CONTRIBUTIONS TO PROCESS MONITORING BY LASER-INDUCED BREAKDOWN SPECTROSCOPY

By

DAVID ALEXANDER RUSAK

A DISSERTATION PRESENTED TO THE GRADUATE SCHOOL
OF THE UNIVERSITY OF FLORIDA IN PARTIAL FULFILLMENT
OF THE REQUIREMENTS FOR THE DEGREE OF
DOCTOR OF PHILOSOPHY

UNIVERSITY OF FLORIDA

1998

ACKNOWLEDGMENTS

I would first like to thank Jim Winefordner for the opportunity to work in his laboratory. I have only recently begun to appreciate the vast resources and creative freedom available here. Next, I would like to thank Ben Smith who was responsible for introducing me to many of the resources in the lab and elsewhere, and who patiently watched and made suggestions as I learned how to do research. Together, Jim and Ben provided a perfect graduate school environment.

I would also like to acknowledge the members of the Winefordner group who all, at some time, contributed either directly or indirectly to my research. Bryan Castle, Dr. Kobus Visser, Igor Gornushkin, and Rebecca Litteral were especially helpful. Martin Clara, who worked in the Winefordner lab for a number of months, was an invaluable resource as well.

There are certainly a number of other people who contributed to my stay in Gainesville. If I were to list them, Yannis Karayannis, Julie Cordek and Wendy Clevenger would be at the top. Thanks to everyone who shared some of their life with me during the last four years.

Lastly, I would like to acknowledge Marlana Blackburn at Infometrix who provided the principal components analysis in the last chapter, the Engineering Research Center (ERC) for Particle Science and Technology at the University of Florida for financial support, and the members of my committee.

TABLE OF CONTENTS

ACKNOWLEDGMENTS....................ii

ABSTRACT....................v

CHAPTERS

1 INSTRUMENTATION AND THEORY OF OPTICAL EMISSION EXPERIMENTS....................1
  - Instrumentation....................1
  - Theory....................6
    - Temperature Determination....................15
    - Electron Number Density Determination....................22

2 FUNDAMENTALS AND APPLICATIONS OF LASER-INDUCED BREAKDOWN SPECTROSCOPY....................29
  - Introduction....................29
  - Solids....................32
    - Fundamental Studies....................32
    - Analytical Results....................40
  - Liquids....................49
    - Fundamental Studies....................49
    - Analytical Results....................58
      - Bulk Liquids....................58
      - Aerosols and Droplets....................63
  - Gases....................67
    - Fundamental Studies....................67
    - Analytical Results....................68

3 THE EFFECT OF TARGET WATER CONTENT ON PROPERTIES OF A LASER-INDUCED PLASMA....................78
  - $CaCO_3$ Experiments....................78
    - Introduction....................78
    - Background....................79
    - Experimental....................82
    - Results and Discussion....................86

Conclusions....87
Iron Ore Experiments....94
Introduction....94
Background....95
Experimental....95
Results and Discussion....98
Conclusions....100

4 LASER-INDUCED BREAKDOWN SPECTROSCOPY OF AQUEOUS SOLUTIONS....102
Introduction....102
Experimental....103
Results and Discussion....107
Conclusions....111

5 USE OF A FIBER OPTIC LIBS PROBE TO DETERMINE TEMPORAL EVOLUTION OF ELECTRON NUMBER DENSITIES IN LASER-INDUCED PLASMAS ON METALS....114
Construction of the Fiber Optic Probe....114
Measurement of Temporal Evolution of Electron Number Densities....120
Introduction....120
Experimental....123
Results and Discussion....123
Conclusions....125

6 EXCITATIONAL, VIBRATIONAL, AND ROTATIONAL TEMPERATURES IN Nd:YAG AND XeCl LASER-INDUCED PLASMAS....129
Introduction....129
Background....131
Experimental....135
Results and Discussion....138

7 CONCLUSIONS AND FUTURE WORK....148

LIST OF REFERENCES....153

BIOGRAPHICAL SKETCH....163

Abstract of Dissertation Presented to the Graduate School
of the University of Florida in Partial Fulfillment of the
Requirements for the Degree of Doctor of Philosophy

CONTRIBUTIONS TO PROCESS MONITORING BY LASER-INDUCED BREAKDOWN SPECTROSCOPY

By

David A. Rusak

May 1998

Chairman: James D. Winefordner
Major Department: Chemistry

When a pulsed laser of sufficient energy and pulse duration is brought to a focus, multi-photon ionization creates free electrons in the focal volume. These electrons are accelerated in a process known as inverse Bremsstrahlung and cause collisional ionization of species in the focal volume. More charge carriers are produced and the process continues for the duration of the laser pulse. The manifestation of this process is a visible spark or plasma which typically lasts for tens of microseconds.

This laser-induced plasma can serve as a source in an atomic emission experiment. Because the composition of the plasma is determined in large part by the environment in which it forms, elements in the laser target can be determined spectroscopically. The goal of a laser-induced breakdown spectroscopy (LIBS) experiment is to establish a relationship between the concentration of an element of interest in the target and the intensity of light emitted from the laser-induced plasma at a wavelength characteristic of that element.

Because LIBS requires only optical access to the sample and can perform elemental determinations in solids, liquids, or gases with little sample preparation, there is interest in using it as an on-line technique for process monitoring in a number of industrial applications. However, before the technique becomes useful in industrial applications, many issues regarding instrumentation and data analysis need to be addressed in the lab.

The first two chapters of this dissertation provide, respectively, the basics of the atomic emission experiment and a background of laser-induced breakdown spectroscopy. The next two chapters examine the effect of target water content on the laser-induced plasma and the use of LIBS for analysis of aqueous samples. Chapter 5 describes construction of a fiber optic LIBS probe and its use to study temporal electron number density evolution in plasmas formed on different metals. Chapter 6 is a study of excitation, vibrational, and rotational temperatures in plasmas formed by ultraviolet and infrared laser beams. The last chapter is a brief assessment of classification software for analysis of LIBS data and a discussion of future work.

CHAPTER 1

INSTRUMENTATION AND THEORY OF OPTICAL EMISSION EXPERIMENTS

Instrumentation

There are three basic units of instrumentation which appear in some form in all emission experiments. They are an excitation source, wavelength selector, and radiant power monitor. The excitation source serves to produce free atoms from the sample and to excite the atoms to the upper energy levels. Excitation sources include flames, arcs, sparks, plasmas, low pressure discharges, and lasers.

Flames are the oldest excitation source used in emission experiments. In the mid-1800s Kirchhoff and Bunsen used a flame for qualitative identification of many elements and discovered the elements cesium and rubidium by use of flame emission.[1] In the 1920s quantitative flame emission was established by Lundegardh for studying plant metabolism, and the first commercial instrument was produced in the mid-1930s by Siemens and Zeiss in Europe.[1] The flame is still used today for determination of elements such as Na and Li which can have significant populations of upper energy levels at relatively low temperature.

Because flames did not provide for efficient excitation of some solids, particularly refractory materials, there was an interest in the years of WWII in developing a more energetic excitation source. Arcs and sparks, which had seen very limited use until this time, were more thoroughly developed, particularly during the Manhattan Project, and used to excite nearly all the stable elements in the periodic table. The dc arc, because of its somewhat lesser stability, was used primarily for qualitative and semi-quantitative analysis, while the more stable (and more energetic) spark was used in quantitative determination. Arcs and sparks are still used as excitation sources in the analysis of many solids, and are also used as part of the sampling unit in techniques where the excitation is accomplished by another plasma.

In the 1960s the development of stable high-frequency and dc plasma devices offered an even more energetic excitation source.[2] The higher degrees of excitation that could be achieved with these plasma sources translated into lower detection limits for many elements, and by the mid-1970s inductively coupled and dc plasmas were available commercially as excitation sources. Today, these plasma sources dominate the field of emission spectrometry.

Low pressure discharges have been extensively characterized by physicists and have relatively recently been employed in spectrochemical analysis.[3] Because the discharge operates at low pressure, the source must be evacuated by a vacuum pump every time the sample is changed and so rapid sample analysis is not possible. However, this source is unique in that it suffers much less from selective volatilization than any of the other sources mentioned and so has become of interest for researchers if not for commercial instrument manufacturers.

Although the laser is included in the list of excitation sources, the actual emission produced in a laser plasma is very similar to that produced by a spark. The laser is unique, however, in that only optical access to the sample is required to produce this spark, and the spark can be produced on non-conductive as well as conductive samples.

The wavelength selector is the next unit of instrumentation in emission spectrometry. The purpose of the wavelength selector is to provide only a chosen range of wavelengths to the detector at any one time. Wavelength selectors can be based on absorption, spatial dispersion, interference filters, or interferometry. Spatial dispersion devices are by far the most common; the prism and grating are the most common dispersive devices.

In a spatial dispersion selector the light collected is resolved into its component wavelengths with a spectral dispersion which can be on the order of mm per nm. This implies that each mm of the spectrum contains light which covers a wavelength range of only 1 nm. Placing a 1 mm exit slit in the spectrum at a given position allows light of a wavelength range of 1 nm to pass to the detector at any given time. The wavelength range passed can be changed with time by rotating the dispersive device so that a different portion of the spectrum falls on the exit slit at different times.

In most modern spectrometers gratings are used as the dispersive element. A grating is a plane or concave plate that is ruled with closely spaced grooves. Different wavelengths of light striking the plate are reflected and constructively interfere at different angles relative to the position of the plate. Hence, as the grating is rotated, different wavelengths of light fall on the exit slit and reach the detector.

The radiant power monitor (detector) is the third unit of instrumentation required for emission analysis. It is intimately connected to the wavelength selector, and the properties of the detector to be used in any experiment depend greatly on the characteristics of the wavelength selector. Photographic plates, photomultiplier tubes, photodiodes, photodiode arrays, charge-coupled devices (CCDs) and charge-injection devices (CIDs) have all been employed as detectors of radiant power.

Photographic films or plates were the first used radiant power detectors. They consisted of an emulsion containing silver halide crystals which were converted to silver atoms by incident photons. After exposure to incident photons, the plate was subjected to a complexing agent which removed remaining silver ions leaving only the exposed silver on the film. After development, a densitometer could be used to determine the spatial concentration of silver atoms across the film and thus the relative intensity of the light striking the film in the given region.

Even by today's standards, photographic plates are quite sensitive. Only about 10 incident visible photons are required to produce a discernable spot on the plate. The major drawback of using a photographic plate detector is the time required for development of the plate and subsequent analysis by densitometry. Moreover, the photographic plate has a limited dynamic range, although this can be dealt with to some extent by varying the exposure time. Despite these drawbacks photographic plates are still commonly used in astronomy for obtaining images of faint objects viewed through telescopes.

The remainder of the photon detectors in wide usage operate by converting incident photons into an electrical signal. Photomultiplier tubes and photodiodes are inherently single channel detectors, producing a single output which is a function of the total intensity of radiation reaching them. They are less expensive than array detectors, CCDs, and CIDs, but can monitor only one wavelength at a time. In absorption or fluorescence experiments which attempt to determine only one element at a time, these detectors are used extensively; however, because emission experiments lend themselves nicely to simultaneous multi-element determination, detectors which can realize this goal are preferred.

Photodiode arrays, CCDs, and CIDs are all multichannel detectors. They consist of a number of discrete sensing elements arranged in a linear or 2-dimensional configuration. When these detectors are used in conjunction with spatially dispersive wavelength selectors, the entire width of the sensor array can be considered to be the exit slit of the wavelength selector and an entire spectral window can be viewed simultaneously. When these detectors are used, a wavelength region encompassing several transitions of interest is often chosen so that concentrations of several different analytes can be determined at the same point in time.

Recently, a new type of detector has been used experimentally in the field of astronomy. Superconducting tunnel junctions (STJs) which are a novel type of charge-coupled device have been used to obtain wavelength dispersive images of faint objects.[4] The devices, which at present are not practical enough for common use in a laboratory, are unique in that at low photon fluxes they not only can form a 2-dimensional image of the object projected onto them, but can also determine with moderate resolution the wavelength of light responsible for the image, effectively disposing of the necessity for a wavelength selector. Although much work remains to be done in the field of STJs, they are certainly of interest to the analytical chemist as well as the astronomer.

Instrumentation for emission analysis varies widely in appearance from large laboratory set-ups encompassing hundreds of square feet to portable equipment for analysis in the field. All instrumentation includes in some form each of three components:

an excitation source, wavelength selector, and radiant power monitor. Figure 1 shows the basic scheme of emission analysis and lists the devices used for each type of instrumental component.

Theory

In emission spectrochemical methods data acquired are the radiation emitted per unit wavelength by the analyte. The excitation step in such a method produces a distribution of excited states which can be described statistically by the Boltzmann distribution

$$n_i = \frac{n_t g_i e^{-E_i/kT}}{Z(T)} \qquad (1\text{-}1)$$

when conditions of thermal equilibrium are met.

Here, n_i is the number of atoms per cm^3 in level i, n_t is the total number of atoms per cm^3, g_i is the degeneracy of state i, E_i is the excitation energy in joules relative to the ground state, k is Boltzmann's constant, T is the absolute temperature, and Z is the partition function

$$Z(T) = \sum_{i=0}^{\infty} g_i e^{-E_i/kT} \quad . \qquad (1\text{-}2)$$

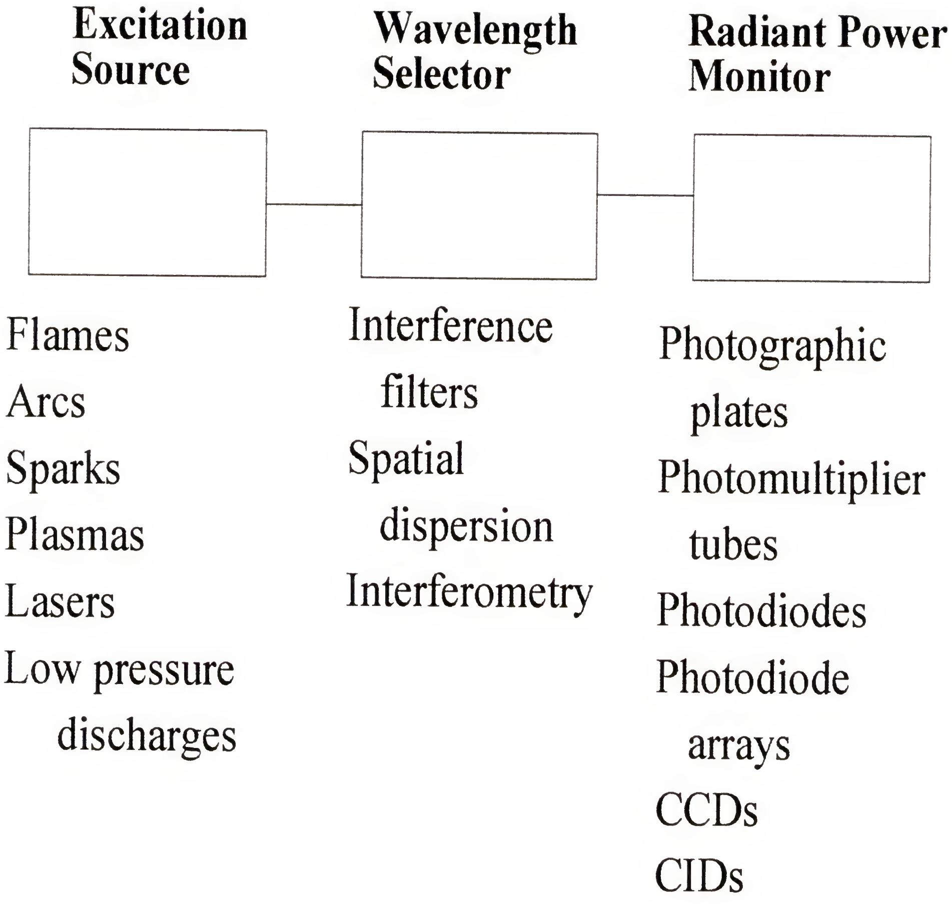

Figure 1-1. Instrumentation for atomic emission spectroscopy.

As these discrete excited states relax to lower energy states, photons of a wavelength inversely proportional to the energy difference between the two states are emitted. The radiant power of emission ϕ_E from state i to state h is equal to the population density of the excited state n_i (cm^3), times the probability A_{ih} (s^{-1}) that the transition will occur, times the energy per emitted photon $h\nu_{ih}$, times the volume observed V (cm^3).

$$\phi_E = A_{ih} h\nu_{ih} n_i V. \quad (1\text{-}3)$$

Even when conditions of thermal equilibrium are not met, ϕ_E will be proportional to analyte concentration as long as n_i is proportional to analyte concentration. It is this relationship which enables quantitative determination of elemental analytes by emission spectroscopy. Figure 2 is a representation of the excitation and emission process.

In order to determine the concentration of an analyte in a sample from measurement of emission due to a certain transition it must first be assumed that the measured intensity of the transition is proportional to the real radiant power emitted due to the transition.

$$I_M \propto \phi_E \quad (1\text{-}4)$$

Several factors are of interest in determining whether or not this condition holds. First, the light collected by lenses, fiber optics, or mirrors and directed into the entrance of a spectrometer is invariably only a fraction of the total light emitted from the plasma. Often this amount of light collected is described by the solid angle of acceptance of the

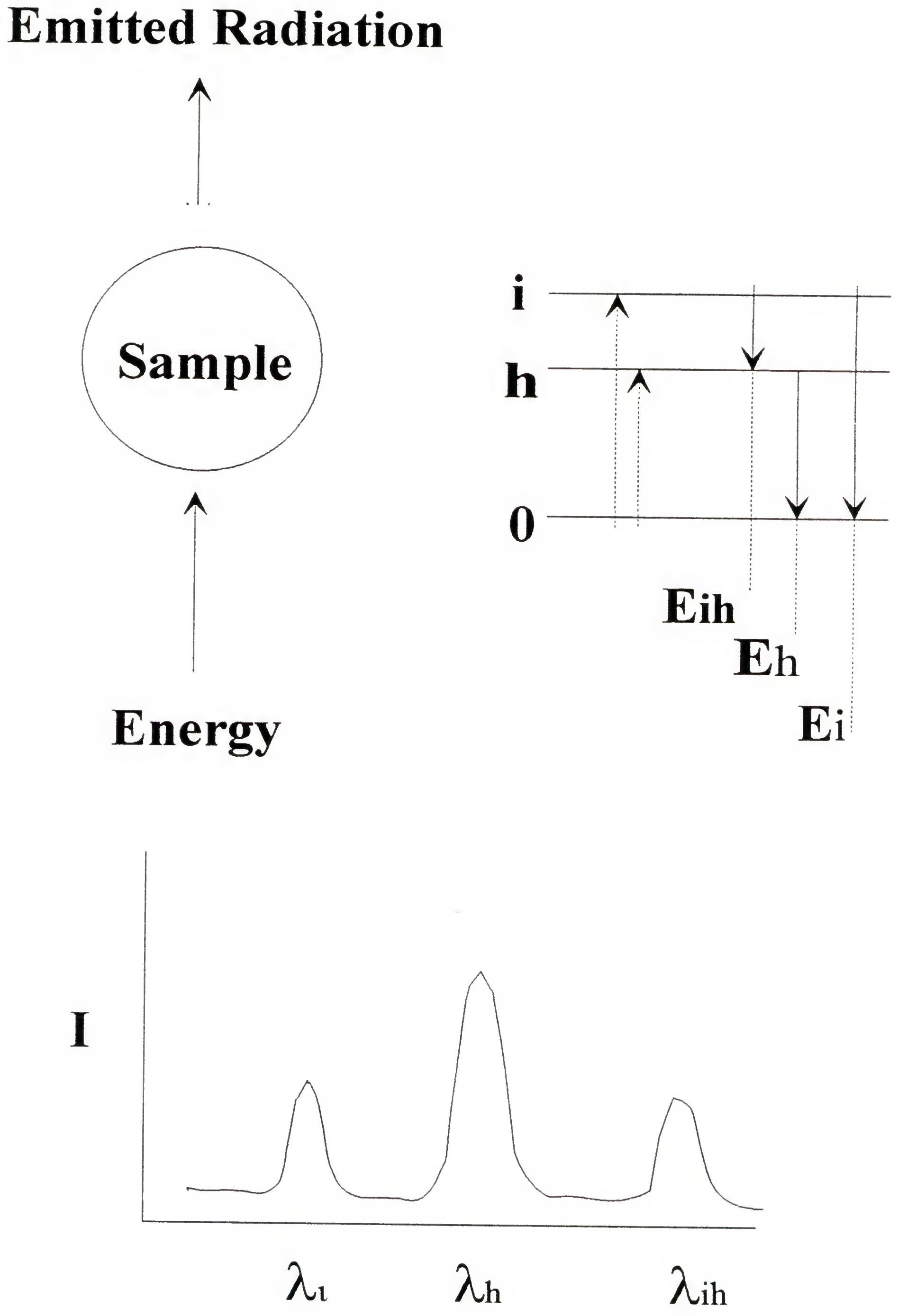

Figure 1-2. The processes of excitation and emission.

optics system. Total acceptance corresponds to 4π steradians, and implies that light emitted in all directions from the sample is collected by the optics. In practice, the solid angle of acceptance is almost always much less than 4π.

The symmetry of the source also must be considered. Any optics system with a solid angle of acceptance less than 4π steradians will have a line of sight through the source. When the source is not spherically symmetric, the orientation of the line of sight through the plasma will affect the observed intensity of emission. In practice this fact is often exploited to discriminate against unwanted or background emission which may not be distributed similarly to the emission of interest.

Another factor which is of interest here is the optical thickness of the plasma. In any excitation source, there exists a gradient between the high energy source and the lower energy surroundings. When this gradient is large, emission generated in the high temperature region from relaxation of excited levels can be reabsorbed by unexcited species in the cooler region. The extent to which this occurs is expressed as the optical thickness of the source and the phenomenon, known as self-absorption, is potentially most severe for transitions in which the lower energy level is the ground state. A source is preferred to be optically thin.

A last factor which affects the proportionality between the measured intensity of emission and the real intensity is the wavelength sensitivity of the detector. A number of detectors which convert incident photons into electrical signals depend on the photons themselves to penetrate a certain distance into a substrate and promote an electron from a valence band to a conduction band. The ability of a given photon to penetrate a certain substrate will therefore effect the electrical signal produced by the photon. In general, UV photons are more readily absorbed by substrates and produce less signal per incident photon than visible photons. Data can be corrected to account for this wavelength sensitivity of the detector by calibrating the detector using sources of known irradiance.

Even with solid angle of collection, source symmetry, optical thickness and wavelength sensitivity affecting the measured intensity relative to the real intensity, it is often the case that the measured intensity is in fact proportional to real intensity and the first criteria is met. So we can begin with the assumption that the measured intensity is proportional to the real intensity of the transition.

From the equation for ϕ_E, it is shown that the radiant power of a transition is proportional to the population density of the higher energy level in the transition. The last, and what turns out to be most difficult, step is to show that the population density of the higher energy level is proportional to the population density of the element (atoms and ions) in the plasma.

The Boltzmann equation can be rearranged to give the fraction of atoms in a source which are in a given energy level i.

$$\frac{n_i^A}{n_t^A} = \frac{g_i e^{-E_i^A/kT}}{Z(T)} \qquad (1\text{-}5)$$

Z(T), the partition function is the sum of the populations of all the energy levels as given above. In practice the partition function manifests itself as a tendency for certain energy levels to be more favorably populated than others at a given temperature. When this function is known the calculation of the number of atoms in the plasma is obtained by rearranging the Boltzmann expression

$$n_t^A \propto \frac{Z(T)}{g_i e^{-E_i^A/kT}} I_M \quad (1\text{-}6)$$

If the partition function is known and if only atoms are present in the source, then this is all we need to calibrate the technique. A problem, however, is that an element is present in the excitation source not only as atoms but also as ions and, at lower temperatures, molecules such as oxides and halides. Ions may have an entirely different energy level distribution and partition function than atoms and must be treated accordingly.

Neglecting the presence of molecules, the total concentration of a given element in the source can be expressed as the sum of atoms and ions.

$$n_t = n_t^A + n_t^A \quad (1\text{-}7)$$

The probability of an element being in its atomic form is given by

$$w^A = \frac{n_t^A}{n_t^A + n_t^I} = \frac{1}{1 + \frac{n_t^I}{n_t^A}} = \frac{1}{1 + \xi}. \quad (1\text{-}8)$$

where ξ is then the ratio of ions to atoms. Under conditions of thermodynamic equilibrium, the Saha equation can be used, provided the electron density is known, to calculate this ratio.

$$\xi = 2 \cdot \frac{1}{n_e} \cdot \frac{Z^I(T)}{Z^A(T)} \cdot \frac{(2\pi mkT)^{3/2}}{h^3} e^{\left(-E_\infty - \Delta E_{red} / kT\right)} \qquad (1\text{-}9)$$

The ΔE_{red} term in the exponential is the reduction in energy of ionization due to shielding by the free electrons. It will be neglected in solving the equation because it is small, typically 0.1 eV for $E_\infty \cong 4$ eV, and is calculated with a large error. The partition functions $Z^I(T)$ and $Z^A(T)$ appear as a ratio. This ratio can be approximated using the degeneracy of the ground state of the ion and atom.[5] The m term is the rest mass of an electron (kg), k is in units of J/K, T is temperature (K), h is in units of J s, and n_e is electron number density (m^{-3}). Now, we need only the temperature (T), electron number density (n_e), and ionization energy (E_∞) to solve for the ratio of ions to atoms (ξ). The determination of temperature and electron density by experiment will be discussed shortly. For now we will assume that these values, as well as ionization energy (E_∞), can be determined or found in a reference.

With ξ from the Saha equation, the total concentration of an element in the plasma can be calculated from the concentration of either atoms or ions.

$$n_t = \frac{n_t^A}{w^A} = n_t^A \cdot (1 + \xi) \qquad (1\text{-}10)$$

$$n_t = \frac{n_t{}^I}{w^I} = n_t{}^I \cdot (\frac{1 + \xi}{\xi}) \qquad (1\text{-}11)$$

And the concentration of either atoms or ions is proportional to the measured intensity of any atomic or ionic transition by a Boltzmann factor which depends on temperature and ionization energy as well.

In summary, the total concentration of an element in an excitation source can be determined by measuring the radiant power of either an atomic or ionic transition when the temperature, electron density, ionization energy, transition probability, and degeneracy are known. In practice, the radiant power is seldom measured with acceptable accuracy. For this to be true, the angle of acceptance of the optics would have to be 4π steradians or a known fraction thereof, the plasma would have to be optically thin, and the spectrometer would have to be calibrated against a source of known irradiance at the wavelength of interest. Even if this were accomplished, the transition probabilities for selected transitions are known only with limited accuracy so that conversion from irradiance to concentration would still introduce much error.

As a result, the measured intensity of a transition is taken to be proportional to the number of atoms or ions in the source and calibration curves are used to establish this proportionality.

Temperature Determination

The determination of the temperature of an excitation source and how it varies with time, sample type, and instrumental parameters is an integral part of the characterization of any emission technique. It has been shown that the relative intensities of different transitions observed from a given sample are exponentially affected by temperature. Moreover, different sample matrices inevitably produce different effects on temperature when introduced to a source. These matrix effects on temperature dictate that the same concentration of analyte in two different sample types may not give the same analytical signal.

Instrumental parameters also affect the temperature of an excitation source. Factors like the rate of sample introduction and the amount of energy provided to the source have large effects on the temperature achieved and thus, on the emission intensities measured. The temperature of a source may also be changing with time. This change is exceedingly more apparent in the use of pulsed sources than in continuous sources and will be discussed later. For now suffice it to say that without at least an understanding of trends in the temperature of the excitation source, a truly useful emission experiment cannot be devised.

In an ideal gas the temperature can be expressed as a measure of the mean kinetic energy per particle.

$$E = \frac{3}{2}kT \qquad (1\text{-}12)$$

Here k is the Boltzmann constant in J K^{-1}, E represents kinetic energy in J, and T is the temperature in K. This equation assumes the presence and isolation of enough particles for a time long enough to establish thermodynamic equilibrium, a concept to be discussed later.

The measurement of kinetic energy of particles in a source *per se* is not a particularly easy task as it involves measurement of mass and velocity at the molecular or even atomic level. However, photons which are emitted from the source share an energy distribution similar to that of the particles and this energy is in practice much easier to measure. Planck derived a relationship between the energy distribution of photons emitted from a source and the temperature of that source. The source considered in this relationship is the blackbody radiator.

A blackbody radiator occurs when the characteristic atomic wavelength dependence disappears due to re-absorbtion and re-emission of photons within the source. In a blackbody radiator, the light emitted is a function only of temperature, not of chemical composition. Measurement of the light emitted as a function of wavelength allows determination of the temperature within the source according to Planck's law,

$$\rho_\lambda(T,\lambda)d\lambda = \frac{8\pi hc}{\lambda^5}\frac{1}{e^{\left({}^{hc}\!/_{\lambda kT}\right)}-1}d\lambda . \qquad (1\text{-}13)$$

Integrating with respect to wavelength gives the Stefan-Boltzmann law for total radiation energy density,

$$\rho = \int_0^\infty \rho\lambda d\lambda = \frac{2k^4\pi^5}{15h^3c^2}T^4 \quad (1\text{-}14)$$

The maximum of the Planck distribution occurs at the root of the first derivative and is given by the Wien displacement law,

$$\lambda_{max}T = hc/5k. \quad (1\text{-}15)$$

This relationship has also been used to approximate the temperature of a blackbody.

In practice, it has been hard to use these laws for temperature determination because it requires that a detector have a uniform and numerically known wavelength response or be calibrated against a source of known irradiance across the entire range of wavelengths. However, this relationship is the basis for optical pyrometry in which the brightness of the source in question is matched to that of a filament of known temperature usually at a wavelength in the infrared.

Like the kinetic energy distribution of particles in an excitation source and the photon energy distribution observed in a blackbody, the population distribution of energy levels over the internal energy states is a function of temperature. As has been discussed already, this population distribution is described by the Boltzmann equation. With a few assumptions about the excitation source, the Boltzmann equation becomes a useful means for determining electronic temperature within the source.

The first criteria that must be met is that the source, or more exactly, the spectral lines observed, must be optically thin. This implies that emission reaching the detector is not reabsorbed to any significant extent by particles in the cooler portions of the source. Observation of non-resonant transitions, and adjustment of a few parameters of the excitation source often provide this optically thin condition.

The second criteria which must be met is that the source is in thermodynamic equilibrium and is homogeneous. In practice, this is rarely, if ever, entirely true. However, at certain times or at specific locations within the source there may be conditions which are close to thermodynamic equilibrium. At these times, in these regions, there is said to exist a local thermodynamic equilibrium. The Boltzmann equation then applies and can be used to calculate an electronic temperature with the understanding that the temperature is valid only inasmuch as the assumption of local thermodynamic equilibrium is valid.

In theory, only one transition need be observed to determine the temperature. The spectral radiance integrated over a single line profile is given by

$$\phi = \frac{\mathrm{hcl}}{4\pi \mathrm{z}} \frac{\mathrm{N_t g_i A_{ij}}}{\mathrm{Z(T)}} \mathrm{e}^{\left(-\mathrm{E_i}/\mathrm{kT}\right)} \quad . \qquad (1\text{-}16)$$

To calculate the temperature, the detector must be calibrated for absolute spectral radiance at the solid angle of acceptance used, and the total particle density N_t, the partition function Z, the effective pathlength l, and the transition probability A_{ij} must all be known. This all makes calculation of temperature by observation of a single transition extremely difficult.

If two transitions which occur from different upper energy levels are observed for the same element in the same ionization stage the equation becomes much more attractive because the constants, and the partition function, will cancel out of the equation

$$\frac{\phi_1}{\phi_2} = \frac{g_1 A_1 \lambda_2}{g_2 A_2 \lambda_1} e^{\left(E_2 - E_1 / kT\right)} \quad . \qquad (1\text{-}17)$$

Now the temperature can be calculated with no knowledge of total particle density, pathlength, or partition function, and with only a relative calibration of the detector at the two wavelengths corresponding to transitions observed.

This method can be extended to include a number of transitions all originating from different upper energy levels of the same element in the same ionization state. The equation for radiance can be rewritten as

$$\frac{\phi_i \lambda_i}{g_i A_i} = \frac{hclN_t}{4\pi z} e^{\left(-E_i / kT\right)} \quad . \qquad (1\text{-}18)$$

Taking the natural logarithms,

$$\ln\left(\frac{\phi_i \lambda_i}{g_i A_i}\right) = -\left(\frac{1}{kT}\right)E_i + \ln\left(\frac{hclN_t}{4\pi z}\right) \qquad (1\text{-}19)$$

Now, plotting ln $(\phi_i\lambda_i / g_iA_i)$ *vs* E_i gives a line with a slope of $-1 / kT$ and intercept of $\ln(hclN_t / 4\pi z)$. This plot is called a Boltzmann plot, and an example is given in figure 3.

In using Boltzmann plots, there are several practical matters that need to be considered. First, it is convenient to choose transitions for the Boltzmann plot which can be observed in a relatively narrow wavelength region. The reasons for this are two-fold. Even with a multichannel detector (photodiode array, CCD, etc.) often only 20 to 30 nm can be observed simultaneously. Emission acquired simultaneously at the wavelengths of interest does not suffer from source fluctuations and is constant in all parameters regarding angle of collection, line of sight, and source homogeneity. Secondly, differences in detector sensitivity at different wavelengths are more likely to be insignificant over a narrow spectral range. Often, temperature determination is done without even relative calibration of the detector at the wavelengths observed.

Next, it is preferable to choose transitions which have a large difference in the upper energy levels. This is because in the Boltzmann plot these upper energy levels constitute the independent variable. The slope of the line over a large range of upper energy levels is more likely to be indicative of the temperature than the slope of a line over a small range where other factors can have significant influence on the intensities observed. When transitions which arise from a wide range of upper energy levels can be observed in a narrow wavelength range, the Boltzmann plot is most likely to yield reliable results.

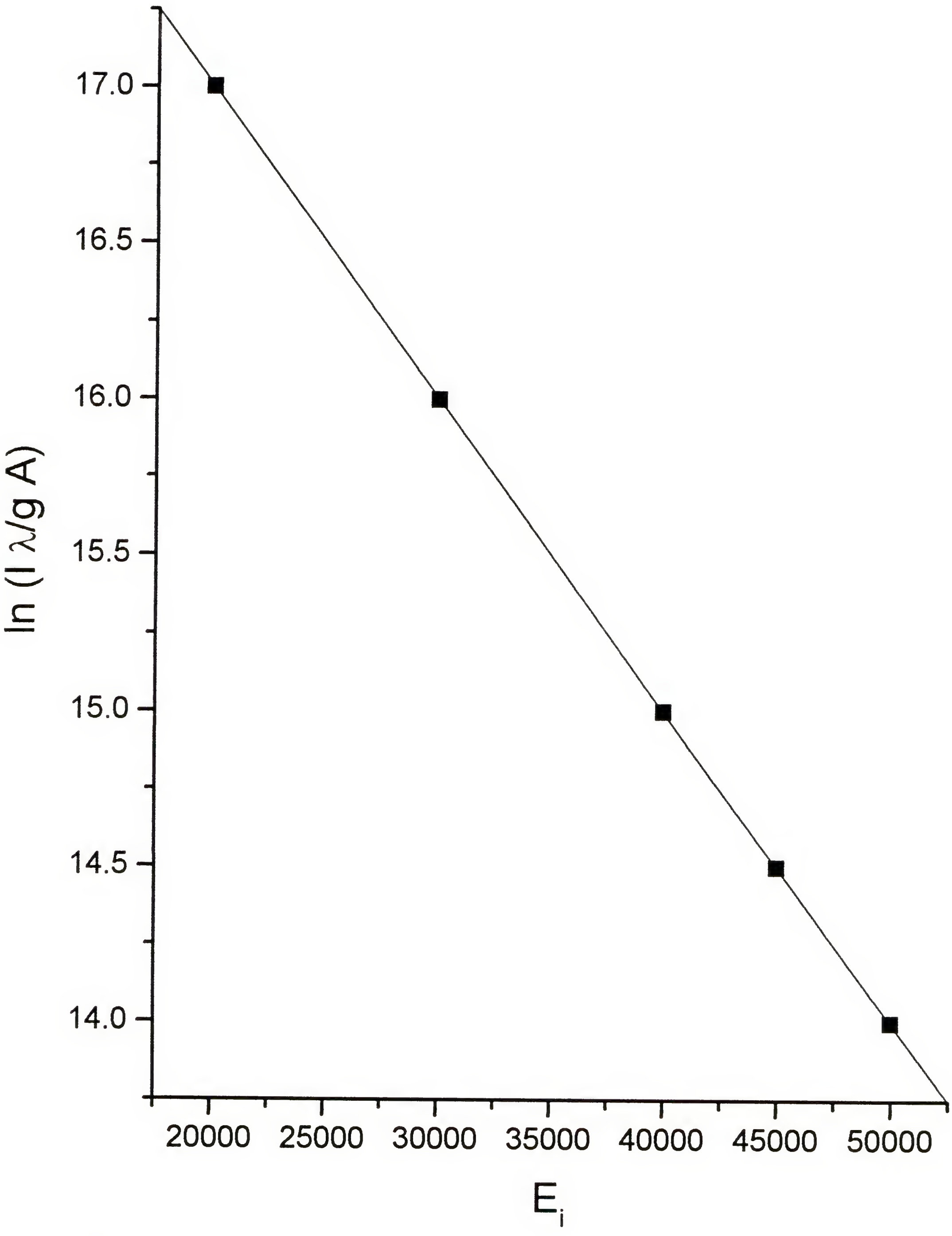

Figure 1-3. An example of a Boltzmann plot

Electron Number Density Determination

Individual hydrogen emission lines are often referred to as belonging to a series named for the scientist who first observed them. These three series are the Lyman (L), Balmer (H) and Paschen. Within each series there exist analogous transitions which are often denoted by greek subscripts (α, β, etc.). Because of their location in the visible region of the spectrum and their sensitivity to electron densities in the range between 10^{15}-10^{19} cm^{-3}, the Balmer alpha (H_α) and Balmer beta (H_β) lines at 656.2 and 486.6 nm, respectively are most commonly used in calculation. Extensive tables of $\alpha_{1/2}$ values for these two lines have been tabulated and confirmed by a number of sources and they are the lines most often used in emission source diagnostics.[6,7]

Because it appears in the Saha equation which is used in the determination of ion to atom ratios, the electron number density is an important parameter of an excitation source, and a practical method to determine it is a valuable diagnostic tool. In order to devise a method to accomplish this, the potentially observable effects of changes in electron density must first be identified. These effects must then be described by physical and mathematical models so that measurement provides a means of calculation.

In the presence of an electric field the degeneracy of certain components of a spectral line can be removed by the Stark effect, and the different components of the original spectral line observed at slightly different wavelengths. The wavelength difference between the components is often much less than the width of the components themselves so that the observed effect is a broadening of the original spectral line.

For a hydrogen line the Stark effect produces splitting which is proportional to field strength. The broadening of a hydrogen line is then a first-order Stark effect. In more complicated atoms the removal of degeneracies and broadening of the spectral line is less apparent. The splitting in these atoms is proportional to the square of the electric field due to the quadratic Stark effect.

In arcs, sparks, and plasmas there exists an electric field which is composed of electrons and ions. This field is often strong enough to produce an observable Stark effect in emitted lines. When the broadening due to the Stark effect can be determined for a hydrogen line, it provides a method for calculating an electron number density in the source. This broadening must be distinguished from other sources of broadening, such as Doppler broadening and instrumental broadening due to resolution of the spectrometer used to view the line.

When the temperature of the source in question is known, the broadening due to Doppler effects can be calculated and subtracted from the observed line width to isolate the broadening due to the Stark effect. For these hydrogen transitions, at high electron densities ($>10^{16}$), Stark broadening tends to dominate Doppler broadening and the broadening due to resolution of the spectrometer becomes the competing mechanism. However, hydrogen lines at these densities can be several angstroms in width, and when the resolution of the spectrometer is less than 1 angstrom, the observed profile is approximately due only to Stark broadening.

Two approximations of Stark broadening due to perturbers (charge carriers in the electric field) have been proposed. The quasi-static approximation assumes that changes in the electric field as seen by a single particle are slow relative to the frequency of the

Stark shift. The impact approximation assumes that the changes in the field are fast relative to the frequency of Stark shift. Both theories have been treated thoroughly by Griem.[6] Although the true mechanism of line broadening for a specific source is almost certainly a combination of aspects of these two approximations, for hydrogen lines the impact theory gives theoretical line widths which more closely match those observed experimentally.

The impact approximation predicts that peaks broadened by the Stark effect will exhibit a Lorentzian profile. In contrast, Doppler broadening gives a Gaussian profile. This fact can be exploited to separate the effects of Doppler broadening and Stark broadening when the Doppler broadening is thought to be significant. For a Lorentzian peak shape of a hydrogen line (linear Stark effect) the electron density is related to the line width by the exponential

$$\Delta\lambda_{1/2} = 2.50\cdot 10^{-9}\alpha_{1/2}n_e^{2/3} \qquad (1\text{-}20)$$

The $\alpha_{1/2}$ value is a Stark broadening parameter which is dependent on both the temperature and electron density, and so in order to use this equation, the temperature of the source must at least be approximated, and an iterative calculation must be done in order to converge on a value for n_e. This method is commonly used to calculate electron densities from hydrogen peak widths with error which is generally less than 15%.

Excitation temperature determinations from Boltzmann plots of atomic or ionic transitions give values close to 10000 K in the laser-induced plasma after the first microsecond. This temperature is the one at which the $\alpha_{1/2}$ values are interpolated. First, the above equation was rearranged to give

$$n_e = \left(\frac{\Delta \lambda_{1/2}}{2.5 \cdot 10^{-9} \alpha_{1/2}} \right)^{3/2} \qquad (1\text{-}21)$$

Next, a plot of $\alpha_{1/2}$ *vs* log (n_e) was prepared using the values for n_e in Griem. Linear regression of this plot gave an equation which could then be used to determine $\alpha_{1/2}$ values at any temperature. At 10 000K the $\alpha_{1/2}$ values for the H_α line were fitted to the equation

$$\alpha_{1/2} = 4.64 \cdot 10^{-3} \log(n_e) - 6.12 \cdot 10^{-2} \qquad (1\text{-}22)$$

as shown in figure 4.

Substituting the right half of this equation for $\alpha_{1/2}$ in the equation for n_e then gives

$$n_e = \left(\frac{\Delta\lambda_{1/2}}{2.5 \cdot 10^{-9} \left(4.64 \cdot 10^{-3} \log(n_e) - 6.12 \cdot 10^{-2} \right)} \right)^{3/2} \qquad (1\text{-}23)$$

Now, if the half-width is measured and an approximation of the electron density is made, a repetitive calculation can be done which will converge on a single value for n_e.

An even better determination can be done if the $\alpha_{1/2}$ *vs* log (n_e) plot is fit with a second order polynomial rather than with linear regression as shown in figure 5. In this case the the equation for n_e becomes

$$n_e = \left(\frac{\Delta\lambda_{1/2}}{2.5\cdot 10^{-9}\left(-7\cdot 10^{-4} \log(n_e)^2 + 2.72\cdot 10^{-2} \log(n_e) - 2.46\cdot 10^{-1} \right)} \right)^{3/2} \quad . \qquad (1\text{-}24)$$

The repetitive calculation can be done in the same manner as with the linear fit.

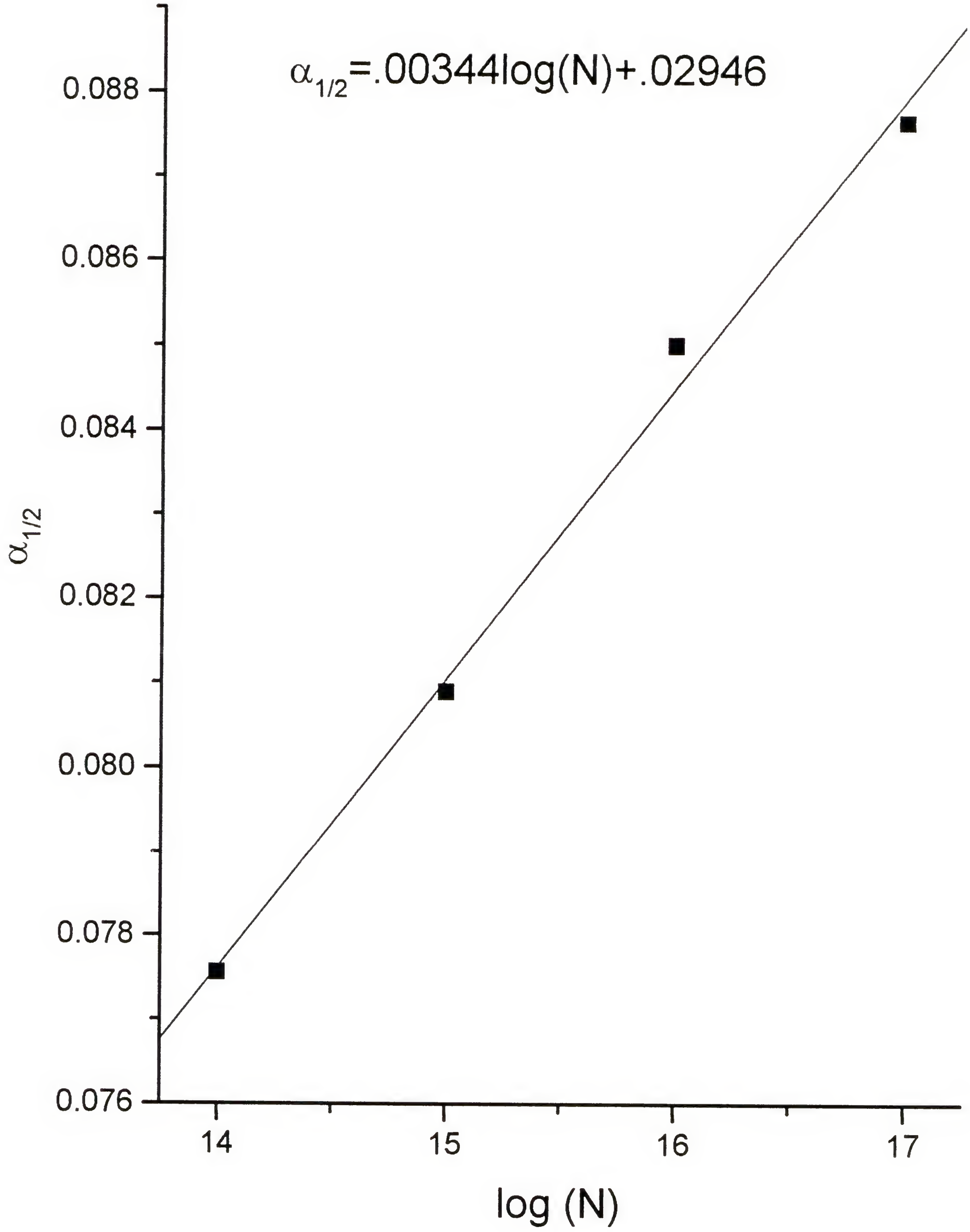

Figure 1-4. A linear fit of $\alpha_{1/2}$ *vs* log (N).

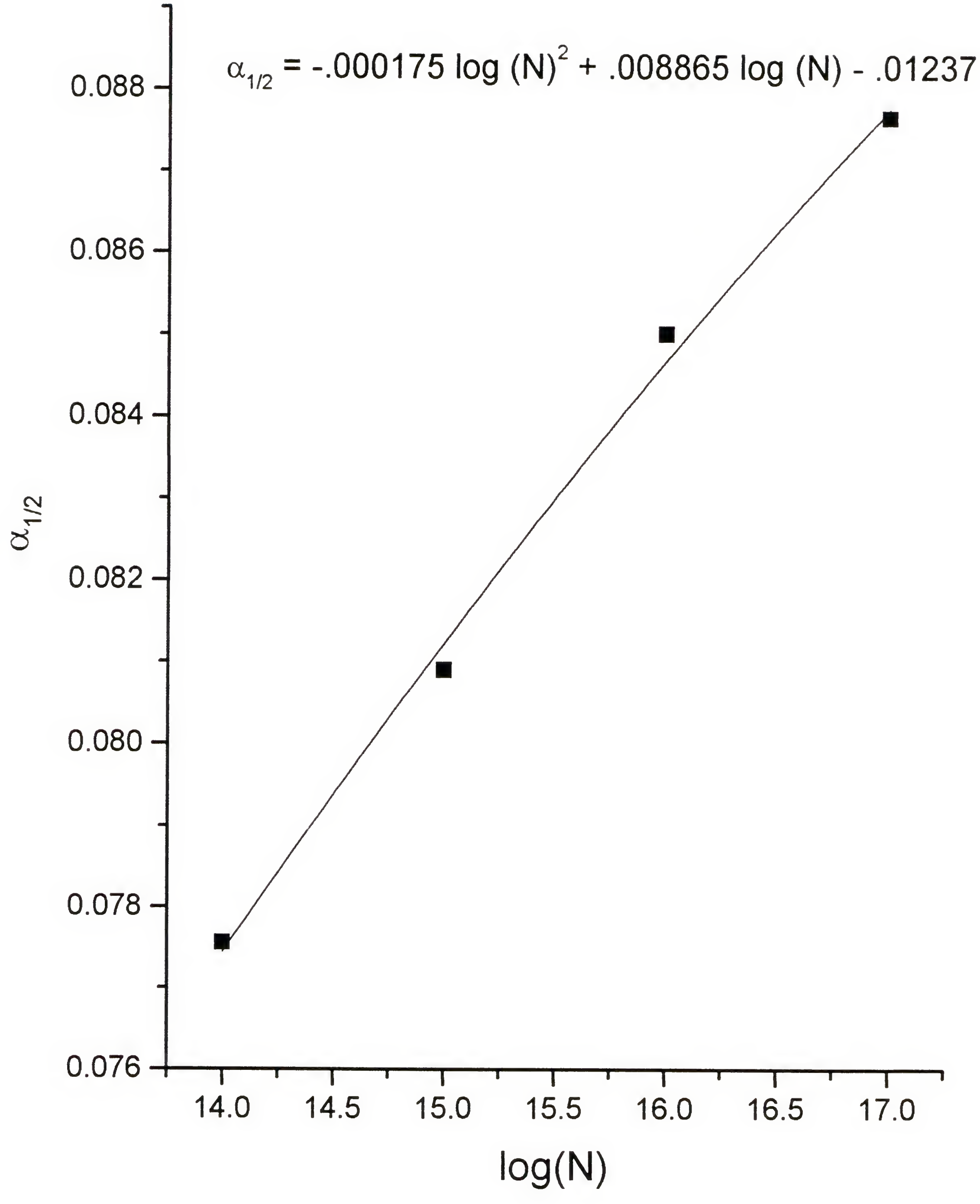

Figure 1-5. A second order fit of $\alpha_{1/2}$ *vs* log (N).

CHAPTER 2

FUNDAMENTALS AND APPLICATIONS OF LASER-INDUCED BREAKDOWN SPECTROSCOPY

Introduction

There have been several publications in the last decade which have reviewed laser-induced breakdown spectroscopy (LIBS) either as a unique method of elemental analysis, or as a member of the family of atomic emission techniques. LIBS has also been addressed in reviews on laser applications, process monitoring, and materials processing. Many spectroscopic studies of laser plasmas have also appeared in the physics journals. In order to construct a meaningful review, the literature must first be reduced to a subset. In this instance, LIBS in analytical chemistry is chosen.

This review will cover fundamental studies and analytical results and applications of LIBS related to the field of analytical chemistry. The review is divided according to target phase. Solids, liquids and gases are treated in sections devoted to each. Articles from the physics literature are included when they are of interest to the analytical chemist. Spectroscopic studies of laser-induced plasmas created in pulsed-laser deposition (PLD) experiments have, for the most part, been omitted under the assumption that these papers are more pertinent to materials science than to analytical chemistry. Fundamentals and applications of laser ablation as a sampling technique are also ignored on the grounds that, in these instances, the laser plasma does not serve as the excitation source.

The time frame to be covered has not been specifically defined because the amount of literature dealing with each of the three phases of targets differs greatly. The literature on solids is easily the largest, and so the review of solids is taken almost entirely from publications within the last 5 years.

Literature on laser-induced breakdown in gases is the oldest. Many of these publications are in the physics literature and deal with mechanisms of breakdown and plasma diagnostics. There are a smaller number of papers that report upon the determination of trace metals in gas phase matrices. Most of these are intended to prove the usefulness of LIBS in hazard monitoring. In the section on gases, the analytical chemistry literature over the past 10 years is reviewed and appropriate additions are made from the physics literature.

The section dealing with liquids includes bulk liquids, isolated droplets, and aerosols generated from liquids. Among the chemistry journals, this literature is the smallest. The physics is of interest primarily because of medical applications of laser-induced breakdown, and publications which are judged to be of interest to the analytical chemist have been included. All publications related to the elemental analysis of liquids by LIBS during the last 14 years are included.

Previous reviews on this topic begin with a 1984 review by Adrain and Watson titled “Laser Microspectral Analysis: A Review of Principles and Applications.”[8] This was followed by Cremers and Radziemski who published “Laser-induced Breakdown Spectroscopy: Principles, Applications, and Instrumentation” in 1990.[9] This paper included a brief review of theory and instrumentation for LIBS followed by a few industrial applications. In 1992, Thiem *et al.* reviewed LIBS theory as part of their paper titled "Lasers in Atomic Spectroscopy: Selected Applications."[10] The section on laser-induced plasma covered laser-material interaction, plasma production factors (wavelength, energy, and properties of target), and emission factors (temperature and electron density).

Majidi and Joseph published "Spectroscopic Applications of Laser-Induced Plasmas" in 1992.[11] This publication has perhaps had the most influence in terms of style and content on the review that follows. Majidi and Joseph reviewed analytical results on solids, liquids, gasses, and mixed phase systems for the years 1987-1992. Emphasis was on applications of LIBS such as determination of hazardous elements in air, toxic elements in wastewater, and elements of interest in coals and iron ores. The authors stressed the fact that LIBS required only optical access to samples.

In 1993, Ibrahim and Goddard published "An Overview of Laser-Induced Breakdown Spectroscopy."[12] They concentrated on the topics of laser-material interaction, local thermodynamic equilibrium, and plasma diagnostics. The instrumentation was described, the use of gated detection was explained, and a few applications were presented. It was not a literature review.

In a 1993 review by Darke and Tyson titled "Interaction of Laser Radiation with Solid Materials and its Significance to Analytical Spectrometry," applications of LIBS were reviewed in the section on laser ablation.[13] In this paper, LIBS was referred to as laser microprobe optical emission.

The following year application of LIBS to process control was briefly reviewed by Noll *et al.*[14] The authors discussed fundamentals of plasma formation and laser-material interaction with respect to optical and heat penetration, laser energy, density, and absorbance. The use of fiber optics and on-line sampling was discussed, and a periodic table was presented showing elements which had been determined and their detection limits in iron ore. This idea was incorporated into the review that follows. Each section is concluded with a periodic table or tables with elements that have been determined and shaded according to detection limit.

Most recently, LIBS was briefly reviewed as a section in the comprehensive review of atomic emission by Sharp *et al.* published in 1995.[15]

Solids

Fundamental Studies

Many papers in this area stem from the need to more fully understand the LIBS plasma in order to obtain useful quantitative results. One such paper is the 1988 publication by Chen and Yeung who used the acoustic signal generated by a laser-induced plasma as an internal standard.[16] They reported that the magnitude of the acoustic wave was proportional to the emission signal for major and minor elements within the solid target. Furthermore, they found that this proportionality was independent of laser power and focus spot size.

In the same year, Wood *et al.* studied the effect of laser pulse duration on soft x-ray emission from a tantalum target.[17] Using a colliding-pulse mode locked dye laser at 620 nm with pulse durations of 100 and 600 fs and a Nd:YAG laser at 1064 nm with a pulse duration of 70 ps, the plasma emission in the range from 10-71 nm was observed. It was found that longer pulses gave relatively more short wavelength emission and longer emission lifetimes than short pulses.

In 1989, Coche *et al.* used laser-enhanced ionization detection in a laser plasma to study the processes of ionization and recombination.[18] They used a N_2 laser (337.1 nm, 5 mJ, 10 ns) to ablate a solid target. A dye laser was used to selectively ionize species in the plasma at different delays relative to the ablation pulse. Optogalvanic detection was used to give an indication of the number of atoms in the probe volume at the chosen time delay. In this way, ionization and recombination rates could be inferred.

Also in 1989, Iida studied the atomic emission characteristics of a laser plasma in reduced pressure argon.[19] Using a ruby laser (1.5 J, 20 ns), a plasma about 10 mm in height, and more than 100 μs in duration was formed at pressures between 0 and 50 Torr. The plasma at 50 Torr had greatly increased line emission and background due to confinement by the Ar atmosphere. The plasma at lower pressure showed less background and less line emission.

Another investigation of plasma expansion was done by Balazs *et al.* in 1991.[20] These authors investigated ruby laser pulses on a copper target, and constructed a two-part model for the interaction. The first part of the model dealt with the heating and melting of the solid and included parameters such as thermal diffusivity, pulse duration, and density. The second part of the model described the plasma expansion into a vacuum.

Mason and Goldberg have characterized a laser plasma in a pulsed magnetic field.[21] The first part of the paper included spatially resolved emission studies. The authors found that when a pulsed magnetic field was oriented normal to the laser beam, it caused radial compression and axial expansion in the plasma. The emission intensities of both atoms and ions were also increased in this magnetically confined plasma.

In the second part of the paper, the authors discuss time resolved emission and absorption studies. They concluded that the increase in emission seen in the plasma was due to Joule heating caused by the induced secondary current in the plasma. This was evident by the fact that the increase in emission was seen later in time than the maximum of the applied magnetic field. Also, the intensity increase was attributed to increased atomization efficiency and longer residence times in the plasma.

The effects of buffer gas type on the plasma produced by a Nd:YAG laser (1064 nm, 100 mJ, 7 ns) on a metal target was studied by Owens and Majidi in 1991.[22] They observed an increase in the ratio of Al II / Al I intensity in helium gas relative to argon gas and air. This increase was attributed to the ability of excited helium atoms to transfer energy to a similar energy level in the aluminum ion.

More metal target studies were performed by Lee *et al.* in 1992.[23] These authors used an ArF laser (193 nm, 100 mJ, 10 ns) to produce plasmas on copper and lead. The lead plasma was much larger than the copper plasma (5 mm *vs* 2 mm) and had a slightly lower excitation temperature as determined by Boltzmann plots. The temperature of the copper plasma was 13200-17200 K, the lead plasma was 11700-15300 K.

In 1992 Marine *et al.* studied plasma expansion by optical time-of-flight measurements.[24] They determined that the velocity distribution of ions produced by a UV pulse of several nanoseconds duration was broad and not well defined. In contrast, the ions produced by a picosecond IR pulse traveled with a velocity inversely proportional to the square root of their mass. Neutral atoms still had a poorly defined velocity distribution. These authors also noted the appearance of a bi-modal temporal profile for YO^+ emission and attributed this to two possible mechanisms for formation of YO^+.

Kuzuya *et al.* studied the effect of laser energy and atmosphere on the emission characteristics of laser-induced plasmas.[25] They used a Nd:YAG laser at 1064 nm and pulse energies from 20-95 mJ in atmospheres of He, Ar, and air from 1 Torr to 1 atm. The authors reported that maximum emission intensity was observed at 95 mJ in 200 Torr of Ar. However, maximum signal to background was obtained in helium at 40 Torr and 20 mJ of power. Images showed the different sizes and shape of these plasmas.

Okana *et al.* studied mass removal in non-metallic inorganic solids and determined relationships between laser power and atom yields.[26] Their paper described vacancy initiated laser ablation as a process by which weakly bound atoms were released from around vacancies and vacancy clusters. The atom yield was determined to be an exponential function of laser fluence.

Time resolved emission studies from a laser plasma on sodium chloride were reported by Yago *et al.* in 1993.[27] They used a Nd:YAG laser of 150 ns duration focused onto a NaCl pellet. The emission spectra showed self-reversal in air but not in a vacuum. The plasma was divided into two zones, a hot core behaving as an emission zone, and a low temperature periphery behaving as a reabsorption zone. The plasma expansion rate was shown to be determined by ambient gas pressure.

In 1994, Kagawa *et al.* used a XeCl laser (308 nm, 15-70 mJ, 20 ns) to produce plasma on a Zn target in vacuum.[28] Time resolved studies showed a number density jump which represented the blast wave expansion into the observed volume. This outermost portion of the plasma was shown to be ideal for analytical measurements because the background in this area was greatly reduced.

In 1994, Tambay and Thareja studied emission in a laser plasma of Cd metal vapor formed in a heatpipe.[29] They showed that emission from the vapor was stronger when the plasma was formed on a tungsten target than it was when the plasma was formed in the gas itself. The authors claimed that this was due to pumping of the vapor by soft x-rays formed on the tungsten target.

Transition probabilities of 28 Si ion lines were determined using a laser-induced plasma as a source by Blanco *et al.* in 1995.[30] Using a Nd:YAG laser (1064 nm, 280 mJ, 10 ns) to produce a plasma on pure silicon, these authors observed emission in Ar and Kr atmospheres. The plasma produced was found to have an excitation temperature of 20000 K and an electron density of 10^{17} cm^{-3}. Absolute transition probabilities for the Si ion lines were calculated.

Jensen *et al.* published mechanistic studies of laser-induced breakdown on model environmental samples in 1995.[31] They used a KrF laser (248 nm, 30 ns) to produce plasmas on SiO_2 containing Eu and Cr, which were added as the solids Eu_2O_3 and $K_2Cr_2O_7$ to the sand. Detection limits of 100 ppb for Eu and 2 ppb for Cr were reported. A sample was also prepared in which the source of Cr was a solution which was added to the sand and then evaporated. This method of sample preparation gave an order of magnitude less signal and a different temporal profile for the Cr emission.

In 1995, Tasaka *et al.* studied the emission of a laser-produced plasma on graphite.[32] They used a Nd:YAG laser in He and in air to form a plasma in which they observed a “triple plume” composed of three distinct regions. The authors claimed that these regions appeared because of three different speeds in the expanding plasma. The fastest region was composed of carbon ions from the target and N and O ions when the experiment was done in air. The second plume was composed of the compressed neutrals in the vicinity of the shockwave. The slowest plume was then the target vapor composed of larger molecules. Thareja *et al.* also studied graphite plasmas at low pressure and found similar temporal profiles.[33]

Intense emission from the CN radical has been observed in plasmas produced on graphite. With the use of a high resolution spectrometer, several authors have resolved the vibrational and rotational structure in the CN emission bands. The emission from the violet band of CN around 388 nm has been used to calculate vibrational and rotational temperatures in the laser plasma.[34-37]

In 1996, Al-Wazzan *et al.* studied three-dimensional number densities of species in laser produced plumes.[38] They used absorption of an expanded dye laser beam to form shadow images of Ba ions in a plume produced by excimer laser ablation at 248 nm. They also used fluorescence from planar slices of the plasma to obtain sequential cross section images which could be built into a three-dimensional image.

Al-Wazzan *et al.* also carried out an experiment in which they observed plasma in vacuum and in ambient oxygen.[39] In oxygen, the expanding plume showed increased temperature and electron number density at the shock front due to increased collisional excitation rates. In a vacuum, enhancement at the shock front was not observed.

Bulatov and Liang obtained full spectra at each pixel in the image of a laser-induced plasma as depicted in Figure 2-1.[40] They used this technique to create classification maps which gave location of any species of interest within the plasma. They studied the effects

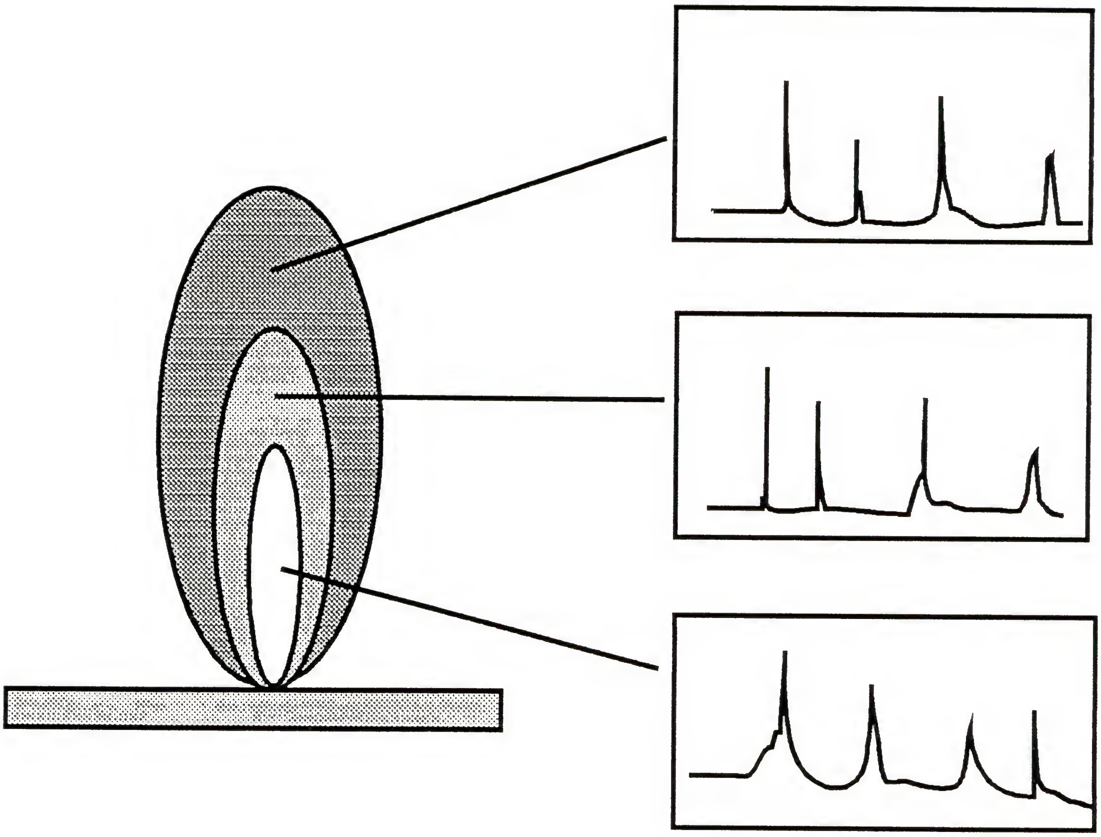

Figure 2-1. Spectroscopic imaging of a laser-induced plasma.

of different focal length lenses and different sampling geometries on plasma formation and location of species within the plasma.

In 1996, Mulatari *et al.* obtained time resolved images from a laser plasma formed on a sample at non-normal incidence.[41] They varied the angle of the incident laser beam with respect to the target from perpendicular to nearly parallel. It was found that the plume was generated in the perpendicular direction regardless of the laser angle. However, the maximum emission signal was obtained with normal incidence.

Mulatari and Cremers also published a second study that year reporting on the use of an acousto-optic tunable filter to capture spectrally resolved images.[42] They used a series of different lenses to examine the different distributions of elements within each plasma. By collecting light from the outermost edge of the plasma, they were able to use ungated detection to obtain analytically useful spectra with low background.

Nemet and Kozma studied the shape of emission lines produced on gold targets at different delays relative to the ablation laser.[43] The 406.51 and 389.79 nm lines were observed. These lines were asymmetric and shifted relative to their natural wavelength at times up to 1000 ns after the laser pulse. These lines could be described by asymmetric Lorenz-type profiles. After 1000 ns, the lines appeared to be very close to their natural wavelength and were Lorentzian and symmetric.

In 1997, Kurniawan and Kagawa used a long pulse Nd:YAG laser to produce plasma on a brass target in vacuum.[44] The authors were especially interested in the secondary plasma formed by compression in the vicinity of the shock wave. The emission in this secondary plasma was captured, and it was observed that when a wedge of aluminum was placed very close to the target, the emission signal increased in the vicinity of the wedge.

The authors attributed this effect to increased compression provided by the shock wave interaction with the immovable aluminum wedge.

In 1997 Martin *et al.* used a laser-induced plasma to establish spectral calibration of their detector.[45] A Nd:YAG laser (1064 nm, 350 mJ) was focused onto targets of ceramic, polyethylene, ZnS, and aluminum, all in vacuum. Line pairs in the deep UV were used with known transition probabilities to determine the relative efficiency of the detection at each wavelength.

Most recently, Granse *et al.* modeled laser-induced plasma and compared their model to experiments with different lasers and different materials.[46] The model they derived accounted for fluid dynamics of the plasma, absorption of laser energy *via* inverse bremsstrahlung, and the dynamics of ionization and recombination.

Analytical Results

The number of papers describing analytical results of LIBS studies on solids is easily larger than the number of papers dealing with either liquids or gases. For this reason, only publications after 1992 are considered in this section. Figures of merit given for specific determinations differ greatly from one author to the next. In the periodic tables which follow this section, the lowest published detection limits for the elements in the matrix of interest are used to determine the shading.

Carbon content in steel was determined by Aguilera *et al.* in 1992.[47] The authors observed the emission from the 193.1 nm carbon line because the 247.9 line had an interference. The experiment was done in a CO_2 free environment, and a neighboring iron line was used as an internal standard. A Nd:YAG laser at 1064 nm was used, and it was found that the slope of the calibration curves generated decreased with increasing laser power. Also, there was a slight difference in slope for stainless and non-stainless steels. At a laser power of 100 mJ, the detection limit for carbon was 65 ppm and the RSD was 1.6 %.

Also in 1992, Hader used LIBS for on-line quality control of rubber mixing.[48] The author called the technique "remote laser microanalysis" and used the acronym RELMA. The existing technique for quality control of rubber mixing involved a discrete sampling step in which a small portion of rubber was taken from a batch and analyzed. This led to problems when it became neccessary to distinguish between bulk composition fluctuations and inhomogenieties; with on-line sampling by LIBS in a number of randomly chosen positions in the rubber mix, the two problems could be distinguished. Analytes were elements found in the cross-linkers and plasticizers added to the raw rubber.

Lorenzen evaluated other on-line applications of LIBS in the same year.[49] This time the technique was referred to as "laser-induced emission spectral analysis" and given the acronym LIESA. The authors described applications such as the determination of minor elements in liquid steel, and depth profiling of layers on metallic substrates.

In 1993, Sabsabi *et al.* used a KrF laser (248 nm, 100 mJ) to analyze aluminum alloys.[50] They carefully optimized the delay time by using a PMT to look at the temporal evolution of several different emission lines. An aluminum line was used as an internal standard and magnesium was determined at a few ppm.

The following year Thiem *et al.* investigated LIBS of alloy targets.[51] They determined Al, Cu, Fe, Ni, and Zn using a Nd:YAG laser at 532 nm in a vacuum chamber. Using non-resonant lines for all the elements, the authors were able to generate linear calibration curves from a few hundred ppm to a few percent for each element. For the determination of these elements at the percent level, the authors have found many potential emission lines in the spectral window from 300 to 400 nm.

Thiem and Wolf used LIBS to analyze mining ores and compared the results to those obtained by a digestion ICP-AES method.[52] Al, Ca, Cu, Fe, K, Mg, Mn, Si, and Ti were determined in aluminum and manganese ore. The comparison showed that both methods gave roughly the same accuracy, but the ICP technique had better precision. The authors also pointed out the similarity in cost for the two techniques, about $100 K for either.

Investigations of the use of resonant wavelengths in laser ablation had been made as early as 1992 by Borthwick *et al.*[53] Although most of the work was carried out with time-of-flight mass spectrometry, the paper is included because of its relevance to LIBS. The authors noted that when an ablation laser was scanned through specific wavelengths, an enhanced ion yield was detected. More specifically, an enhancement in Ga ions in the ablation of GaAs, and an enhancement in Al ion yields in ablation of steels were noted. The ion yields were even more pronounced when grazing angles of incidence of the ablation laser were used.

In 1995, Allen *et al.* employed resonant wavelengths in LIBS of thin films.[54] The authors used resonant laser ablation time-of-flight mass spectrometry to investigate copper thin films on a silicon substrate. Using a XeCl excimer laser pumped dye laser (5 mJ pulse energy at 463.51 nm) multi-photon ionization of copper was observed. By using an unfocussed laser continually and watching the decay of the copper signal, the authors were able to determine the thickness of the film between 20 and 100 Å. It was calculated that between 10^{-3} and 10^{-2} Å per shot was removed by the laser, although this was at a power below the breakdown threshold, so emission could not be collected.

Anderson *et al.* used LIBS for depth profiling without the resonance feature of Allen's experiment.[55] A Zn/Ni coating between 2.7 and 7.2 μm thick on a steel substrate was analyzed and a calibration curve of signal duration with thickness was found to be linear. The depth resolution was far poorer than in the mass spectrometric experiment of Allen because the energy density at the target was much greater. Nonetheless, Sn coatings of less than 1μm, and Cr coatings on the order of a few nm on steel could be determined by this technique.

Arnold and Cremers used LIBS to determine metal particles on air sampling filters.[56] Tl was collected on filter paper by passing contaminated air through a filter or by wiping a filter on a Tl surface. The laser beam from a Nd:YAG laser at 1064 nm was formed into a line at the focus by a pair of cylindrical lenses. The detection limit for Tl was 40 ng/cm^2 of filter paper, and the calibration curve was linear up to 40 μg/cm^2. The 535.05 nm Tl line was used for detection.

Sattmann and Sturmalso investigated the use of a multiple Q-switch Nd:YAG laser for analysis of steel samples.[57] Single, double, and multiple pulses were used to produce plasma on a low-alloy steel. Material ablation, emission intensity, electronic temperature, and electron number density were determined for each plasma type. All of these parameters were greater for the double and multiple pulses than for the single pulses presumably because of a smaller shielding effect in these cases. Calibration curves were correspondingly steeper.

Davies and Telle used a 100 m fiber optic pair to perform remote LIBS on ferrous targets.[58] A pair of 550 μm (OD) fiber optics were used to transmit laser light to the target and to return plasma emission to the spectrometer. Detection limits of 200 ppm or less were found for Cr, Cu, Mn, Mo, Ni, Si, and V. A number of potential emission lines to use for calibration were given for these elements.

Cremers *et al.* used a fiber optic probe to determine Ba and Cr in soil.[59] A single 1.5 mm fiber was used both to deliver laser light and collect emission. A glass plate was used to reflect the emission to the spectrometer. The Ba ion line at 493.41 nm and the Cr atom line at 425.44 were used for calibration which was linear over 4 orders of magnitude for both elements. The detection limit for Ba was 26 ppm, and the detection limit for Cr was 50 ppm.

Cremers also determined at what distance LIBS could be performed using conventional optics rather than fiber optics.[60] By using a beam expander to increase the diameter of the laser beam and a pair of lenses with adjustable distance to focus this expanded beam onto a target, he was able to produce a plasma and collect light at a distance of 24 m. Detection limits in a simulated moon rock were at the level of a few percent due mostly to the small solid angle of collection at this distance.

Bescos *et al.* analyzed aluminum samples again in 1995.[61] The authors simultaneously determined Mg, Mn, Fe, and Pb in aluminum using a spectral window from 380 to 410 nm. Detection limits were around 100 ppm and calibration curves were linear up to about 1%.

Gonzales *et al.* also analyzed steel samples.[62] Their 1995 publication dealt with sulfur determination. They reported a detection limit of 700 ppm using the 180.73 nm atom line.

The analysis was done in a N_2 atmosphere, and the Fe ion line at 186.47 was used as an internal standard. Precision was 7%.

Hakkanen and Korppi-Tommola used LIBS to study elemental distributions of paper coatings.[63] A XeCl laser at 308 nm was used to generate a plasma on paper, and Ca or Si was used as an internal standard. A spatial resolution of about 250 μm could be achieved with a laser pulse power of 200 mJ. It was estimated that 2 ng of paper coating were vaporized per shot. Al, Si, Mg, Ca, and C were were monitored quantitatively in a spectral window from 220-290 nm.

Sabsabi and Cielo once again analyzed aluminum alloys by LIBS in 1995.[64] The authors characterized the laser plasma on aluminum targets using Stark broadening of Al ion lines to determine electron number densities and using a series of Fe atom lines to make Boltzmann plots to determine electronic temperature. Calibration curves for Mg, Mn, Cu, and Si were constructed and detection limits were as low as 10 ppm, for Mg.

Soil was analyzed by Ciucci *et al.* in 1996.[65] They used both a Nd:YAG laser at 1064 nm and a XeCl laser at 308 nm. The authors found that the background decay in the laser plasma was faster for the 308 nm pulse than for the 1064 nm pulse, and used a correspondingly shorter delay time with the XeCl laser. Cu, Pb, and Cr in soil were determined, and an entire spectra from 350-700 nm was shown with lines identified for the geological survey soil sample GXR-2.

Ernst *et al.* used LIBS to determine Cu in A533b steel.[66] The first attempt was carried out with fiber optic delivery of the laser. This method would have been significant because in the hazardous environment of a nuclear reactor pressure vessel, Cu concentration in the steel is an indicator of radiation embrittlement and of expected material lifetime. Because the fiber optic could not deliver enough power to produce sensitive detection, beam delivery was done with conventional optics. The Cu line at 324.75 was used for calibration, and by using a second order calibration curve, Cu could be determined in the range between 100 ppm and 5%.

Geertsen *et al.* revisited LIBS for aluminum samples in 1996.[67] Using a Nd:YAG at 1064 nm and a pulse power of 230 mJ the authors formed craters ~5 μm deep in aluminum with a single shot. The detection limits for Mg and Cu were 4 and 40 ppm, respectively, with a precision of about 8 %. Spatial resolution was assessed by rastering the beam over a sharp Al-Cu junction. The best spatial resolution obtained was 6 μm.

Marquardt *et al.* determined Pb in paint using a Nd:YAG laser at 532 nm coupled into a fiber optic probe.[68] The probe consisted of two fibers, excitation and collection, terminated in a probe head with an aspheric lens to focus the laser light to a spot and focus plasma emission into the collection fiber. The common end of this fiber is shown in Figure 2-2. Different combinations of excitation/collection fiber diameters were tried. The detection limit for Pb was 140 ppm, and precision was 5-10 % even when analysis was carried out through layers of non-lead containing paint.

Miziolek also reported on a LIBS probe in 1996.[69] This application was for determination of heavy metals in soils, and the probes were to be used in a cone penetrometer truck. In one probe, a compact laser was mounted in the probe head. In the other probe, laser light was carried through a fiber optic to the probe head. The compact laser head provided the more sensitive probe with detection limits for Pb, Hg, Cr, Cd, and Zn of 1-10 ppm in sand and silt. The fiber optic delivery provided less power but a higher laser repetition rate; 15 mJ *vs* 28 mJ, 30 Hz *vs* 1/3 Hz.

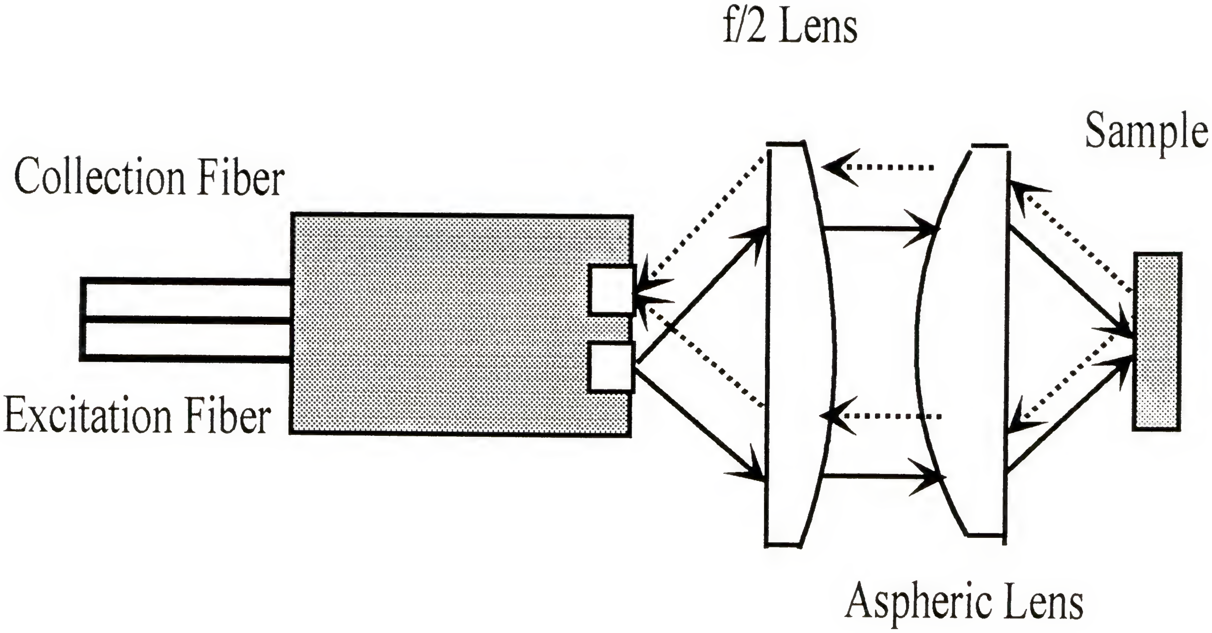

Figure 2-2. Common end of fiber optic LIBS probe used by Marquardt *et al.* for determination of lead in paint.

Also in 1996, Cremers *et al.* introduced a portable LIBS instrument and used it to determine hazardous elements in soil, in paint, and in samples on filter paper.[70] A compact laser head was used as the probe. Ba, Be, Pb, and Sr were determined in soil with detection limits of 265, 9.3, 298, and 42 ppm respectively. In paint, the detection limit for lead was much greater because the 405.8 nm line could not be used due to spectral interference. On filter paper, Be and Pb were determined with detection limits of 21 ng/cm^2 and 5.6 $\mu g/cm^2$ respectively. In the filter paper studies, some particle size effects were evident.

Palleschi *et al.* used a 400 mJ Nd:YAG laser at 1064 nm for a variety of determinations including Hg in air (5 ppm detection limit), and pollutants in powerplant smoke and soil.[71] These authors analyzed the geographical survey GXR-2 sample and determined concentrations for 18 elements.

Vadillo and Laserna analyzed geological samples of vanadinite, pyrite, garnet, and quartz.[72] These determinations were done in vacuum to increase the lifetime of the ionic species and of the ion lines observed. Fe, Mn, Mg, and Si were determined in each of the rocks, and Al was also determined in garnet. Differences in composition were as expected.

Laserna *et al.* used LIBS to analyze the surface of solar cells.[73] A N_2 laser at 337.1 nm was focused onto the cell and the cell was rastered under the focus providing spatial resolution of about 30 μm. The C ion line at 588.9, Ag atom line at 546.5, Si atom line at 634.7, and Ti atom line at 625.9 were used in determinations of these four elements. The concentration of each element was mapped across the surface of the solar cell.

In another application of LIBS to alloys, Kim *et al.* determined aluminum in a zinc alloy.[74] The authors used a Nd:YAG laser (1064 nm, 105 mJ, 3 ns) in vacuum, air and argon. The presence of Al in the Zn alloy was important because of its detrimental effect on its welding properties. The delay and the distance from the surface of the target were optimized in each atmosphere. Because the Al atom line at 308.22 nm was used for calibration, large delay times were used to insure no contribution from a shorter-lived Zn interference. In air, a 30 μs delay was used and in Ar a 50 μs delay was used. The Zn line at 307.59 was used as an internal standard.

In 1997, Maravelaki *et al.* used LIBS to monitor the laser cleaning of marble artifacts.[75] Although lasers had been used previously for the cleaning of such treasures, these authors were the first to examine the emission from the plasma. Crusts of 20-600 μm consisting of gypsum, iron oxides, soot, and calcite were ablated from the marble by a Nd:YAG laser. The plasma formed in this ablation was analyzed spectroscopically to determine the endpoint of the cleaning.

Figures 2-3 and 2-4 show graphically the detection limits for elements that have been determined using LIBS in sand, ore, or soil and in steel or alloy.

Liquids

Fundamental Studies

Besides papers in the field of analytical chemistry, there have also been a number of

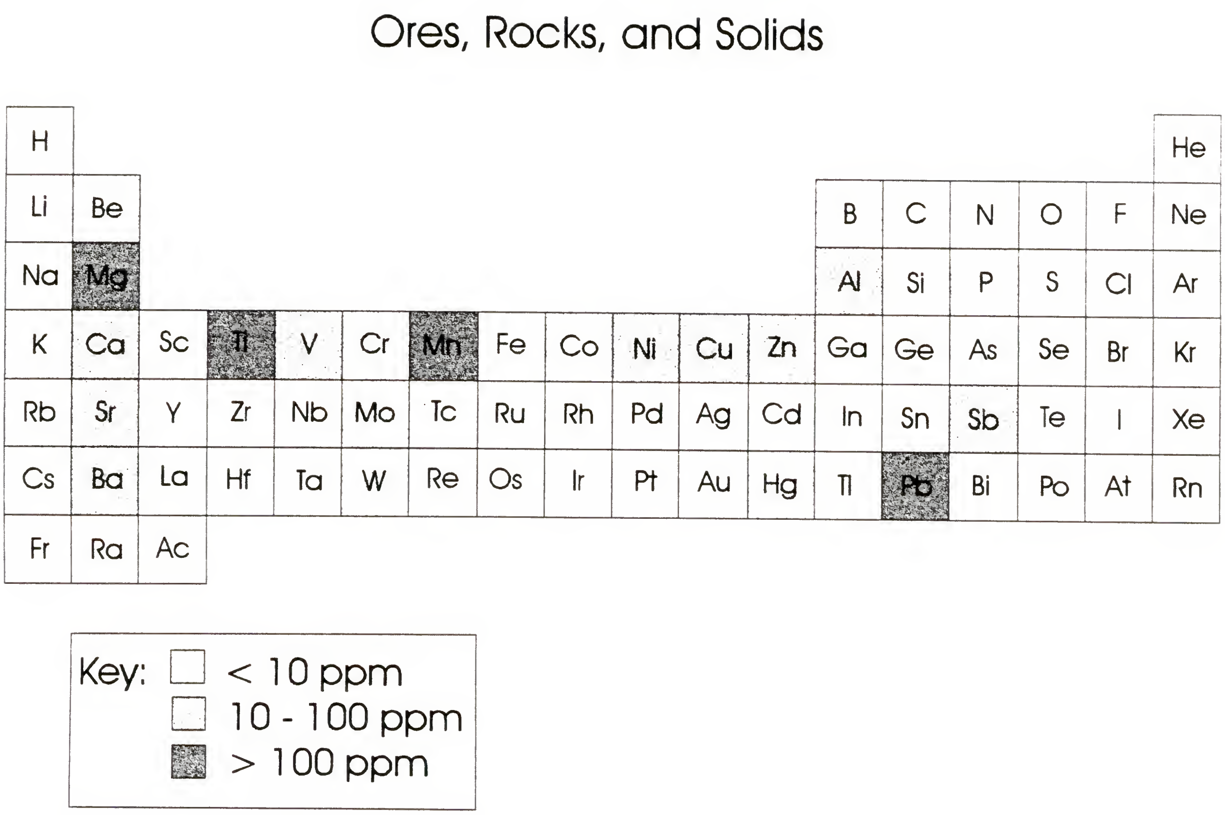

Figure 2-3. Elements determined in ores and soils shaded according to detection limit.

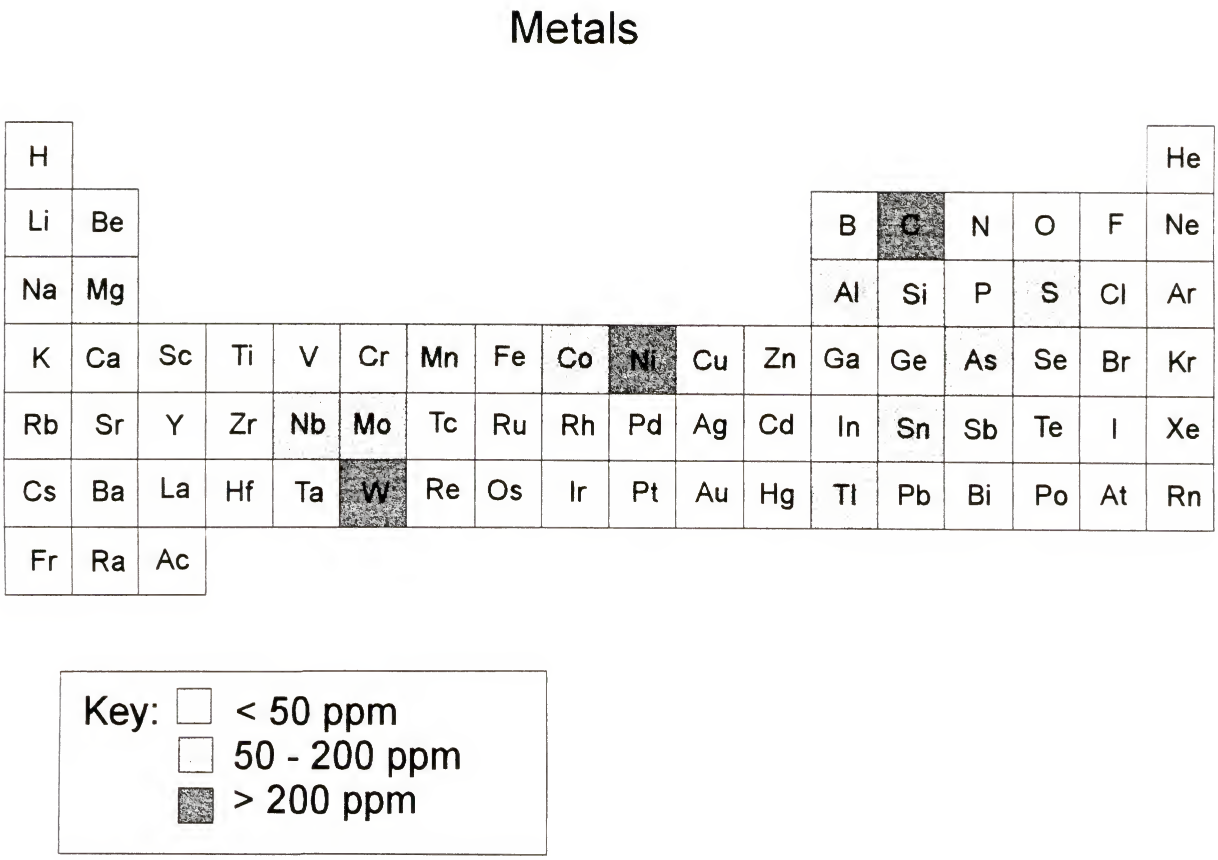
Metals
H He
Li Be B C N O F Ne
Na Mg Al Si P S Cl Ar
K Ca Sc Ti V Cr Mn Fe Co Ni Cu Zn Ga Ge As Se Br Kr
Rb Sr Y Zr Nb Mo Tc Ru Rh Pd Ag Cd In Sn Sb Te I Xe
Cs Ba La Hf Ta W Re Os Ir Pt Au Hg Tl Pb Bi Po At Rn
Fr Ra Ac
Key:
< 50 ppm
50 - 200 ppm
> 200 ppm

Figure 2-4. Elements determined in metals shaded according to detection limit.

papers which have dealt with the physics of laser-induced breakdown in aqueous solution. Most of these deal with the processes of cavitation and the factors which can effect the breakdown threshold.

In 1984, Armstrong identified three time domains in the heating of an aerosol: the acoustic regime, the internal conductive regime, and the external conductive regime.[76] He explained the phenomenon of aerosol-enhanced air breakdown as being caused by increased electron collision frequency in the hot, dense, vapor surrounding the heated aerosol particles in the beam.

Three years later Armstrong used a CO_2 laser at 10.6 μm to explode aerosols generated by a vibrating orifice aerosol generator.[77] A UV laser was used to produce shadow images of the exploding droplet, and a phase Doppler particle analyzer system determined size and velocity of the expelled particles at a distance of 2 mm from the original drop. It was found that the CO_2 laser power affected the size of particles produced in the breakdown for original drop sizes between 30 and 50 μm. The speed of the particles produced was independent of laser power.

Chylek *et al.* studied the effect of size and material of liquid aerosols on breakdown thresholds in 1986.[78] The setup that they used is shown in Figure 2-5. A Nd:YAG laser (532 nm, 10 ns) was focused onto droplets generated by a Berglund-Liu vibrating orifice aerosol generator. Breakdown thresholds were determined on aerosols of different size generated from liquids of various refractive index, density, surface tension, and chemical structure. Thresholds were seen to decrease with droplet size. Refractive index had no apparent effect. Density, surface tension, and chemical structure had effects which could not be independently examined.

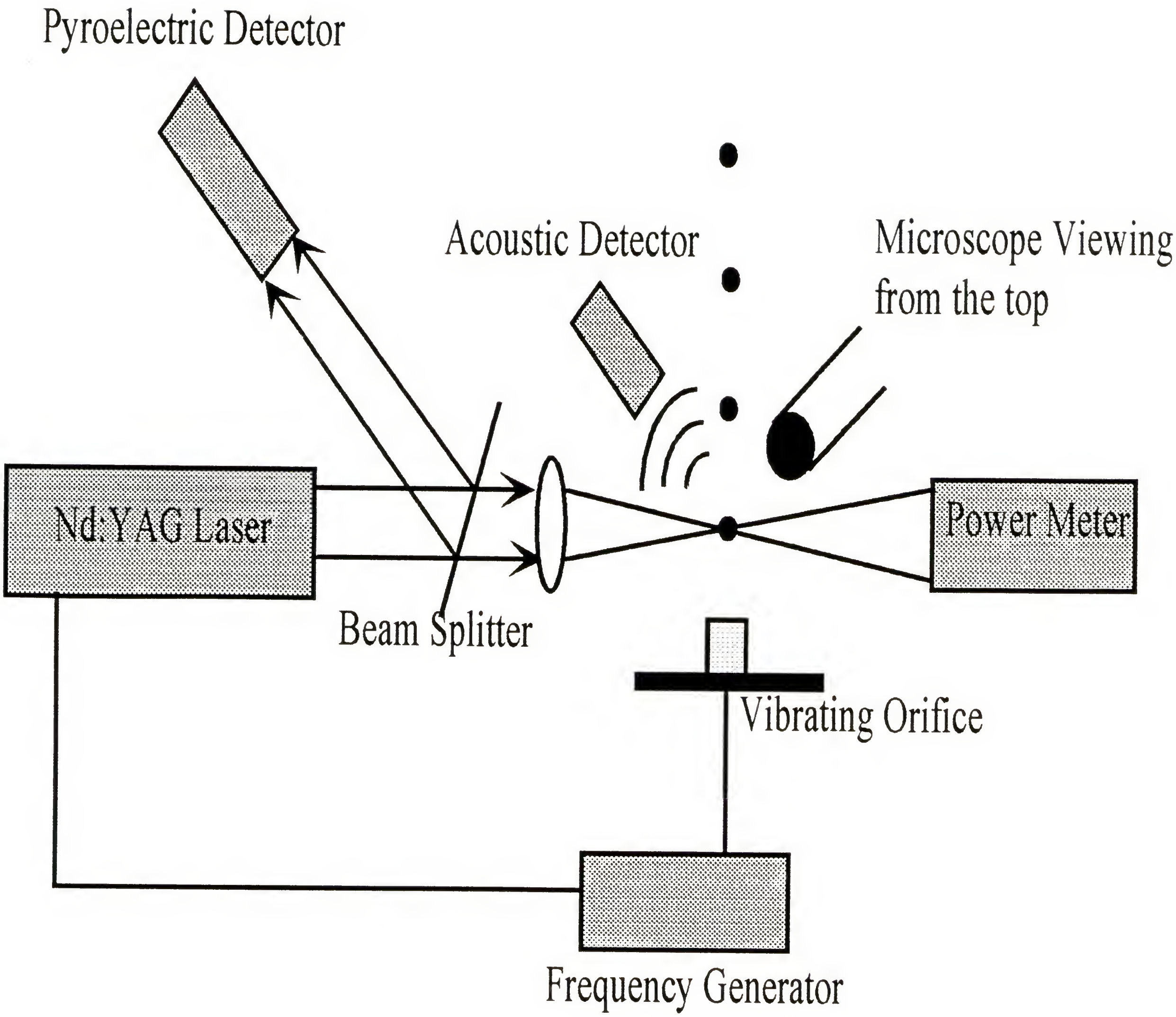

Figure 2-5. Schematic of experimental setup used by Chylek *et al.* to investigate LIBS of aerosols.

In 1987, Hsieh *et al.* used a Nd:YAG laser at 532 nm to examine the exact location of breakdown initiation on water droplets generated by a Berglund-Liu vibrating orifice.[79] They found that as the energy of the laser increased, the breakdown moved from outside the droplet to the inside. Theoretical calculations showed that the curved liquid gas interface of a water droplet in air focused laser energy at one point just inside the illuminated face and at another point just beyond the shadowed face.

The effect of laser wavelength and irradiance on spectra from laser-induced breakdown of single levitated aerosol droplets was examined by Biswas *et al.* in 1988.[80] Droplets of glycerine saturated brine solution approximately 18 μm in diameter were optically levitated and probed with a Nd:YAG laser at 1064, 532, and 355 nm. Emission lines of Na, C, and N were observed. It was shown that the energy required for breakdown, and the time of plasma emission increased with increasing wavelength. The optimum time delay for determination of these elements increased with laser wavelength and showed more variance from element to element at longer laser wavelength.

Also in 1988, Zheng *et al.* acquired temporally and spatially resolved spectra of laser-induced breakdown of a 40 μm 4 M NaCl droplet using a Nd:YAG laser at 532 nm.[81] Using fiber optic ribbons and a streak camera, these authors observed that emission began first at the shadowed face of the droplet and propagated toward the illuminated face.

Hammer *et al.* also examined thresholds with ultrashort laser pulses.[82] Using pulses of 2.4 ps, 400 fs, and 100 fs from a pulsed dye amplifier, they determined breakdown thresholds in saline solution, high purity water, and tap water. The thresholds in these media were not significantly different. With the 2.4 ps pulse the breakdown threshold was found to be 5 x 10^{11} W cm^{-2}, with a 400 fs pulse it was 1.3 x 10^{12} W cm^{-2} and with a 100 fs pulse it was 5.65 x 10^{12} W cm^{-2}.

Kitamori *et al.* used the acoustic wave generated during particle-induced breakdown to detect polystyrene particles in aqueous solution.[83] A Nd:YAG laser (532 nm, ~1 mJ, 6 ns, 10 Hz) was focused into a solution. In pure water, the energy density produced by this beam was not sufficient to cause a breakdown. When a particle entered the probe volume, however, a breakdown occurred and subsequently an acoustic wave was generated. By detecting these acoustic waves, the probability of breakdown was determined. By analyzing solutions of known particle concentration, a calibration curve of breakdown probability *vs* concentration was generated. This curve was used in the analysis of solutions of unknown particle concentration.

Vogel *et al.* used a Nd:YAG laser to produce and image a breakdown in water.[84] The fundamental wavelength of 1064 nm was focused into the water to produce a breakdown. A portion of the beam was frequency doubled to produce 532 nm light which was put through a beam expander and allowed to pass through the underwater breakdown, providing a shadow of the plasma and the cavitation bubble. The size of the plasma and cavitation bubble were examined for 1064 nm laser pulse durations of 30 ps and 6 ns.

Sacchi discussed the mechanisms of laser breakdown in water and described the differences in threshold for short pulse and long pulse lasers in 1991.[85] He claimed that the avalanche breakdown process or inverse bremstrahlung was responsible for breakdown when nanosecond laser pulses were used. In this case, the breakdown threshold behaved probabilistically. The probability of breakdown scaled linearly with the log of laser power for low powers, and scaled parabolically with the log of laser power at higher power. In contrast, with laser pulses of less than nanosecond duration, multi-photon ionization appeared to be the mechanism of plasma formation, and a definite threshold above which breakdown would occur could be determined.

Sacchi returned to this topic in 1996 and produced images of laser-induced breakdown on solids under water. By using a dye laser oriented parallel to the underwater target and delayed relative to the ablation laser, the authors obtained shadowgraphs of the evolving plume and shock wave. A series of images followed the growth and decay over a total time of about 700 μs. A schematic of the setup used is shown in Figure 2-6.

In 1992, Pinninck *et al.* studied the effect of resident particles on laser-induced breakdown thresholds.[86] It was found that even at wavelengths where the particles did not absorb laser light, there was a decrease in breakdown threshold in particle laden air versus clean air. This was taken to mean that particles were focusing laser light. Location of plasma formation (inside, shadowed side, or illuminated side) was found to depend on ionization potential, gas pressure and laser wavelength. Refractive index had no effect on breakdown threshold, in agreement with the observations reported by Chylek in 1986.[78]

In 1993, Nyga and Neu created a plasma on calcite submerged in water using two fiber optics to deliver two pulses from two XeCl lasers.[88] Both pulses were 30 ns pulses at 308 nm through 600 μm fibers which were brought in close proximety to the target with no focusing lenses. The pulses were separated in time by ~300 μs, and the second fiber was equipped with a 308 nm dielectric beam splitter and used to collect emission from the calcite. No quantitative results were reported.

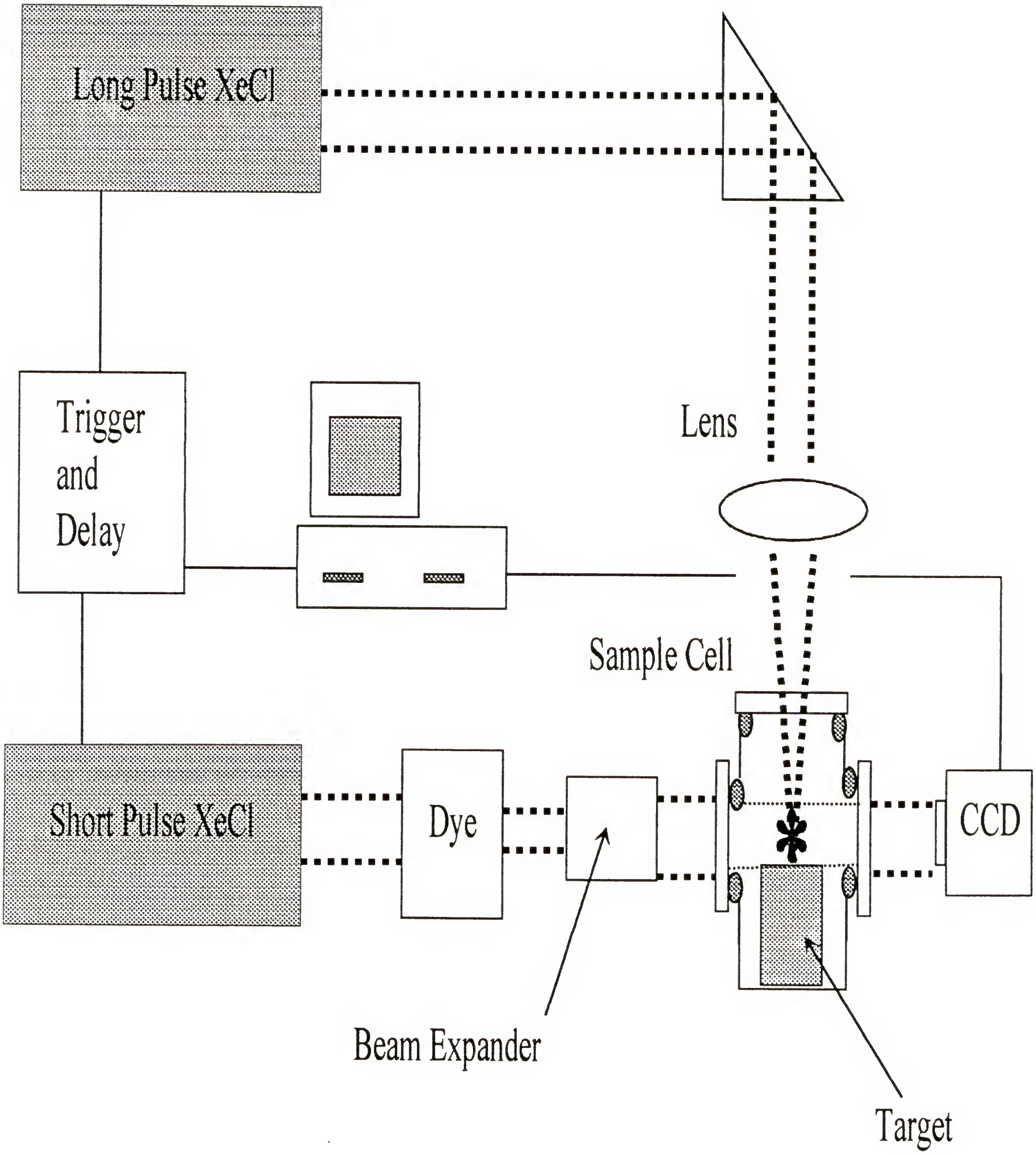

Figure 2-6. Schematic of experimental setup used to obtain shadowgraphs of a laser induced plasma.

Feng *et al.* also examined the effect of laser pulse duration on breakdown thresholds in water.[89] In their 1997 paper, they determined the mechanism of breakdown with nanosecond pulses to be due to cascade ionization, and the mechanism of breakdown with ultrashort pulses to be multi-photon ionization, similar to Sacchi's findings.[85] These authors, however, went on to model the breakdown phenomenon in water relating the breakdown threshold to laser power, spot size, and pulse duration. They derived an extended non-linear Schrödinger equation to describe the relationship.

Analytical Results

Quantitative results for LIBS with liquid samples will be presented in two sections based on the nature of the analysis. The first section will cover determinations done in bulk liquid. This implies that a laser spark is generated either on the surface or beneath the surface of a relatively large liquid sample. The second section will cover determinations done in aerosols or droplets generated from liquid samples. Analysis of dry aerosols generated from solids are included in the last section on gas phase determinations.

Bulk Liquid

In 1984, Cremers *et al.* reported the use of a repetitive single spark (RSS) and repetitive spark pair (RSP) for the determination of Li, Na, K, Rb, Cs, Be, Mg, Ca, B, and Al in aqueous and organic solutions.[89] With the single spark, detection limits for all elements except Li were >1 ppm. The detection limit for B was 1200 ppm. When a second spark which was generated from a second laser and delayed by 18 μs relative to the first was used to form the plasma, the detection limit for B was reduced to 80 ppm.

This improvement was attributed to formation of the plasma within a cavitation bubble when the RSP method was used. The experimental setup is shown in Figure 2-7.

In 1987, Wachter and Cremers reported a detection limit of 100 ppm for uranium in solution by LIBS.[90] The plasma used was formed by a Nd:YAG laser (1064 nm, 260 mJ) on the surface of a 4 M nitric acid solution contained in a small glass vial. Each analysis was done by averaging 1600 laser shots. This averaging was necessary to overcome poor shot-to-shot precision due mainly to small variations in lens to sample distance.

In 1987 Cremers conducted an experiment to determine the maximum lens to sample distance (LTSD) that could be used in a LIBS experiment.[60] With a 250 mJ pulse from a Nd:YAG laser at 1064 nm, it was found that a 2 m focal length lens could produce breakdown on molten metal. The larger problem was collection of the emitted light. A fiber optic could collect enough light at 0.5 m from the plasma for modest figures of merit to be obtained. At distances farther than this, the sensitivity of the experiment decreased rapidly.

In 1993, Aragon *et al.* used LIBS to determine carbon content in molten steel.[91] They used a Nd:YAG laser (1064, 200 mJ, 8ns) focused onto molten steel in a crucible under an argon atmosphere. In order to provide a homogeneous sample, a jet of argon gas was directed downward into the crucible. This served to remove the topmost layer of molten liquid which would be enhanced in the lighter elements. Carbon was determined by ratioing of the C 193.09 nm to Fe 201.07 nm intensity and a detection limit of 250 ppm was found with an RSD of 6%.

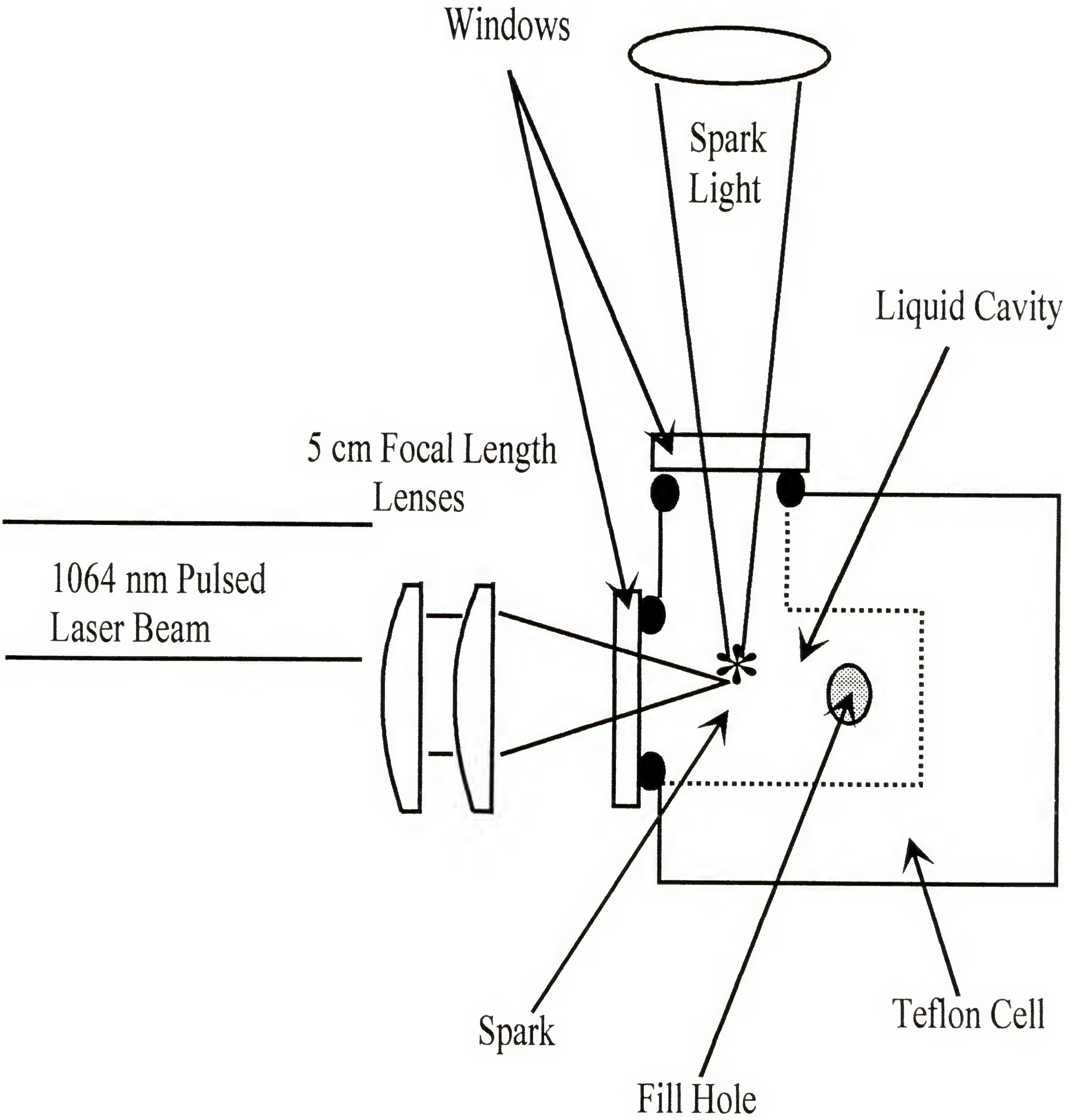

Figure 2-7. Experimental setup used by Cremers *et al.* to analyze aqueous solutions with LIBS.

In 1995, Stolarski *et al.* produced sub-surface plasmas in saline solution, triple-distilled water, and tap water with Nd:YAG laser pulses of <5 mJ and pulse durations of 5 ns and 80 ps.[92] The focussing lens used was 2.54 cm. in diameter and had a focal length of 17 mm. This lens was chosen to approximate the lens in the human eye. The authors found that an energy of 1.5 mJ was enough to produce a breakdown at either pulse duration, and found that the plasma temperatures and electron number densities depended little on pulse duration for the two studied. These authors observed sodium emission around 590 nm in a 0.9% NaCl solution, but no quantitative analysis was performed.

Also in 1995, Ito *et al.* used LIBS to determine colloidal iron in water.[93] They focused a Nd:YAG laser (1064 nm, 100 mJ, 10 ns) into a flowing stream of water containing FeO(OH) as submicron particles. The detection limit for iron was in the ppm range. This technique differed slightly from previous techniques in that it relied on particle-induced breakdown for the formation of the plasma. A plasma was formed only when a FeO(OH) particle was present in the probe volume. Because of the extremely small size of the particles, however, it was essentially a determination of iron in water. The following year, the same authors used a second laser delayed by 1 μs relative to the first in a technique similar to Cremer's repetitive spark pair. With this technique, they were able to improve the detection limit for iron to 16 ppb.[94]

In 1996, Knopp and Scherbaum used a dye laser at 500 nm with a pulse energy of 22 mJ to produce a sub-surface breakdown in aqueous solution.[95] They reported detection limits for Cd, Pb, Ba, Ca, Li, and Na of 500 ppm, 12.5 ppm, 6.8 ppm, 130 ppb, 13 ppb and 7.5 ppb respectively. No signal was obtained for either Hg or Er at 0.1% in solution. When micron-sized particles of $ErBa_2Cu_3O_x$, rather than a soluble salt, were used as the source of Er, the detection limits decreased by a factor of 10^3. The improvement illustrated the increased sensitivity of particle-induced breakdown as compared to breakdown in particle-free solution. This experiment also suggested that 500 nm laser light had analytical advantages over 1064 nm light.

In 1997, Ho and Ng used both a Nd:YAG laser (532 nm, 12 ns) and an ArF laser (193 nm, 15 ns) to determine Na in aqueous solution.[96] In order to increase absorbance of the laser light, methyl violet was added to the solution to be analyzed. It was found that the 532 nm laser light produced a more visibly intense plasma; because the continuum emission was higher in the 532 nm produced plasma, the 193 nm laser light actually gave better detection limits for Na. A detection limit of 230 ppb was reported for Na in the methyl violet solution with the plasma formed by the ArF laser.

In 1996, a similar experiment was performed by Paksy *et al.* who used a Nd:YAG (1064 nm, 15 mJ, 4 ns) focused onto the surface of a molten alloy in an argon atmosphere.[97] Because the laser power used was significantly less than that used by most authors, the delay of the detection relative to the laser was also less. A 100 ns delay and 1000 ns gate width were used. Detection limits were 0.001% for Si in Fe, 0.006% for Cr in Fe, 0.06% for Si in Al, and 0.007% for Mn in Al.

Arca *et al.* determined Cr, Pb, and Cu in aqueous solution with a single laser shot on the surface of the water.[98] Detection limits were 100, 100, and 50 ppm for the three elements, respectively. Calibration curves were linear over 1 order of magnitude. The authors also analyzed aqueous solutions by placing a drop of water to be analyzed on a KBr pellet. When this technique was used, detection limits were improved by almost an order of magnitude.

Aerosols and Droplets

In 1983, Radziemski *et al.* used a nebulizer/heat chamber system to produce an aerosol from a liquid solution and analyzed the aerosol with LIBS.[99] Detection limits for Na, P, As, and Hg were reported to be 6 ppb, 1.2 ppm, 0.5 ppm, and 0.5 ppm, respectively. The authors determined that local thermodynamic equilibrium existed in the aerosol spark for time delays greater than 1 μs relative to the laser.

In 1987, Eickmans *et al.* spatially resolved the emission from laser-induced breakdown of an aerosol.[100] Approximately 45 μm diameter droplets were formed by a vibrating orifice aerosol generator which was synchronized with the Nd:YAG laser beam at 532 nm. Emission of Li, Na and H was observed in 5 M salt solutions of either NaCl or LiCl. Spatial resolution of the emission revealed that in the plasma plume in the vicinity of the illuminated face of the droplet, emission lines showed Stark broadening and self-reversal. Near the shadowed face of the droplet emission lines were narrower and less intense.

In 1988, Essien *et al.* used LIBS to determine Cd, Pb, and Zn in an aerosol.[101] A Nd:YAG laser (1064 nm, 100 mJ, 5 ns) was focused onto an aerosol generated by a nebulizer/heat chamber. Detection limits were 19 ppb, 210 ppb, and 240 ppb for Cd, Pb, and Zn, respectively.

Also in 1988, Archontaki and Crouch used an isolated droplet generator to produce equally spaced, uniformly sized droplets.[102] The experimental setup was such that a single drop of known size was always in the probe volume of the laser for a given repetition rate. A Nd:YAG laser (1064 nm, 100 mJ) was used to determine detection limits for Li, Na, Mg, Ca, Mn and Al of 0.3, 2.2, 1.9, 0.4, 7.2, and 5.2 ppm, respectively. Droplet diameter had little effect on the detection limit for sizes between 58 and 75 μm.

In 1992, Ng *et al.* used an ArF laser (193 nm, 150 mJ) to analyze an aerosol generated by a concentric glass nebulizer/spray chamber traditionally used for ICP-AES.[103] The authors determined the optimum delay for detection to be 6 μs relative to the laser pulse. Detection limits for Na, Li, In, Al, Ga, Ca, Mg, K, and Sr were determined to be 0.9, 0.3, 10, 3, 3, 8, 3, 2, and 20 ppm, respectively.

The following year Parigger and Lewis used a picosecond XeCl laser (308 nm, 4 mJ) to produce LIB in 66 μm water droplets.[104] Plasma diagnostics showed a temperature of ~10 000 K and an electron number density of 10^{18} cm^{-3}. The H_α line at 656 nm was used as an internal standard and the detection limit for sodium was ~1 ppm. Poulain and Alexander performed a very similar experiment in 1995 using a KrF laser (248 nm, 200 mJ). The detection limit for Na was found to be 165 ppm.[105]

Haisch and Paine reported on the characterization of colloidal particles by LIBS in 1996.[106] Field flow fractionation was used to sort particles by size and deposit them onto filter paper using partitioned pumping to retain time resolution. A cylindrical lens was used to focus the laser onto the paper to avoid ablation of the paper which could occur if the energy density became too high. Detection limits for Si were in the ppb range.

Figures 2-8 and 2-9 show graphically the detection limits for elements that have been determined using LIBS in bulk liquids and in aerosols generated from liquids.

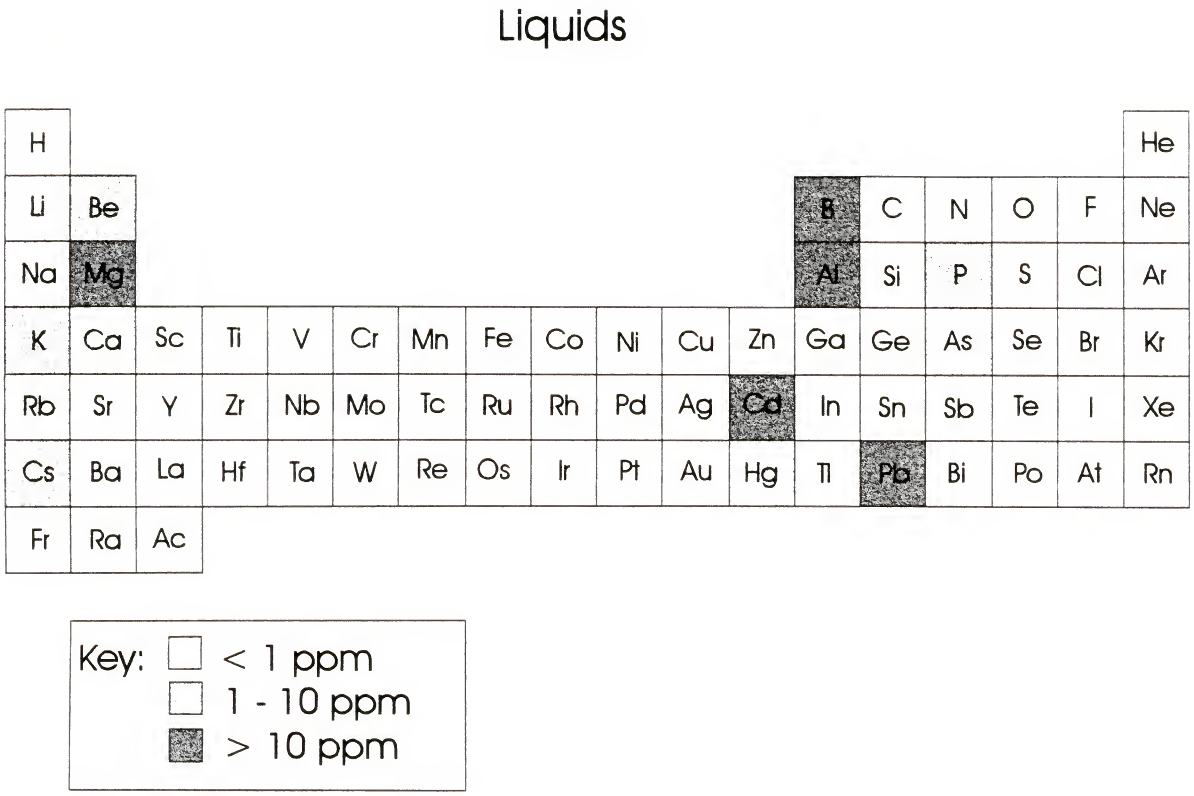

Liquids

H																	He
Li	Be											▨ B	C	N	O	F	Ne
Na	▨ Mg											▨ Al	Si	P	S	Cl	Ar
K	Ca	Sc	Ti	V	Cr	Mn	Fe	Co	Ni	Cu	Zn	Ga	Ge	As	Se	Br	Kr
Rb	Sr	Y	Zr	Nb	Mo	Tc	Ru	Rh	Pd	Ag	▨ Cd	In	Sn	Sb	Te	I	Xe
Cs	Ba	La	Hf	Ta	W	Re	Os	Ir	Pt	Au	Hg	Tl	▨ Pb	Bi	Po	At	Rn
Fr	Ra	Ac															

Key: ☐ < 1 ppm
☐ 1 - 10 ppm
▨ > 10 ppm

Figure 2-8. Elements determined in bulk water shaded according to detection limit.

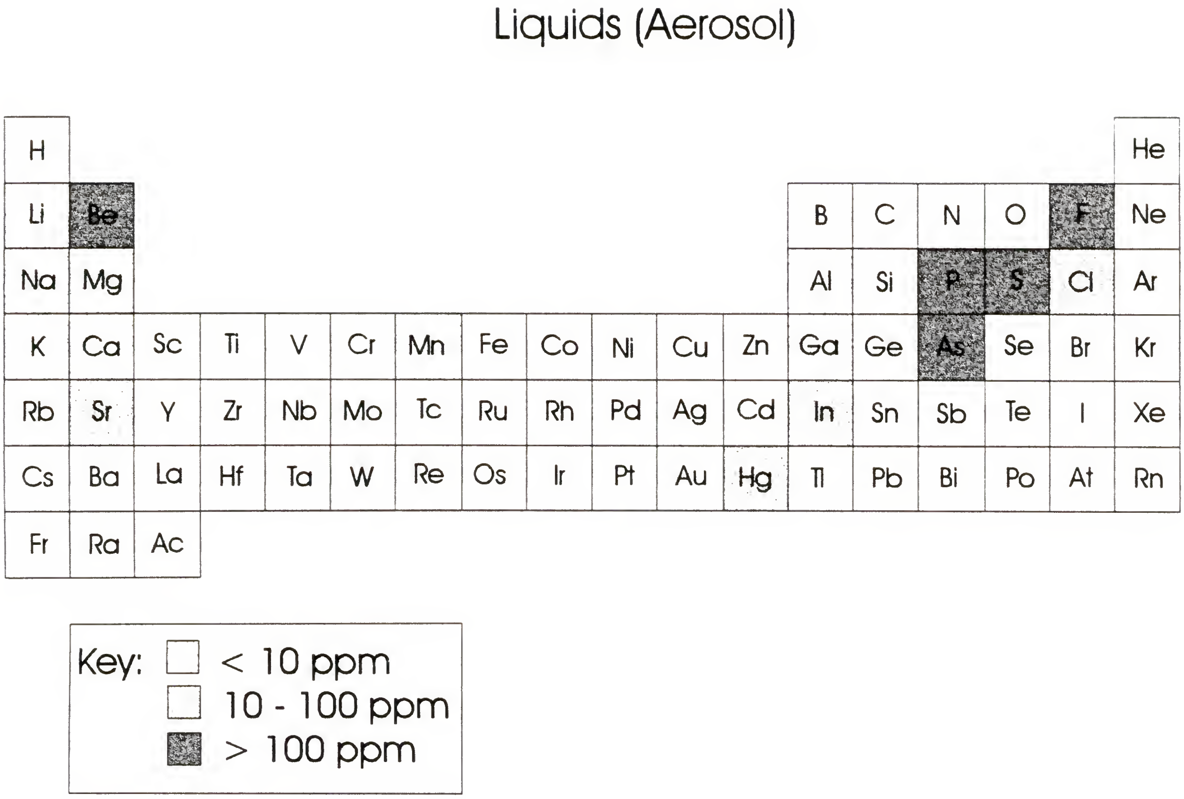

Liquids (Aerosol)

H																	He
Li	▨ Be											B	C	N	O	▨ F	Ne
Na	Mg											Al	Si	▨ P	▨ S	Cl	Ar
K	Ca	Sc	Ti	V	Cr	Mn	Fe	Co	Ni	Cu	Zn	Ga	Ge	▨ As	Se	Br	Kr
Rb	Sr	Y	Zr	Nb	Mo	Tc	Ru	Rh	Pd	Ag	Cd	In	Sn	Sb	Te	I	Xe
Cs	Ba	La	Hf	Ta	W	Re	Os	Ir	Pt	Au	Hg	Tl	Pb	Bi	Po	At	Rn
Fr	Ra	Ac															

Key: ☐ < 10 ppm
☐ 10 - 100 ppm
▨ > 100 ppm

Figure 2-9. Elements determined in liquid aerosols shaded according to detection limit.

Gases

Fundamental Studies

In 1988, Kumar and Thareja studied laser-induced gas breakdown in the presence of an electric field.[107] They used a XeCl laser (308 nm, 60 mJ, 8ns) focused between two electrodes separated by 6.5 mm. A transverse static electric field was produced by applying different potentials to the electrodes. In order to study the effect of the field on breakdown thresholds, the current on the electrodes was adjusted so that no breakdown occurred using only the field or only the laser. The authors were then able to determine that pre-breakdown electron densities of 10^{10} cm^{-3} created by the field were sufficient to lower the laser energy density needed to produce breakdown.

Parigger and Lewis used a Nd:YAG laser (1064 nm, 300 mJ, 7.5 ns) to produce a plasma in CO.[108] They observed the emission of the C_2 Swan band around 565 nm to determine vibrational temperatures in the decaying plasma. The observed spectra was fit with a model in which temperature was a parameter. At a time delay of 30 μs relative to the laser pulse, a temperature of 6745° K was obtained. This temperature was confirmed by use of the CN violet band around 388 nm to calculate the vibrational temperature in a similar way.

Yagi and Huo investigated breakdown in H_2 gas at different pressures initiated by a KrF laser (248 nm, 250 mJ, 20 ns).[109] This work was related to Raman spectroscopy in that the breakdown threshold determined the maximum energy with which the Raman transitions could be pumped. The authors found that below 600 Torr breakdown thresholds were pressure independent. Thresholds decreased between 600 and 3000 Torr, and increased slightly above 3000 Torr.

Yalcin *et al.* investigated the sensitivity of a laser spark produced by a Nd:YAG at 532 nm to ambient conditions such as variation in background gas, presence of particles, and humidity.[110] This was done in order to assess the potential usefulness of LIBS in toxic metal monitoring. The authors found that excitation temperature and electron number density in the plasma remained essentially constant with variations in the ambient conditions.

Analytical Results

In this field, Cremers and Radziemski again did pioneering work. In their 1983 publication, they detected chlorine and fluorine in air.[111] Detection limits for these two gases were 8 and 38 ppm by weight, respectively. These values corresponded to absolute detection limits of 80 and 2000 ng. In a helium atmosphere, the absolute detection limits improved to 3 ng for both. Experiments were carried out in which molecular gases containing both chlorine and fluorine were introduced to the sampling chamber. The relative intensities of the chlorine and fluorine signal were found to be an indication of the number of each of these atoms in the molecular gas. All experiments were carried out using a Nd:YAG laser (1064 nm, 100 mJ, 15 ns) and detecting Cl at 837.6 nm and Fl at 685.6 nm.

These authors also detected Be in air.[112] The limit of detection in this experiment was 0.5 ppb by weight. The Be was introduced into a chamber by laser ablation and diluted by air. A second laser produced a breakdown in the chamber from which the emission was measured. It was found that the emission from the Be II doublet at 313.1 nm was stronger than any atomic emission even at delay times of 20 μs. This doublet was used for calibration which was linear over 4 orders of magnitude.

Cremers *et al.* used LIBS to determine sodium and potassium in a coal gassifier stream as early as 1983.[70] These elements were present as particulates in the stream and so again the question of whether or not the target was a gas or solid arises. Regardless, the authors were able to determine Na with a detection limit of 4 ppb by weight using the doublet at 589 nm. Figures of merit for potassium were not given. In conclusion, the authors noted that sulfur could also be monitored.

Sneddon extended this technique to the determination of P in air and lowered the absolute detection limit of Cl in air. In a1988 paper, he detected phosphorous at 15 ppm and Cl at 60 ppm by weight in air.[113] A calculated plasma volume of 0.010 cm^3 was used to determine an absolute detection limit of 60 pg for Cl.

Ottenson *et al.* reported on the application of LIBS to analyze particulates in a coal combustion vent in a 1989 publication.[114] A Nd:YAG laser was triggered on the scattering from a HeNe laser to explode particles detected in the probe volume. The experiment used on-line temperature correction to account for different excitation conditions in plasmas formed on different size particles. Moreover, the size of particles to be sampled could be adjusted by adjusting the laser power. With lower laser power, only larger particles were sampled, the smaller ones were not sufficient to provide plasma formation. The on-line temperature correction automatically accounted for differences in excitation conditions with varying laser power.

In 1990, Morris *et al.* used laser-induced breakdown as a detector for gas chromatography.[115] The UV laser light was focussed into the effluent from a gas chromatograph at a power below the breakdown threshold of the carrier gas. When eluting carbon containing molecules were present in the effluent, the threshold for breakdown was lowered and a plasma formed. The organic analytes were indirectly detected by optically detecting plasma formation. A schematic is shown in Figure 2-10. No emission from the plasma was measured, and so the potential of this technique was only as a universal detector.

In 1991, Cheng *et al.* studied polyatomic molecular impurities in helium gas at ppm levels.[116] Using ungated detection, they determined B_2H_6, PH_3, and AsH_3 with detection limits of 1, 3, and 1 ppm, respectively. The ionic phosphorous lines at 602.4, 603.4, 604.3, and 605.5 nm were used. As lines were observed at 228.8, 235.0, 278.0, and 286.0 nm. B lines were observed at 336.0 and 434.5 nm. The plasmas were produced by a Nd:YAG laser at 532 nm.

Also in 1991, He and co-workers focused a pulsed laser onto a metal rod in an atmosphere of helium or argon seeded with a reaction gas to produce ion-molecule complexes and observe their emission.[117] Ion lenses were used to preferentially draw ions into the He or Ar gas for reaction with the seeded gas. Emission from species such as AlO, AlO-CO, Al-Ar and Al^+H_2 was observed.

Joseph and Majidi used an electrothermal atomizer to create a gas phase sample from a liquid for analysis by LIBS.[118] A few μL sample was deposited in the furnace and was dried, ashed, and atomized. The setup is shown in Figure 11. At the onset of atomization, a Nd:YAG laser (1064 nm, 100 mJ) was focused into the furnace and fired at a repetition

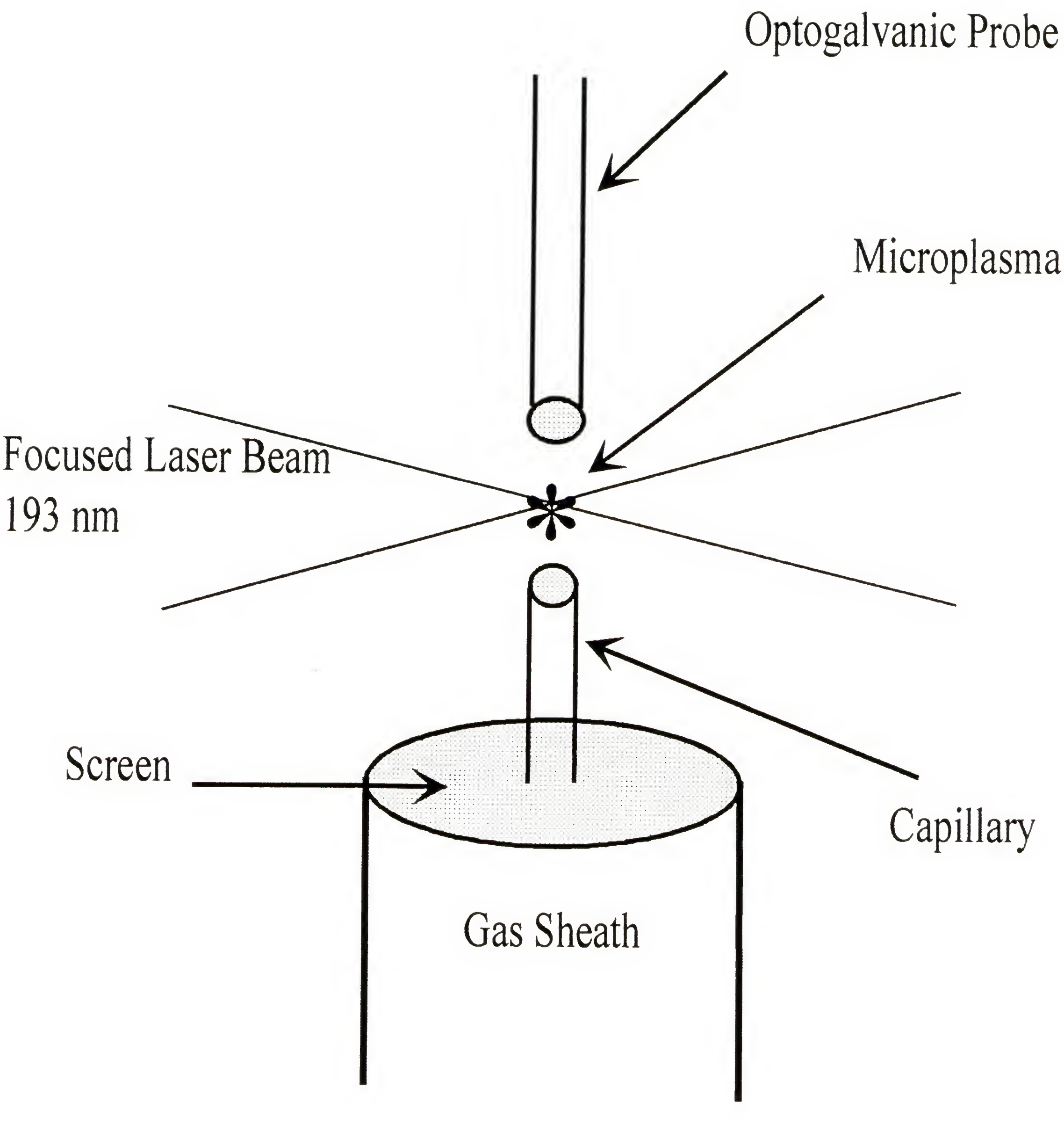

Figure 2-10. Schematic of setup used by Morris *et al.* for use of laser-induced breakdown as a detector in gas chromatography.

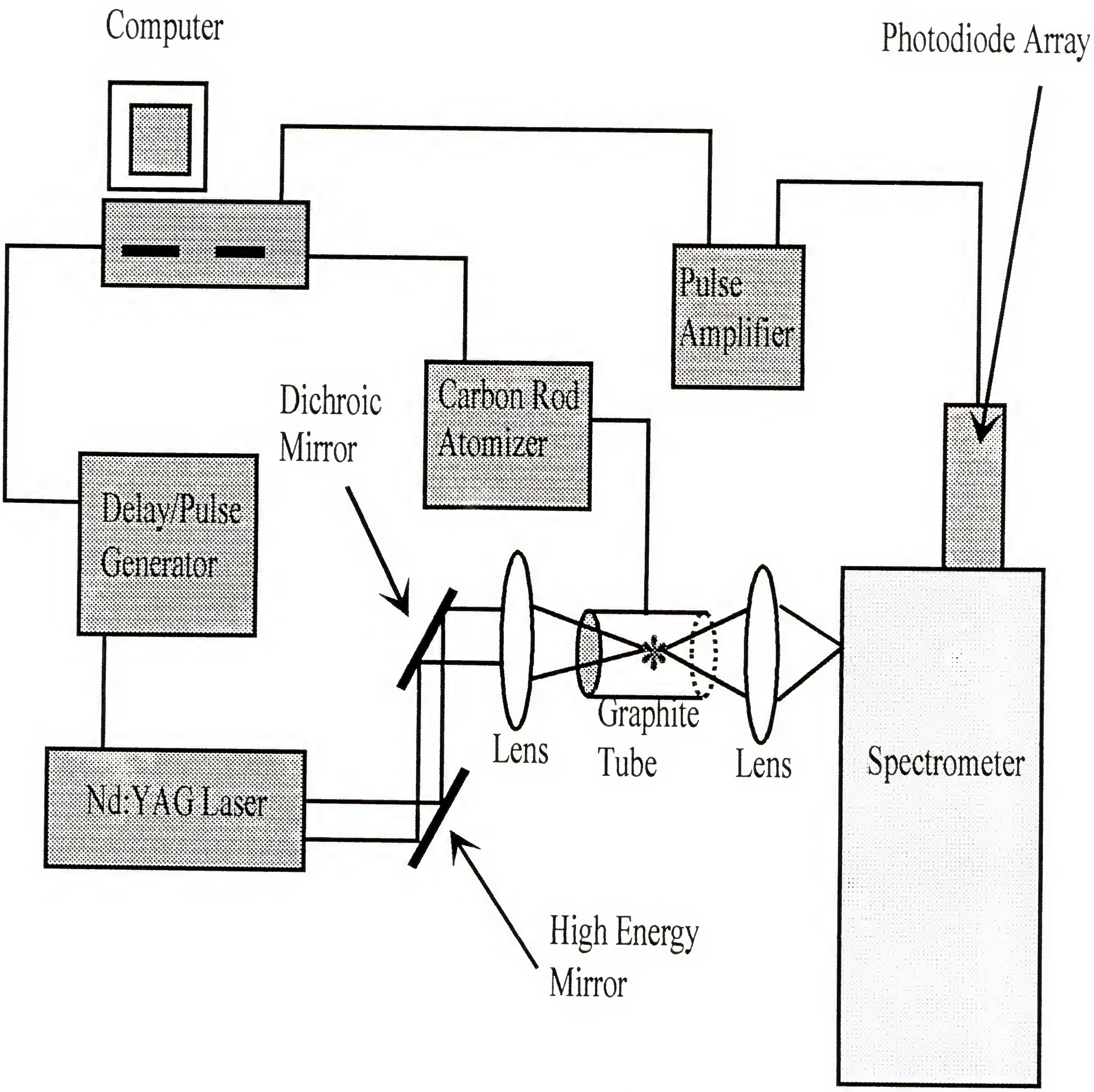

Figure 2-11. Schematic of setup used by Joseph and Majidi for LIBS in a graphite furnace.

rate of 10 Hz. Emission from the plasma was collected through the dosing hole of the tube. Experiments with cobalt and cadmium gave absolute detection limits of 5 and 50 pg.

Casini *et al.* also determined several elements of interest in air using LIBS.[119] Their experiment used a Nd:YAG laser (1064 nm, 40 mJ, 7 ns) to produce plasma in an atmospheric pressure chamber as shown in Figure 2-12. Using the saturated concentrations of air over chosen liquids at the given temperature, and then successively diluting these concentrations in the chamber, yielded calibration curves for a number of elements. Cl was detected at 449.0 nm with a detection limit of 60 ppm, S at 415.3 nm with a DL of 200 ppm, P at 442.1 nm with a DL of 200 ppm, Na at 371.1 nm with a DL of 110 ppm, Hg at 404.7 nm with a DL of 50 ppm, Be at 381.4 nm with a DL of 130 ppm, and As at 454.4 nm with a DL of 130 ppm.

In 1994, Flower *et al.* used LIBS to monitor metal aerosol emission generated by a pneumatic nebulizer.[120] A chromium salt solution was passed through the nebulizer and a heating pipe to produce a gas with known concentration of Cr. The detection limit was 200 ng Cr / standard cubic meter of air (scm). The laser used was a Nd:YAG (1064 nm, 180 mJ) and detection was at 312 nm.

In 1994, Lazzari *et al.* detected mercury in air using LIBS with a Nd:glass laser (400 mJ, 8 ns) to produce plasma in a chamber filled with saturated Hg vapor and successively diluted.[121] With this technique, they obtained a detection limit of 10 ppb by observation of the 253.7 line.

Zhang *et al.* performed LIBS in a particle loaded methane/air flame and in an oil-fueled combustor vent.[122] In their 1995 publication, they described the addition of a flange with four movable windows to a pre-existing combustor vent. LIBS was

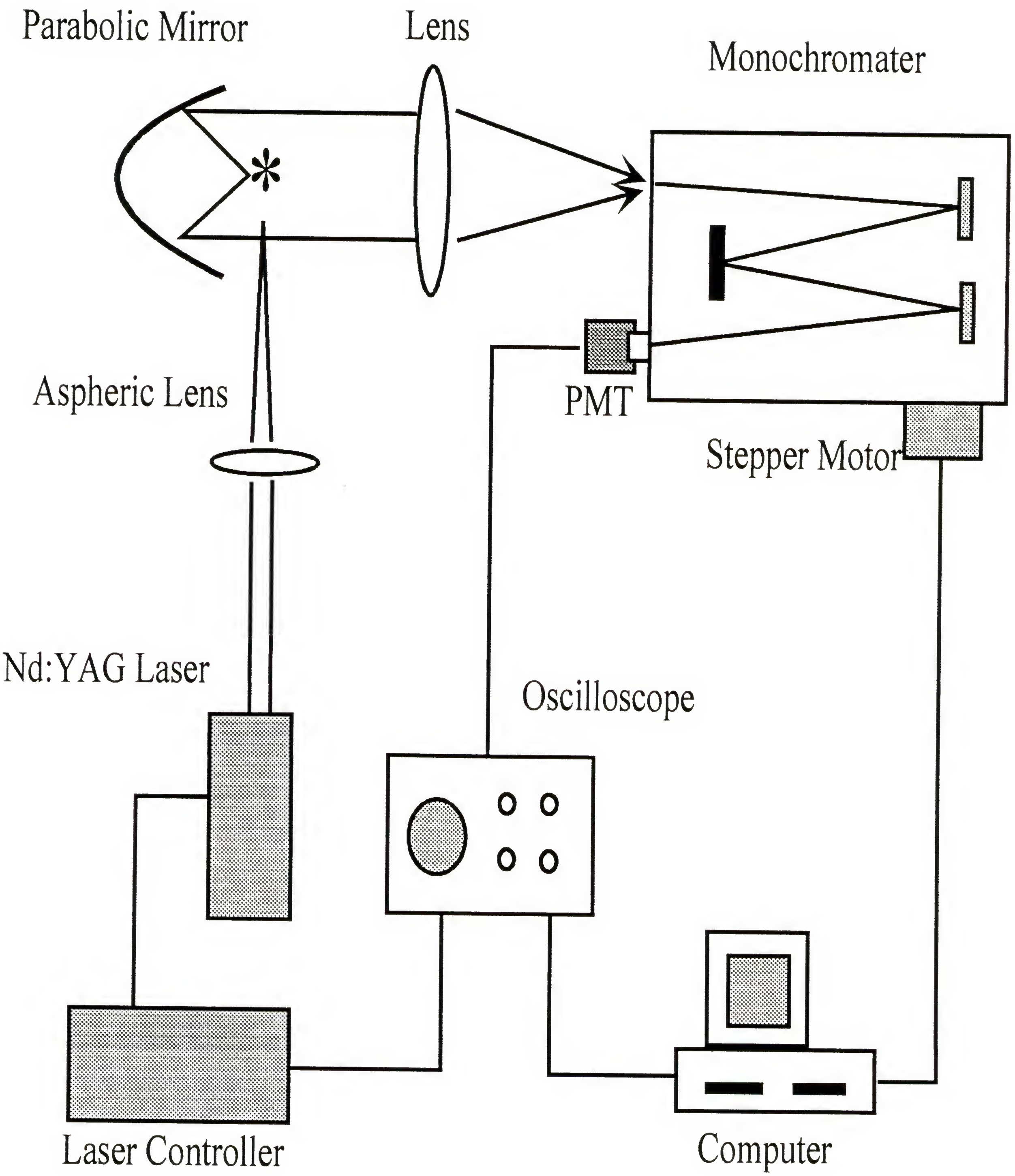

Figure 2-12. Shematic of setup used by Cassini *et al.* for air analysis using LIBS.

performed through these windows which were kept clean by a flow of N_2 gas and could be switched out periodically for cleaning.

In 1995, Nordstrom studied the laser-induced plasma emission spectra of N_2, O_2, and ambient air from 350 to 950 nm.[123] This range was covered with approximately 0.5 nm resolution and atomic, ionic, and molecular emission from a plasma created by a CO_2 laser (10.6 μm, 320 mJ, 200 ns) was observed. Spectra were computed for N, O, and a few molecular species, and a comparison between experiment and calculation was done.

The same year, Parigger *et al.* again published a fundamental paper on laser-induced plasma in the gas phase.[124] This time the breakdown was produced by a Nd:YAG (1064 nm, 220 mJ, 6 ns) in hydrogen at 150 and 810 Torr. The H_α line at 656 nm was used to calculate electron number densities in the decaying plasma with temporal resolution as high as 6 ns early in the plasma and 1 μs at later times. Spatial resolution was also achieved by focusing different portions of the 1:1 plasma image onto the spectrometer entrance slit. Spatial resolution was approximately 50 μm. Surface plots for electron number densities resolved in time and space were then created. Electron number densities varied between 10^{16} and 10^{19} cm^{-3}.

In 1996, Haisch *et al.* again used LIBS to detect chlorine in the gas phase.[125] Two experimental setups were described. The first was a benchtop experiment using a 320 mJ Nd:YAG laser. The second setup used a miniature Nd:YAG laser built into a sensor head. This miniature laser provided 18 mJ of pulse energy. Detection of Cl in chlorinated hydrocarbons was accomplished by focusing the laser onto a copper target in the presence of the gas to be analyzed. This provided for formation of CuCl in the plasma. The luminescence of the D-system of CuCl was then detected around 440 nm. Detection limits were a few ppm.

Figure 2-13 shows the elements determined in a gas phase matrix and their relative detection limits.

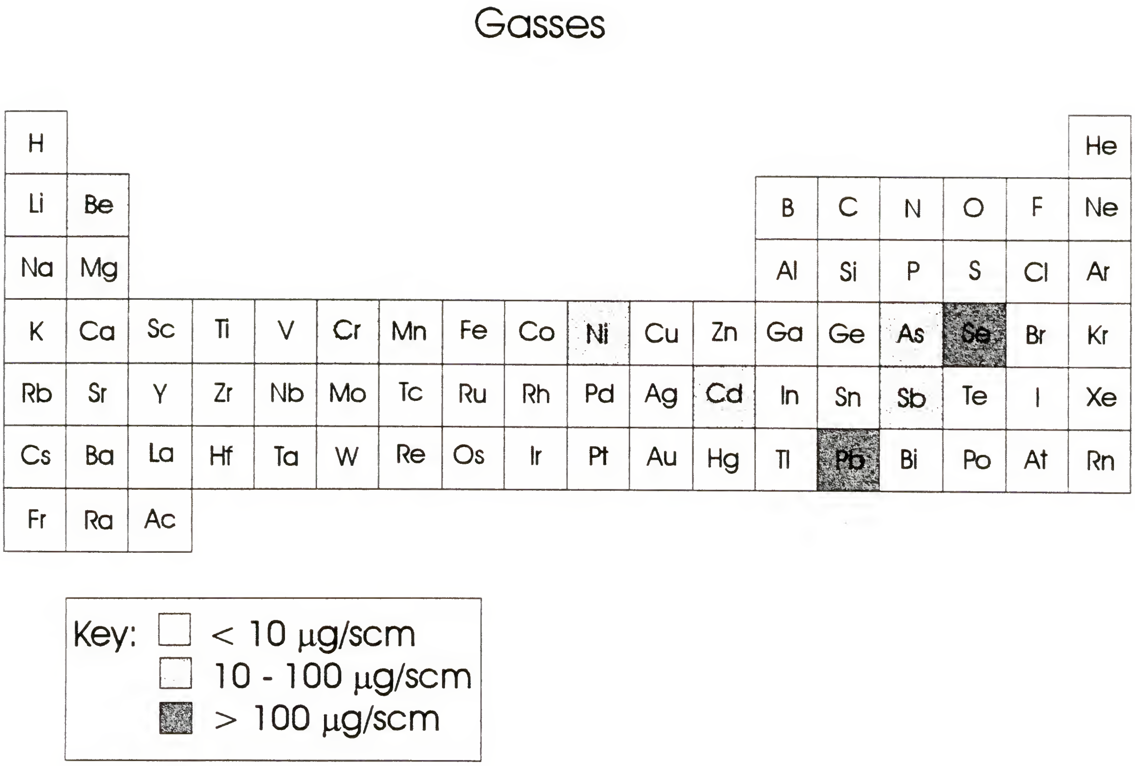
Gasses
H He
Li Be B C N O F Ne
Na Mg Al Si P S Cl Ar
K Ca Sc Ti V Cr Mn Fe Co Ni Cu Zn Ga Ge As Se Br Kr
Rb Sr Y Zr Nb Mo Tc Ru Rh Pd Ag Cd In Sn Sb Te I Xe
Cs Ba La Hf Ta W Re Os Ir Pt Au Hg Tl Pb Bi Po At Rn
Fr Ra Ac
Key: □ < 10 µg/scm
□ 10 - 100 µg/scm
▨ > 100 µg/scm

Figure 2-13. Elements determined in gas phase matrices shaded according to detection limit. The unit scm refers to a standard cubic meter of gas.

CHAPTER 3

THE EFFECT OF TARGET WATER CONTENT ON PROPERTIES OF A LASER-INDUCED PLASMA

$CaCO_3$ Experiments

Because of difficulties with matrix matching in a number of laser solid sampling techniques, plasma diagnostics are often employed directly or indirectly (through internal standardization) as a means of generating working curves. In this study, the effects of water content of $CaCO_3$ powder on size, shape, excitation temperature, electron number density, continuum emission, and line emission of plasmas generated on the powder are investigated. Although the specific wetting properties of the matrix will determine the magnitude of the water content effects, the observations made for $CaCO_3$ powder indicate that emission and electron number density are the two parameters affected significantly by water content, both decreasing with increasing weight % water. In laser-induced breakdown spectroscopy of samples which may have an inhomogeneous distribution of water or of samples in which water content can vary significantly, accounting for the effects of this water is essential to an accurate analysis.

Introduction

In recent years, laser-induced breakdown spectroscopy (LIBS) has received increasing attention as a technique suitable for rapid, often on-site, analysis of environmental samples with little or no sample preparation.[58,65,69,94,126-130] Establishing working curves for elements in real environmental samples is difficult, in large part, due to lack of standards and matrix matching difficulties. The interaction between the laser and the target in LIBS is influenced significantly by the overall composition of the target so that the intensity of the emission lines observed is a function of both the concentration of the elements of interest and properties of the matrix which contains them. One of the properties of the matrix which can affect the observed intensities is the water content or humidity of the sample.

Several authors have observed that in samples capable of absorbing water, the observed intensity of emission lines decreases with increasing water content.[31,131] It has been suggested that when this phenomenon poses a threat to accurate analysis, the calibration curve and sample analysis should be obtained from samples that are thoroughly dried.[131] However, this practice represents an increase in the time with which a sample can be analyzed, especially in on-site applications. In this chapter, some of the effects of humidity on the observed emission lines and on the plasma in general will be discussed. Although a quantitative method to correct for humidity in a variety of samples seems difficult to obtain, the qualitative effects of humidity in a specific LIBS analysis can be described on the basis of laser-target interactions and plasma diagnostics.

Background

Water contained within a solid sample can be classified into one of three categories based on the energy with which it is bound to the sample.[132] Chemically bound water includes water of crystallization and coordination and is the most tightly bound of the three categories. Physiochemically bound water includes water absorbed on the solid by osmotic or dipole forces and is second in binding energy. Unbound water refers to water which is found in voids, pores and grain boundaries of the solid and is held within the solid by the least energy. This last type of water is the one most easily changed by the interaction of a solid with its environment, and is the type capable of greatest variation. Therefore, it is the type most likely to affect a LIBS analysis and is the water which is varied in the following experiments.

Wetting of the external surface of a solid can occur spontaneously when the specific solid vapor interfacial energy (E_{sv}) is greater than the sum of the specific solid liquid interfacial energy (E_{sl}) and the specific liquid vapor interfacial energy (E_{lv}).

$$E_{sv} \geq E_{sl} + E_{lv} \qquad (3\text{-}1)$$

There is then a gain in free energy associated with the formation of a solid-liquid interface and wetting of the internal surfaces of the solid will proceed according to the Rideal-Washburn equation.

$$L = \left(r \frac{(E_{sv} - E_{sl})}{2\eta} t \right)^{1/2} \qquad (3\text{-}2)$$

Here L is the distance of penetration of liquid into the solid in units of m, r is the average pore radius of the solid in m, E_{sv} and E_{sl} are in units of J/m^2 , t is time in units of s, and η is viscosity of the penetrating liquid in Pa s.

In these experiments, water was used to penetrate a $CaCO_3$ powder sample. $CaCO_3$ powder was chosen because it is available in a pure form with a small grain size that wets spontaneously and rapidly and therefore is more likely to give a homogeneous sample. Several matrices (soils, mining ores, etc.) behave similarly to $CaCO_3$ in that they are porous substances which spontaneously wet. Many matrices (alloys, glasses, etc.) behave entirely differently.

In samples which do not spontaneously wet, water can be easily removed. Water content becomes a factor in samples which do spontaneously wet because it effects the laser-target interaction which generates the plasma. Several authors have written equations to describe aspects of this interaction.[14,133] The equation proposed by Ahmad and Goddard is the most straightforward.[133] The minimum irradiance required for breakdown of the sample is given by

$$F_{min} = \rho L_v a^{1/2} t_e^{-1/2} \qquad (3\text{-}3)$$

where F is in units of W/m^2, ρ is density of the target in units of kg/m^3, L_v is the heat of vaporization of the target in units of J/kg, a is the thermal diffusivity, which measures the targets ability to dissipate heat, in units of m^2/s, and t_e is the duration of the laser pulse in units of s. The density, thermal diffusivity, and heat of vaporization of the target should all increase as water takes the place of air in the pores of the solid. The result is that the minimum irradiance required for breakdown should increase with increasing water content. Likewise, for a given irradiance, breakdown intensity should decrease with increasing water content.

Experimental

Figure 3-1 is a schematic of the setup used for these studies. Most notably, a pierced mirror was used to collect light from above the powder samples so that formation of the plasma within the crater formed from previous laser shots would not affect light collection. A Nd:YAG laser operating at 1064 nm (Quantel YG580, Santa Clara, CA) with a pulse width of 20 ns and a power of approximately 200 mJ was focussed onto a sample stage. Emission was focussed with a 2.5 cm f/2 quartz lens into a 1 m spectrometer with a grating of 2400 lines/mm (HR1000, Instruments SA Inc., Metuchen, NJ). A pulse generator (FG-100, Princeton Instruments, Trenton, NJ) was used to gate a 1024 element photodiode array (ST-120, Princeton Instruments) which could simultaneously view a spectral window of 15 nm with a resolution of 20 pm.

Samples were prepared by mixing water with oven dried $CaCO_3$ powder on an electronic balance and stirring with a glass rod. Wetting of the samples by this method assured homogeneous distribution of the water. Samples were smoothed with a scalpel before analysis to minimize the effects of variations in the distance between the sample and the lens used to focus the laser onto it.

Emission intensity on $CaCO_3$ powders of water content between 0 and 40 % was determined for the Ca ion line at 393 nm. The delay time was 1 μs and the gate width was 1 μs. Each sample was analyzed at five different locations by single shots.

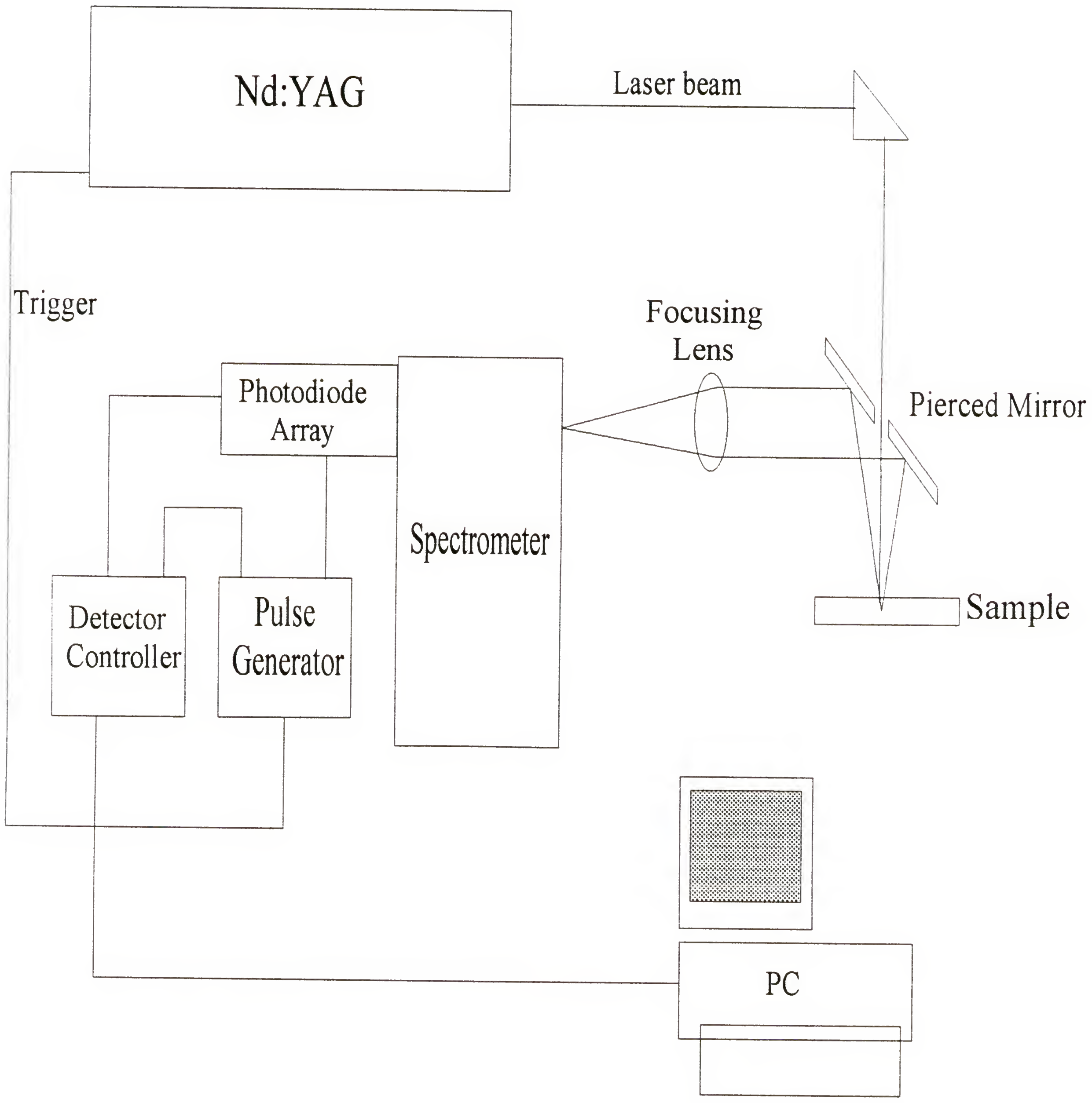

Figure 3-1 A schematic of the setup used to investigate laser-induced plasmas on targets of varying weight % water.

Images of the plasma evolution on $CaCO_3$ powder targets were taken using a CCD camera (ST-135, Princeton Instruments) and pulse generator (PG-200, Princeton Instruments). The gate width was 250 ns and the delay times were 500, 1000, 1500, and 2000 ns, giving four images for each sample. Non-specific emission from the plasma was also measured using a photomultiplier tube with an interference filter centered at 480 nm. The PMT was coupled to a 300 MHz oscilloscope through a 50 Ω resistor. In order to investigate the effect of water content on the excitation temperature, $PbCl_2$ was mixed 5% by weight with the $CaCO_3$ powder. The emission of lead lines at 357, 363, 367, 368, and 373 nm could be viewed simultaneously with the photodiode array at a delay time of 1 μs and gate width of 1.75 μs, which provided sufficient data with which to prepare Boltzmann plots. Four samples of different weight % water were analyzed 8 times each.

Investigation of the effect of water content of the target on electron number density in the plasma was done by observation of the H_α line at 656 nm with a 1 μs delay and 1 μs gate width. The observed width of this line was greater than the spectrometer limited line width by more than an order of magnitude. The FWHM of the line was measured, and an iterative calculation was carried out using the equation

$$\Delta\lambda_{1/2} = 2.50 \times 10^{-9} \alpha_{1/2} n_e^{2/3} \qquad (3\text{-}4)$$

with $\alpha_{1/2}$ values for H_α interpolated from tables by Griem.[6] Similar calculations have been done by other researchers to determine electron number densities in microwave plasmas[134] and inductively coupled plasmas.[135]

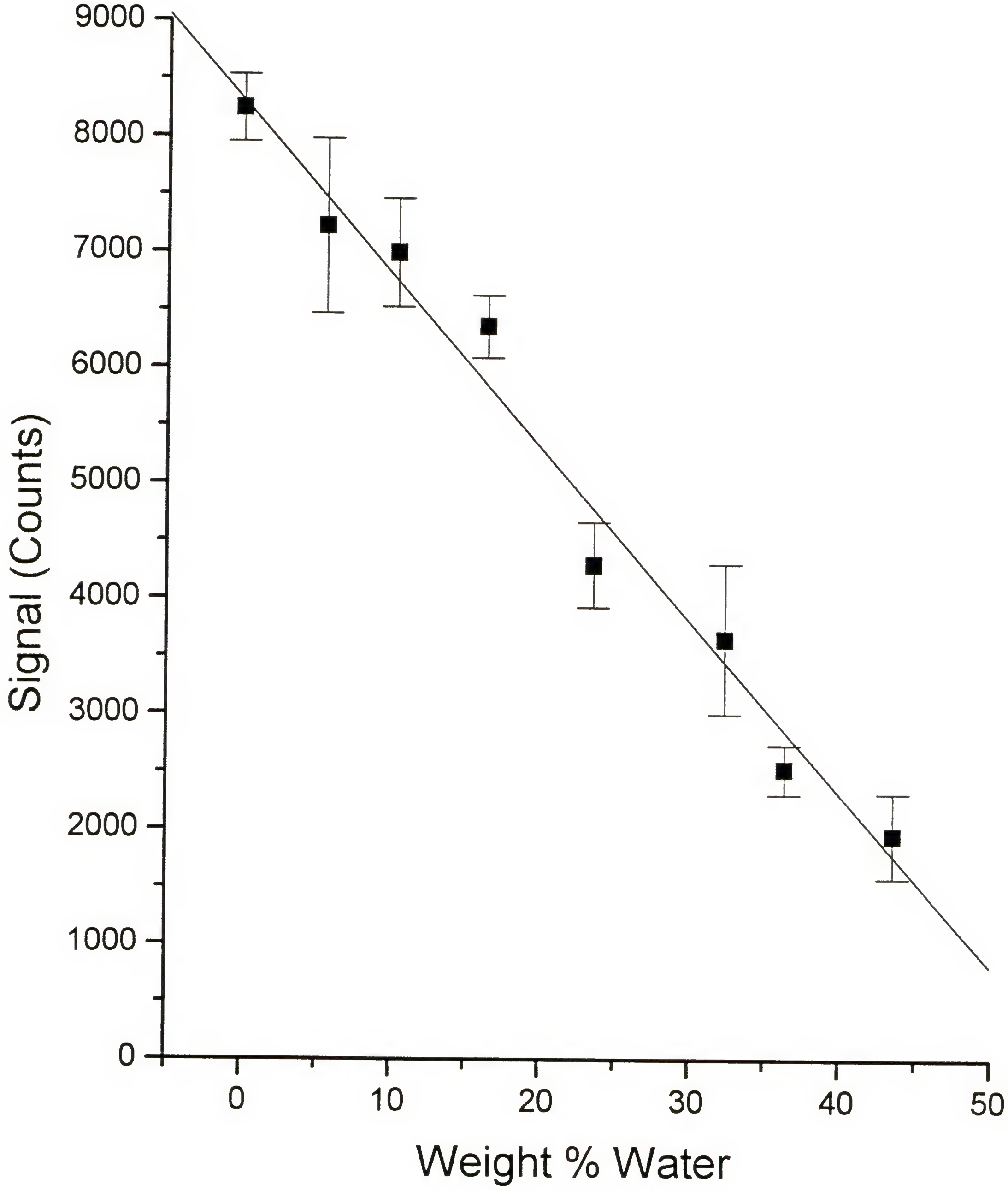

Figure 3-2 Plot of the Ca II 393 nm line intensity vs. weight % water. The targets were $CaCO_3$ powder.

Results and Discussion

Figure 3-2 is a plot of intensity of the Ca 393 nm ion line vs weight % water for $CaCO_3$ powder. The signal intensity decreased linearly by an order of magnitude for weight % water between 0 and 40%.

Figure 3-3 shows the light emission at 480 nm from plasmas generated on $CaCO_3$ powder targets of different water content as determined with the photomultiplier tube and 480 nm interference filter. Because the sample has no emission lines of significant intensity in this region, the signal was produced primarily by continuum emission. Figure 3-4 shows the CCD images obtained at 500, 1000, 1500, and 2000 ns on targets of different water content. Both the CCD and PMT measurements indicate that as water content increases, the intensity of the plasma decreases. The rate of decay of emission appears largely unchanged.

The Boltzmann plots generated from the lead lines of $PbCl_2$ mixed with the $CaCO_3$ and wet with varying weight % water are shown in Figure 3-5. The excitation temperature calculated from the slope of the line is 10000 K for all samples. The emission intensity of lead lines falls by an order of magnitude in the range between 0 and 30%.

The electron number density, like the emission line intensity, shows a significant variation with water content. Figure 3-6 shows the excitation temperature and electron number density for plasmas formed on targets between 0 and 30% water by weight. Calculated electron densities vary from 7×10^{16} cm^{-3} for a plasma formed on a dry target to 1.6×10^{16} cm^{-3} for a plasma formed on a target which was 30% water by weight.

To correct for the decrease in signal with increasing water content, the intercept of the Boltzmann plots of lead lines and the electron number densities at different weight % water found using H_α half-widths were used. From these data the relative plasma densities at each weight % water were calculated from the equation

$$\textbf{Relative plasma density(weight \% water)} = \frac{\ln^{-1}(\textbf{Boltzmann intercept(weight \% water)})}{\textbf{\% of lead appearing as atoms(weight \% water)}} \qquad (3\text{-}5)$$

The % of lead appearing as atoms at each weight % water was calculated with the Saha equation (1-9) using partition functions taken from Winefordner *et al.*[5] The resulting relative plasma densities and the normalized Ca II 393 nm signal at different weight % water are shown in Figures 3-7 and 3-8 respectively.

Conclusions

The decrease in emission intensity observed with increasing water content in targets which spontaneously wet has several possible explanations. From a laser-target interaction perspective, it can be seen that the addition of water to a target can directly affect the density, and thermal diffusivity of the sample, thereby affecting the energy density required for breakdown.

From a plasma diagnostics perspective, the incorporation of water into the target is shown to decrease the electron number density in the plasma while the excitation temperature remains roughly constant. This may result because the water contains less

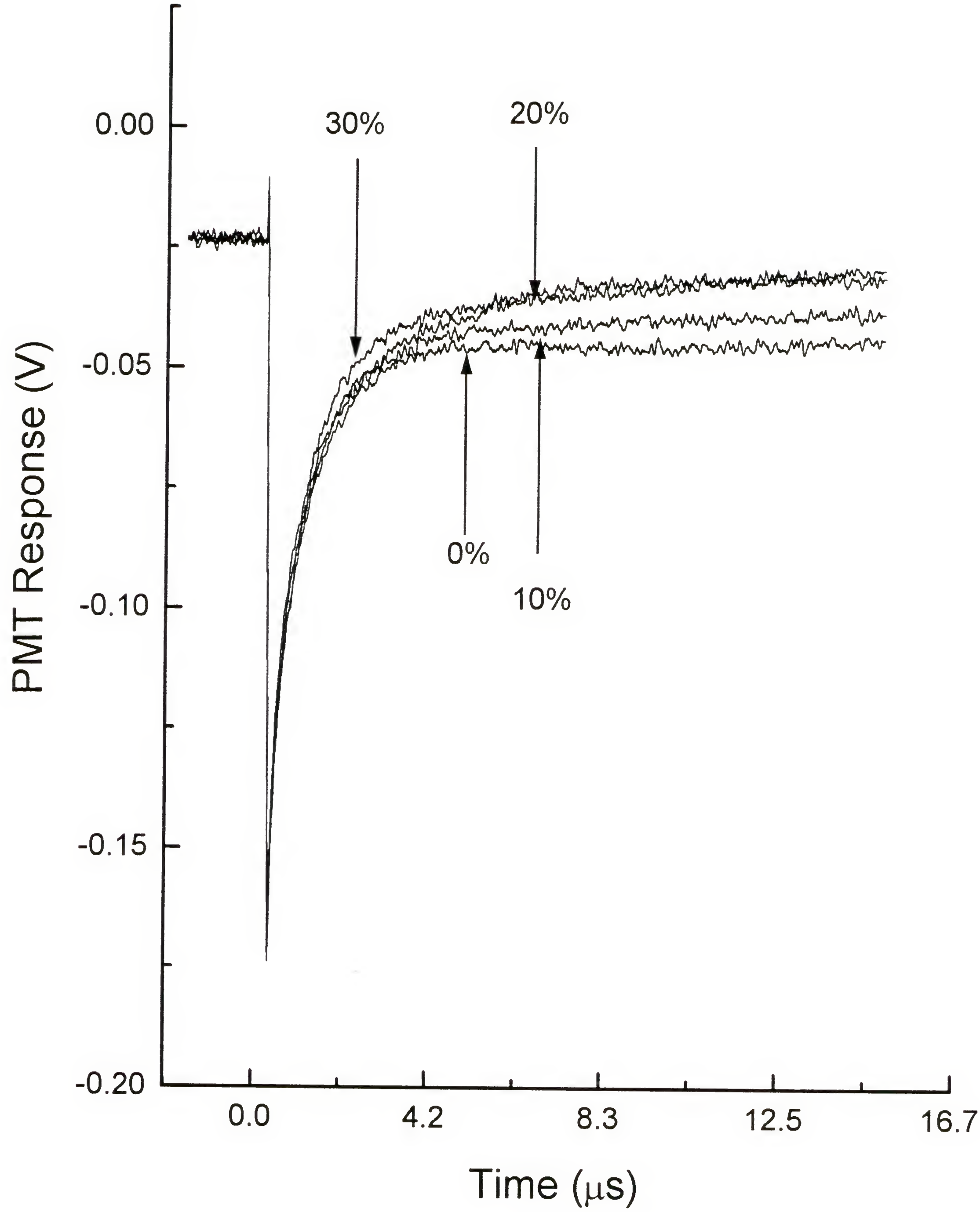

Figure 3.3 Temporal non-specific light emission for plasmas formed on $CaCO_3$ powder targets of varying weight % water.

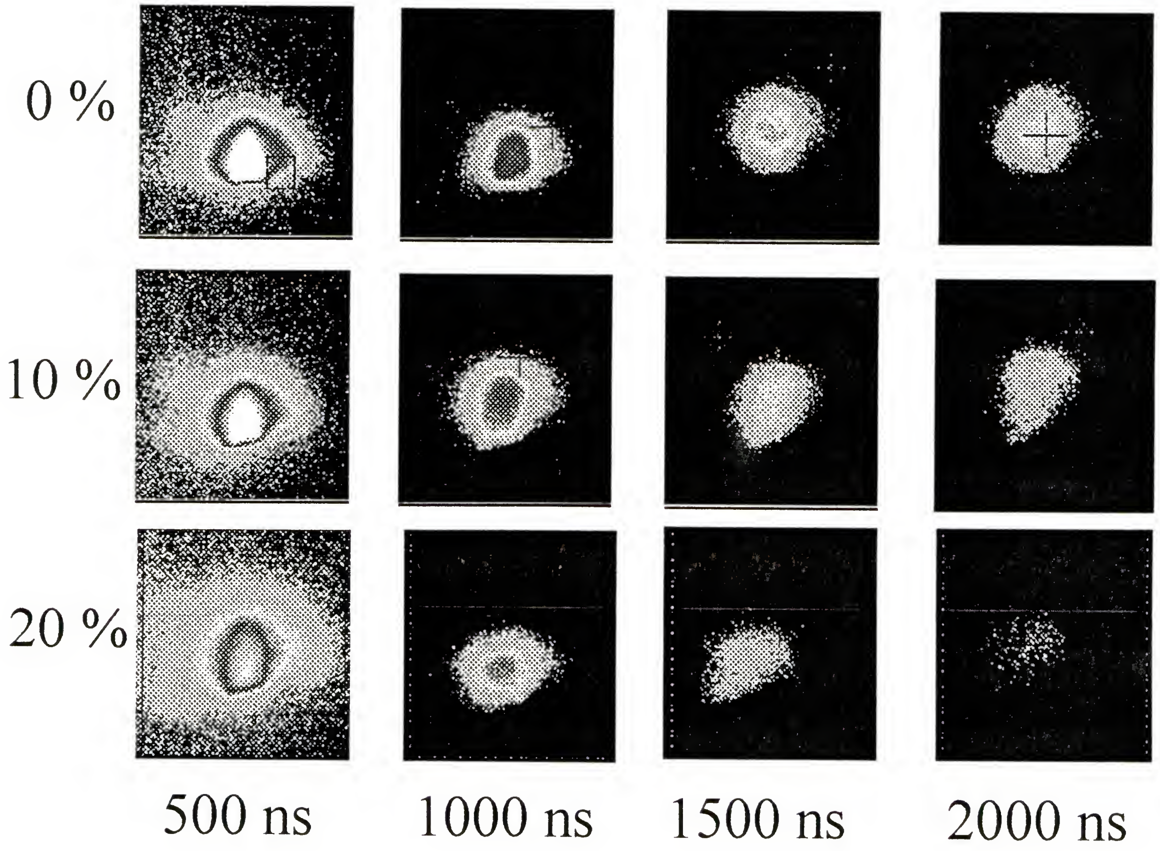

Figure 3.4 CCD images of plasmas formed on targets of varying weight % water.

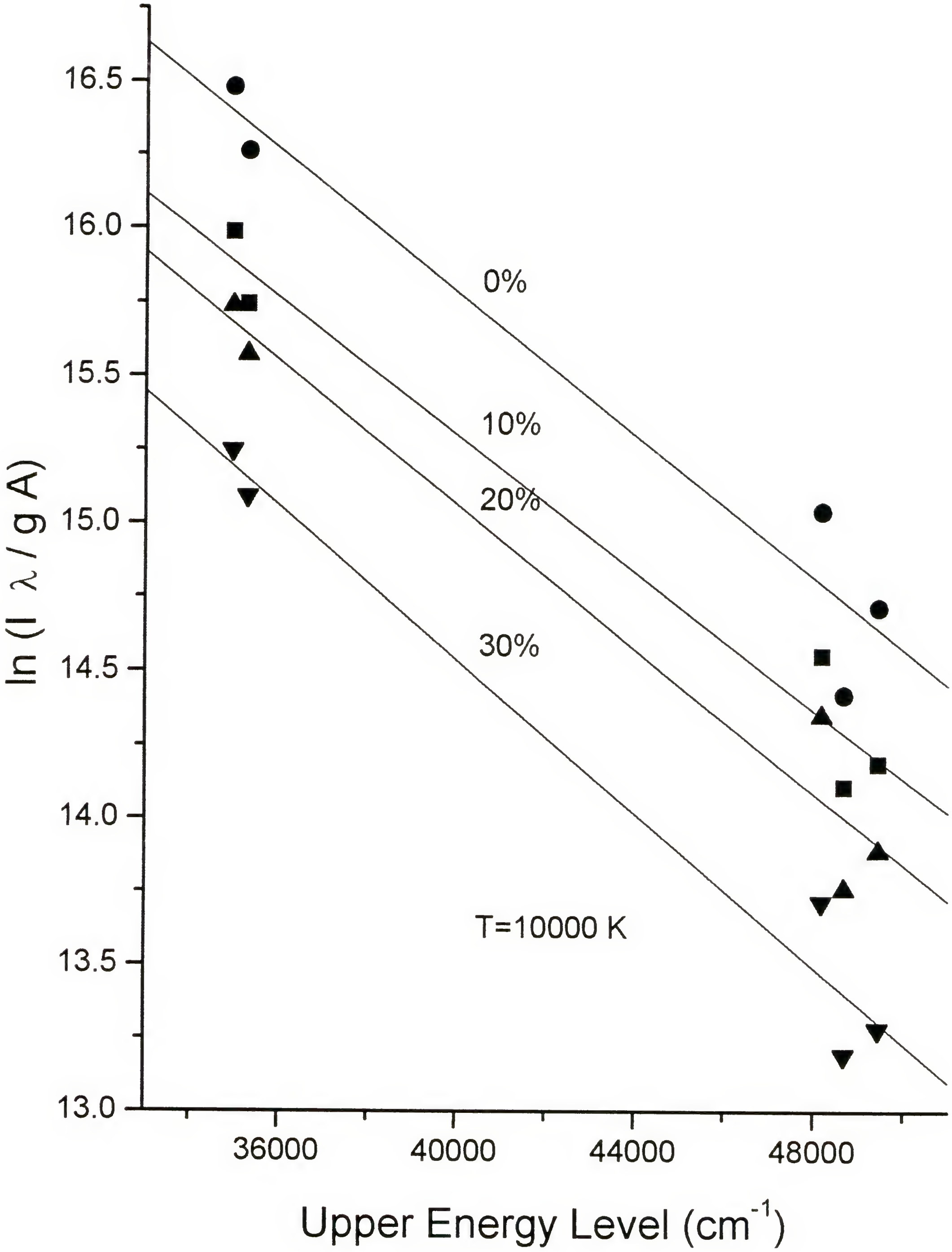

Figure 3-5. Boltzmann plots for $CaCO_3$ powder targets with $PbCl_2$ mixed at 5% by weight at varying weight % water.

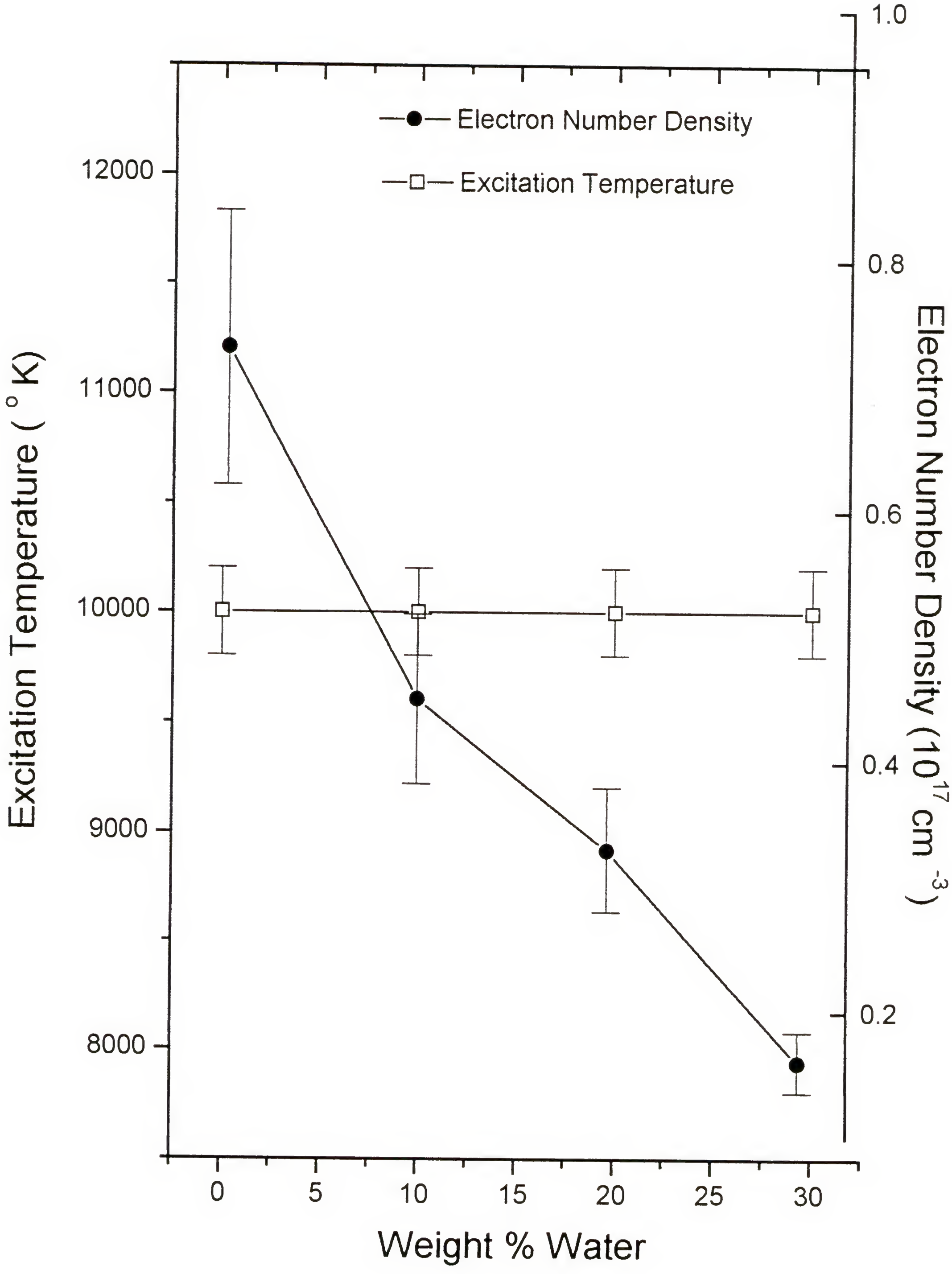

Figure 3-6. Excitation temperature and electron number density vs weight % water.

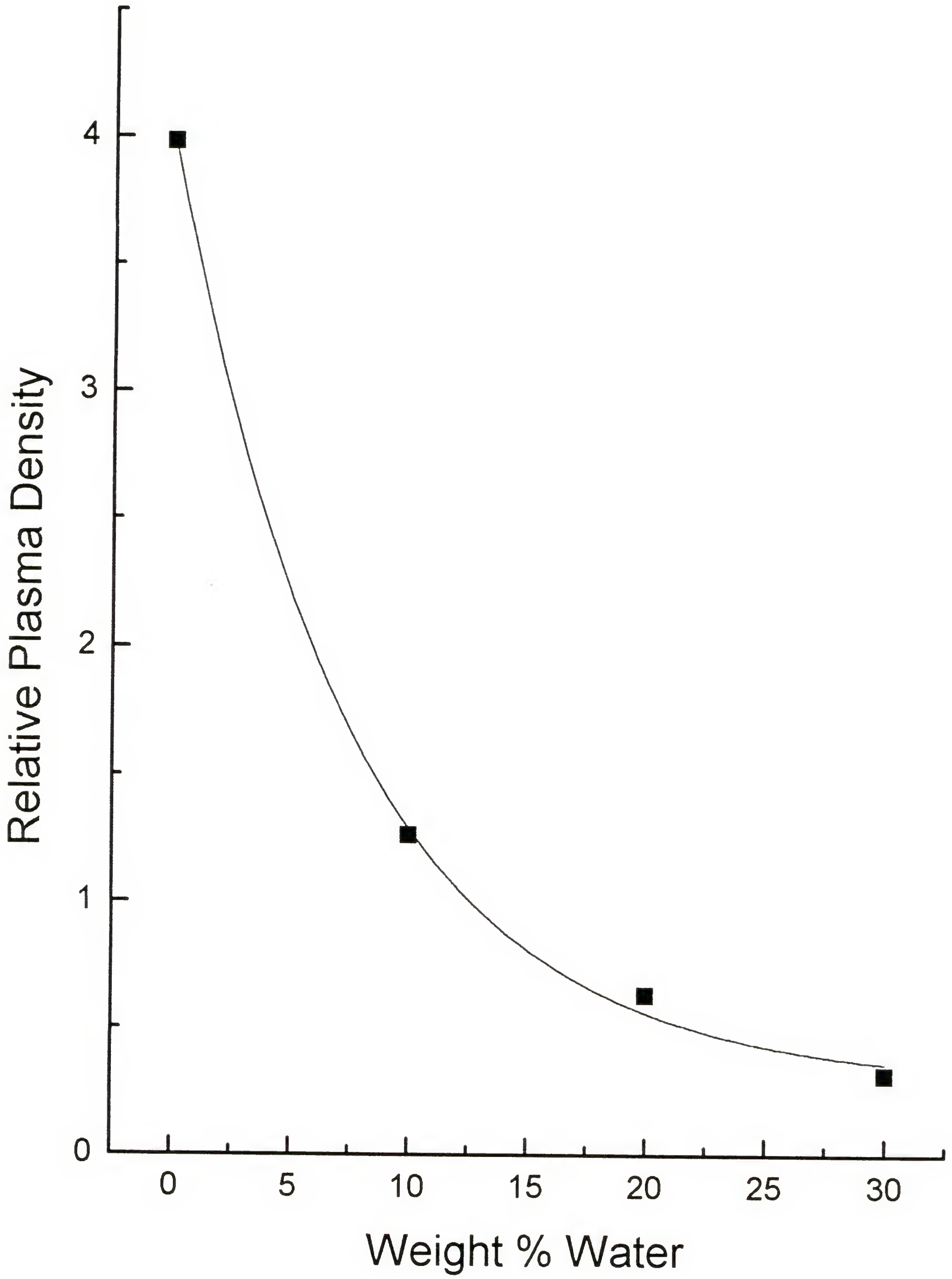

Figure 3-7. Relative plasma densities calculated using Boltzmann intercepts and electron number densities *vs* weight % water.

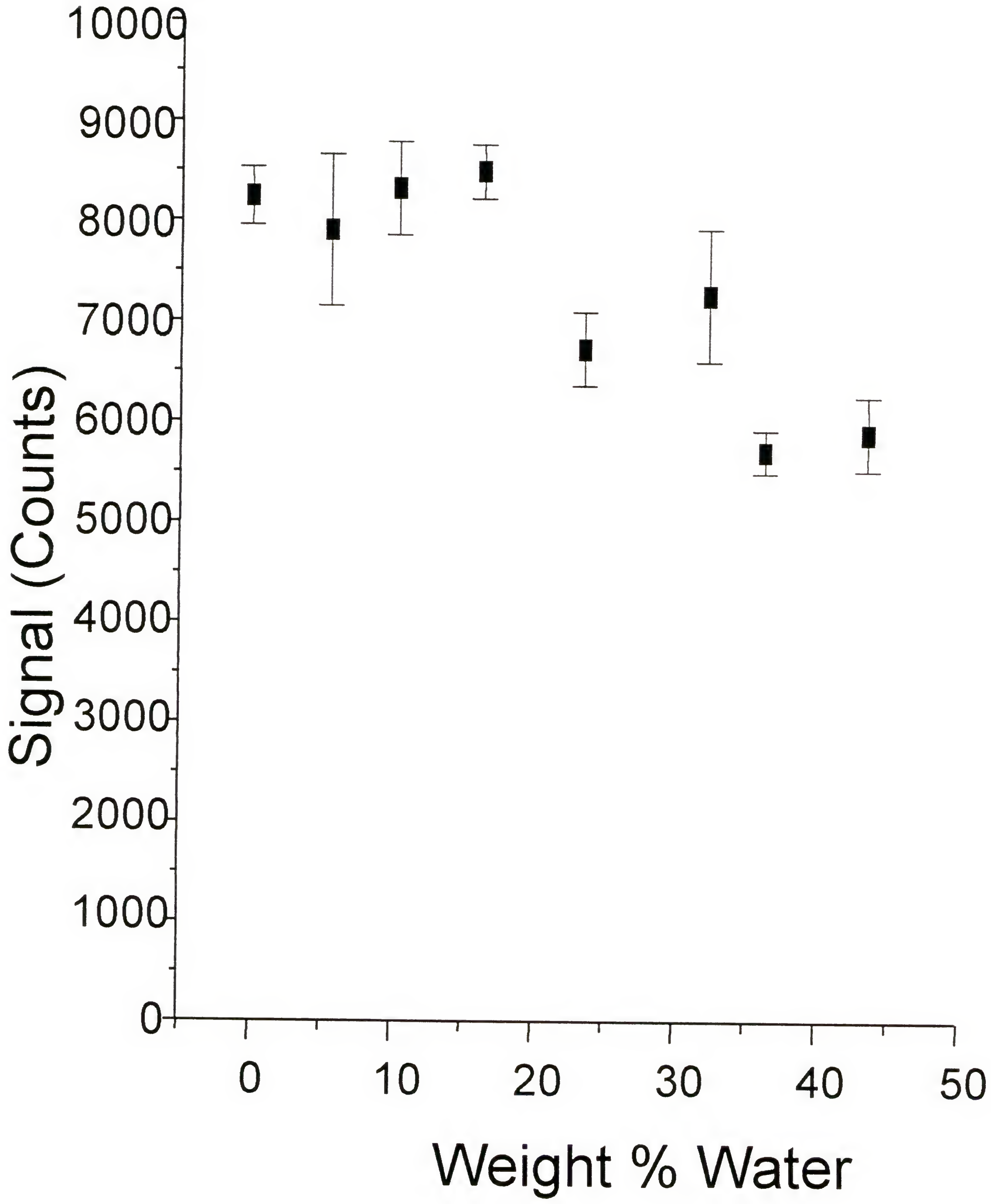

Figure 3-8. Ca II 393 nm signal intensity corrected using relative plasma density *vs* weight % water.

easily ionizable species than the $CaCO_3$ and comprises an increasing portion of the laser-target interaction volume at increasing water content.

Relative plasma densities can be determined at each weight % water using Boltzmann intercepts and electron number densities. These densities can be used to normalize the emission observed and significantly reduce the problem that this matrix effect poses to calibration.

Iron Ore Experiments

Introduction

It has been found that the water content of the sample being analyzed affects characteristics of the plasma in a way which causes observed emission from a given element to decrease with increasing water content.[31] Thus, when sample composition is constant, measuring the intensity of light emitted due to concentration of a given element is sufficient to determine water content of the sample within a limited range.

In this experiment three different iron ores were analyzed by LIBS and a working curve for the determination of water content by observation of emission intensity due to iron concentration was generated. Ores were analyzed both as powders and as pellets, and it was found that the standard deviation in the data obtained was smaller for the pressed samples (pellets) than for the powders. It was also found that the slope of these curves depended on whether the sample water content was determined during permeation of water into the pellet or during evaporation of water from the pellet.

Background

There are currently several methods employed to determine water content of solid samples, the most common of which is the gravimetric method which amounts to weighing of the solid sample before and after drying. Other methods include microwave techniques,[136,137] nuclear magnetic resonance,[138-140] near IR reflectance,[141-143] and time domain reflectometry.[144] Of these methods, nuclear magnetic resonance and near IR reflectance are suited to on-line determination of water content in a solid.

Using emission from a laser-induced plasma to determine water content is similar in several ways to using near IR reflectance. First, the technique must be calibrated for the specific solid to be analyzed. This accounts for inherent differences in IR absorption properties of different samples in the reflectance technique and for different elemental composition of samples in the LIBS technique. Second, both techniques are only suitable for determining water content at, or very near, the surface of the sample where the light from either the IR source or the laser is absorbed.

The LIBS technique has been used to monitor toxic element emissions in smokestacks,[122] colloidal iron in water,[94] and an entire host of elements in solids.[145] It has been employed in toxic environments,[110] as a remote sensor with the use of a fiber optic,[59] and as a technique to analyze single particles with diameters less than 100 μm.[105]

Experimental

The iron ore experiments were done on the same instrument as the $CaCO_3$ experiments. In this study however, the objective was to determine water content of the ore by calibration with the decreasing emission intensity.

Samples of magnetite iron ore (National Bureau of Standards # 29) and crescent iron ore (National Bureau of Standards # 26) were analyzed first in powder form. These samples differed by ~5% in there iron concentration. A known range of water content in each of the ores was prepared by weighing dry powder and adding deionized water. The mixture was homogenized by stirring with a glass rod and a portion of the sample was then placed on weighing paper. The surface of the ore was smoothed with the glass rod to prevent changes in lens to sample distance as the sample was translated under the laser beam.

The pulse generator was set for a delay of 2 μs and a gate width of 1 μs and the average of 50 laser shots taken at 6 Hz. The spectral window observed was from 550-570 nm and included the large hydrogen peak (H_α) at 656.2 nm as well as a number of Fe lines of varying intensity. This window was chosen because the hydrogen line can be used to assess plasma parameters and contains information regarding the charge carrier density within the plasma. Two typical spectra are shown in figure 3-9. The more intense spectrum corresponds to a drier pellet, the less intense to a moist pellet. The Fe 667.8 nm atom line could be observed with little interference, and because it never saturated the detector it was chosen to calibrate on.

Both ores were prepared at four different water contents and run in a similar fashion. After background correction, the peak height was used to construct a plot of signal vs weight % water.

Although the hydrogen peak profile changed slightly with water content, these changes were not as sensitive as the changes in emission of the Fe 667.8 nm line and no calibration of hydrogen line intensity with water content was attempted.

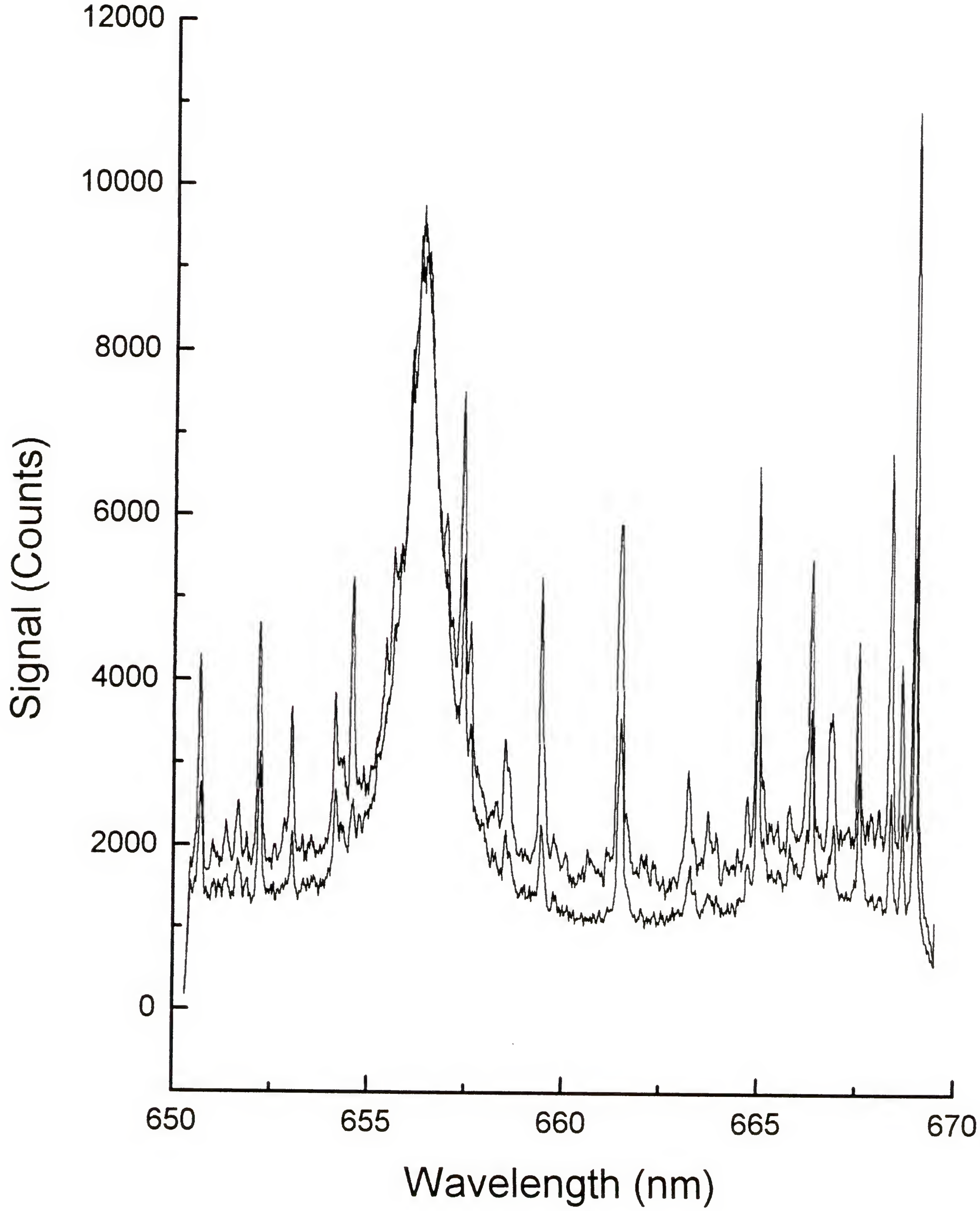

Figure 3-9. Crescent iron ore spectra from 650-670 nm. The large broad peak at 656 is H_α. Fe 667.8 is also shown. The more intense spectrum is taken from a pellet which is dry relative to the pellet which produced the less intense spectrum.

Next the same two ores and a third, sibley iron ore (National Bureau of Standards # 27a), were pressed into pellets. About 0.75 g of powder was placed in a 1 cm pellet press and pressed at a pressure of 10000 Kpa for 2 min. This produced pellets which were approximately 1.5 mm thick. Four different water contents of each ore were prepared by weighing the pellets and then placing them in a sealed chamber in which they were suspended above heated water for differing amounts of time. After removal from the chamber the pellets were quickly reweighed to determine water content and analyzed immediately. The same gate settings were used on the pulse generator, but this time the laser was run at 30 Hz and 250 shots were averaged into a single spectrum. The intensity of the Fe 667.8 nm line vs weight % water was plotted.

Because there was some concern about the homogeneity of water distribution in pellets prepared in this fashion, the experiment was repeated with pellets prepared by a different method. In this second experiment a dry pellet was weighed and then placed in the chamber above the heated water for an extended period of time. After removal the pellet was weighed and analyzed for the point which was to be the maximum water content in the curve. The pellet was then placed in a drying oven briefly, reweighed and analyzed for a point of lesser water content. This was continued until the pellet reached a water content of 2-3 % by weight. Again a plot of Fe 667.8 nm intensity vs weight % water was prepared.

Results and Discussion

The initial plot of the powder analysis is shown in figure 3-10. Although a correlation is definitely apparent, the plot is hardly suitable for calibration. However, the reason for

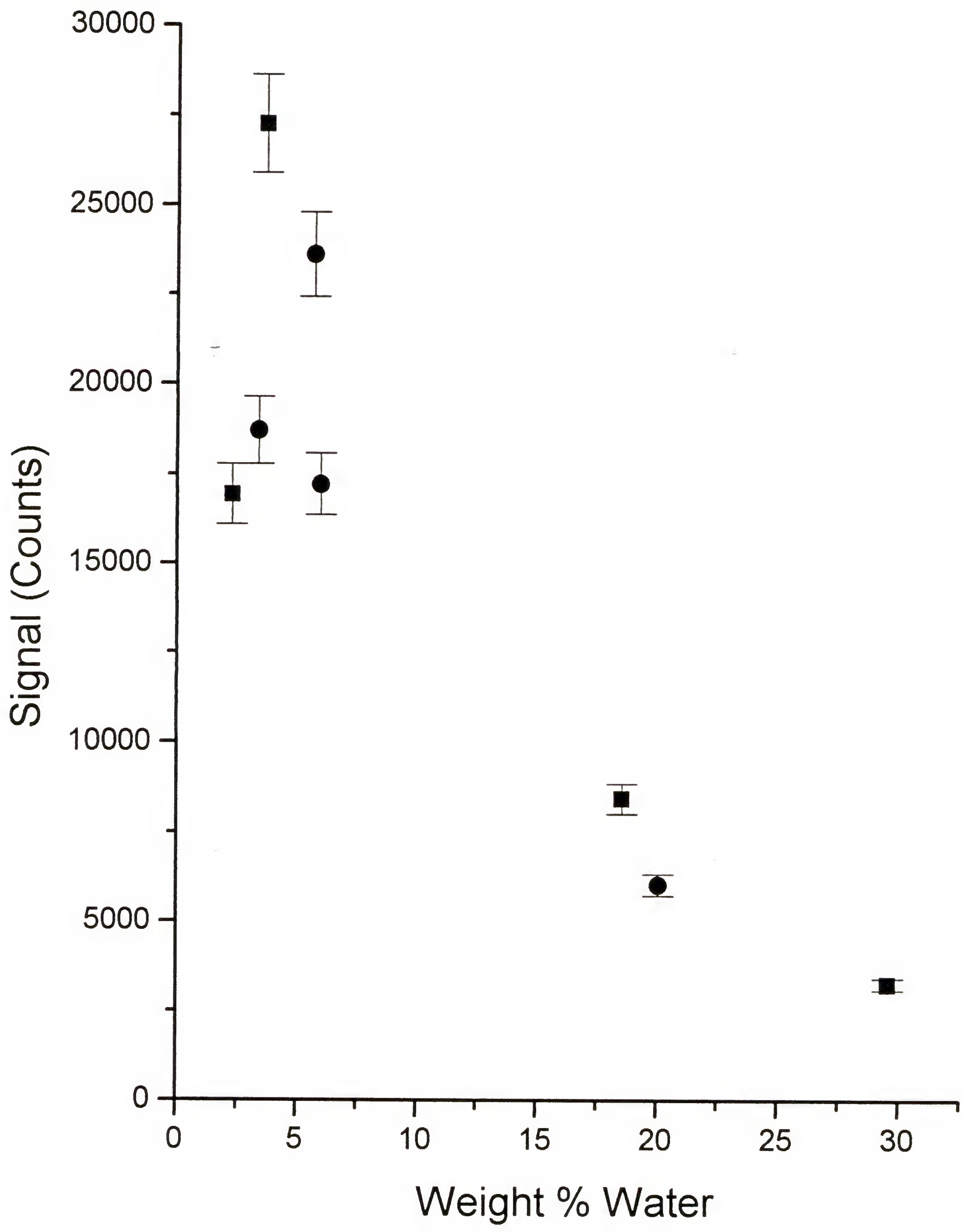

Figure 3-10. Plot of Fe 667.8 nm intensity vs weight % water for the 667.8 nm Fe atom line taken from iron ore powders, crescent (●) and magnetite (■), mixed with water.

the relatively large scatter of the data is readily apparent. In analyzing the powder there was a problem with dust from previous laser shots remaining in the path of the laser beam and either reflecting some of the incident power before it reached the sample or actually causing particle-induced breakdown above the surface of the sample. Even at a laser repetition rate of 6 Hz the problem was apparent and could have certainly been the cause of some deviation in emission signal observed. This problem was less evident on the samples of greater water content as this added water surpressed dust formation. The result is that especially at lower water content (2-8%) larger signals can be obtained for the wet powder than for the dry.

The plots generated from experiments on the pellets showed much less scatter than those on the powder. Figure 3-11 shows the 667.8 nm Fe atom line intensity *vs* weight % water. The different curves represent data taken by addition of water to the sample and evaporation of water from the sample.

Conclusions

Observation of elemental emission from a laser-induced plasma formed on pressed iron ore pellets has been correlated with water content over the range 0-20%. From the slope of the working curve and the precision of the data it is estimated that observation of the atomic transition of iron at 667.8 nm allows determination of the surface water content to within 2-3% in the range from 0-20% in pressed iron ore pellets provided some knowledge of sample history is available.

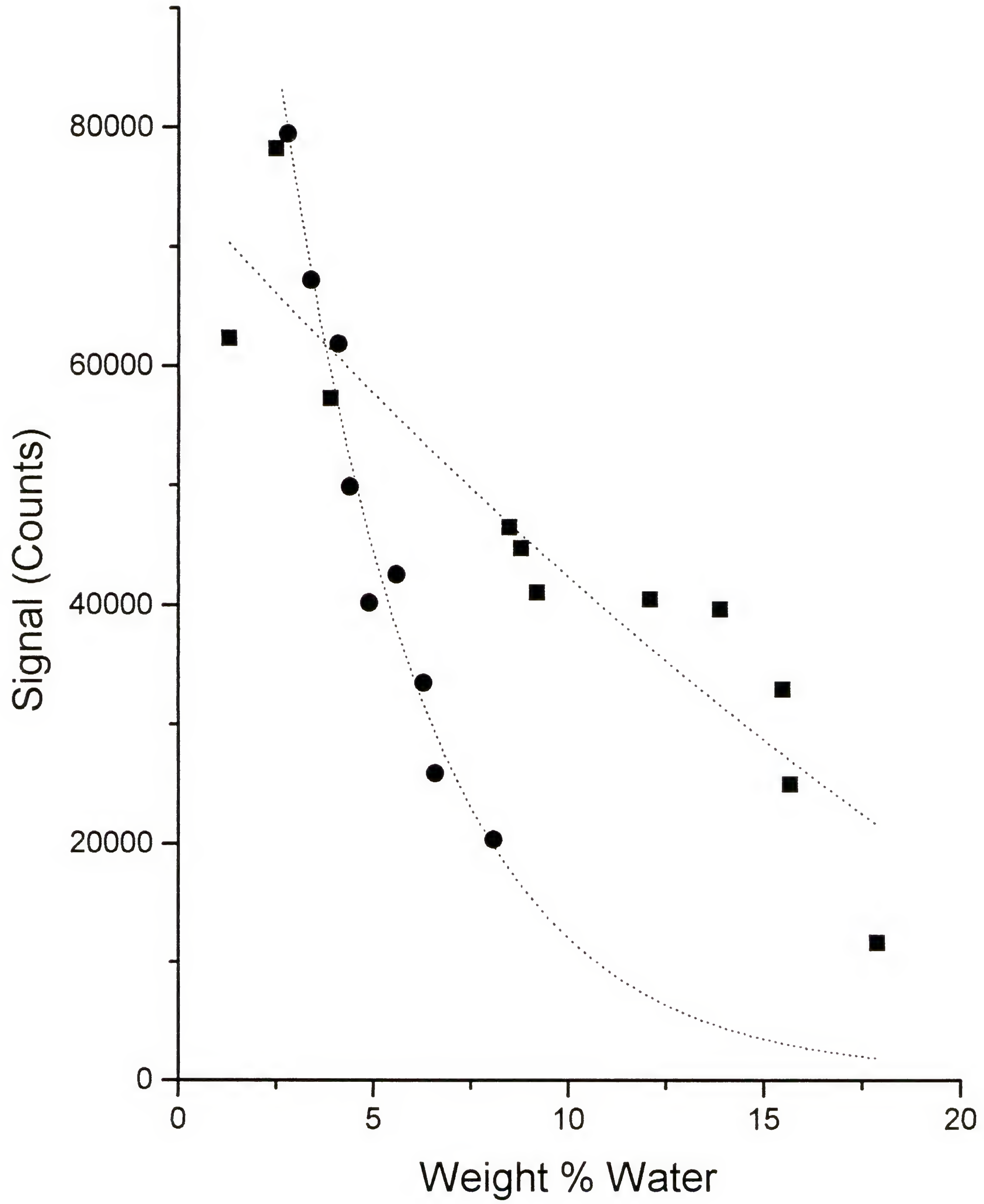

Figure 3-11. Plot of Fe 667.8 nm intensity vs weight % water for the pelletized samples. Data taken by successively adding water (●), data taken by evaporating water (■)

CHAPTER 4

LASER-INDUCED BREAKDOWN SPECTROSCOPY OF AQUEOUS SOLUTIONS

Introduction

In the last chapter it was seen that water content of a target affects the plasma formed by laser-induced breakdown on that target in a way which reduces the electron number density in the plasma and reduces the emission of analytical lines. In this chapter elemental analysis of aqueous solutions by LIBS is investigated. Several different approaches are attempted, including forming a breakdown on the surface of an aqueous solution, forming a sub-surface breakdown, and forming a breakdown at the interface between a solid substrate and the solution to be analyzed.

Work concerning LIBS for determinations in aqueous solution was summarized in chapter 2. Several differences between LIBS on solid targets and LIBS in aqueous solution deserve mention. First, when the laser is focused into a bulk liquid to produce a sub-surface spark, the lifetime of the plasma is greatly reduced relative to its lifetime in air.[98] The optimum delay of the detection relative to the laser pulse is thus much shorter in liquid than on solid; tens of ns rather than a few μs.

Second, when the plasma is formed on the surface of an aqueous solution, the physical effects of the focused laser on the target are much more pronounced than when the plasma is formed on a solid. Maintaining a well defined lens to sample distance and preventing the focusing lens from becoming covered with splashing solution are experimental problems associated with analyzing aqueous solutions by forming the plasma on the surface.[89]

The most successful approaches for analyzing aqueous solutions by LIBS have been the use of a repetitive spark pair to form the plasma inside a cavitation bubble,[84,87,89] and the formation of the plasma on a KBr substrate containing the solution to be analyzed.[98] In the experiments performed here, and attempt was made to perform LIBS with a single spark on the surface of a solution, beneath the surface of the solution, and at the interface between a submerged substrate and the solution.

Experimental

The first approach attempted was the focusing of the Quantel Nd:YAG laser onto the surface of an aqueous solution. Emission was collected at 90°. A schematic of this experiment is shown in figure 4-1. The aqueous solution was held in a petri dish with the meniscus of the solution above the edge of the dish. In this way the light could be collected at 90° without having to first pass through the wall of the dish.

An initial evaluation of this setup was performed by filling the dish with 1000 ppm Na solution and acquiring spectra from single laser shots focused just above the surface of the liquid. Single shots were used to assure that physical effects of the laser pulse on the water, splashing and formation of waves, did not affect the subsequent shots. The laser was focused just above the surface in an effort to minimize these physical effects.

The first experiments were carried out using approximately 200 mJ per 20 ns pulse of laser energy. The spectra obtained at this power were extremely irreproducible. The

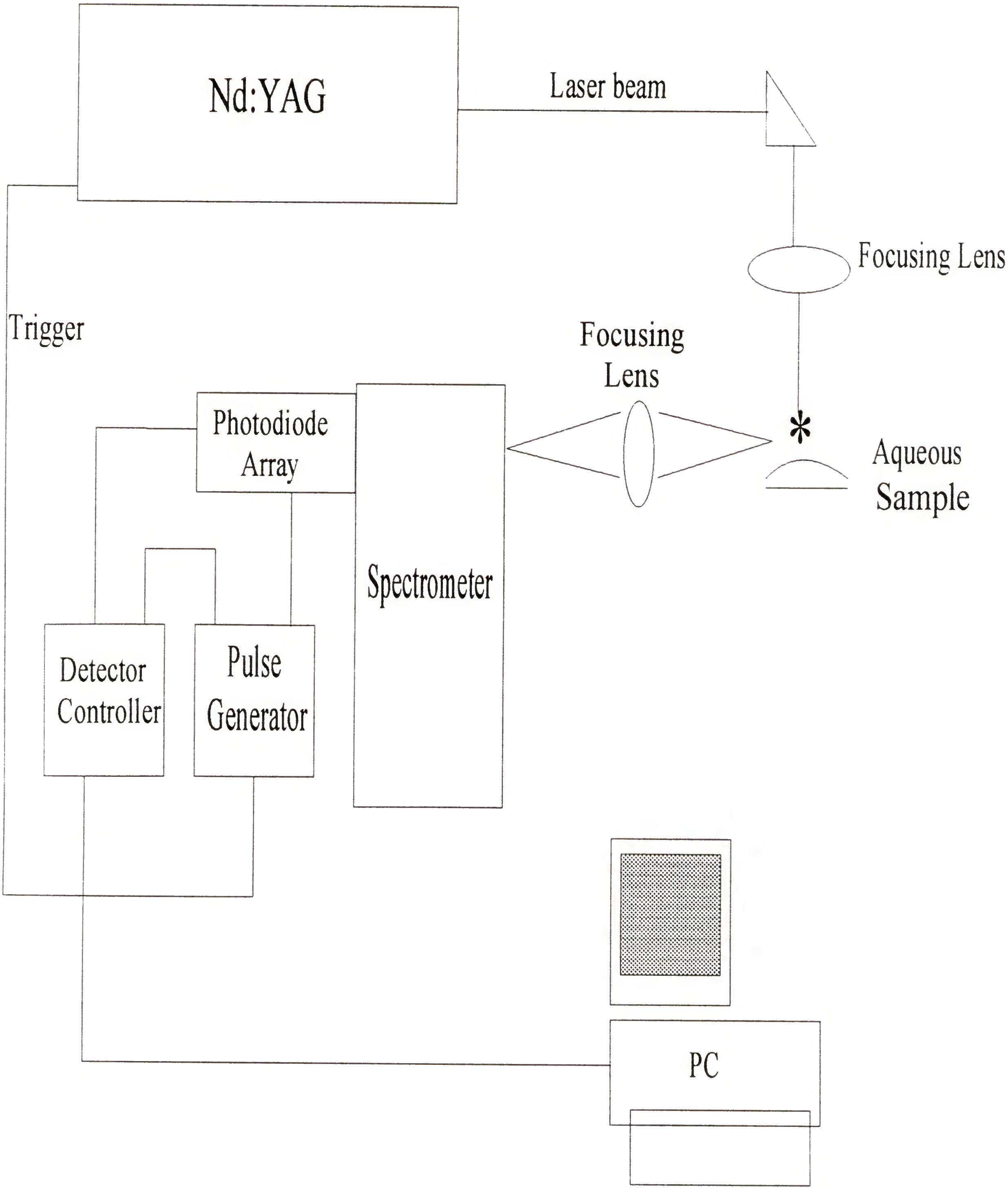

Figure 4-1. Experimental setup for performing LIBS on the surface of an aqueous solution.

reason for this was that the solution reacted violently to the focused laser pulse splashing out of the dish and also onto the focusing lens. Because solution was lost, the lens to sample distance could not be maintained accurately and every shot was effectively performed at a different distance.

When the power was reduced to approximately 100 mJ a breakdown could not be produced on the surface of the solution. At 150 mJ a breakdown could be formed, but the splashing and resultant changes in lens to sample distance persisted. This technique was abandoned in favor of the subsurface technique.

The experimental setup used for the production of a plasma beneath the surface of the aqueous solution was the same as shown in figure 4-1 with the exception that a quartz cell, rather than a petri dish, was filled with the solution to be analyzed, and the laser was brought to a focus a few mm beneath the surface of the solution rather than just above it. It was found that a plasma could be produced beneath the surface of the solution at a laser repetition rate of 30 Hz with a laser power of 200 mJ.

The 1000 ppm sodium solution was again used as a sample and the Na emission at 589.6 and 590.0 nm was chosen for observation. The detector was set to average 30 shots with no delay and a 1 μs gate width. The spectrum obtained is shown in figure 4-2. Because the two Na lines in this spectrum are not well resolved, an effort was made to increase resolution by using a delay of 50 ns. At this delay the resolution was unchanged, but the intensity of the signal fell to almost half. In all subsequent measurements no delay was used.

While investigating the use of this subsurface technique it was noted that the breakdown did not occur at the same location from pulse to pulse. One possible reason

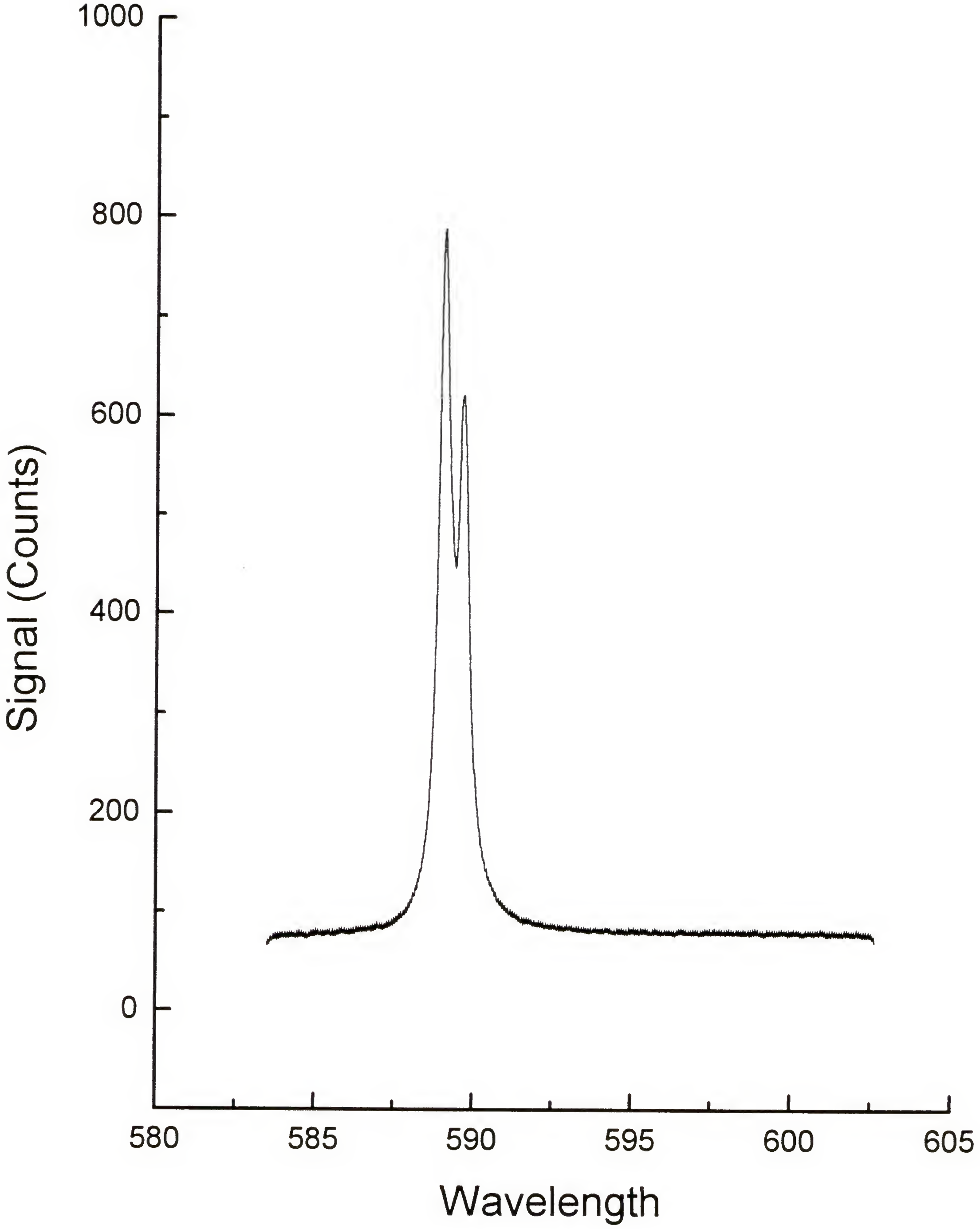

Figure 4-2. Spectra of saline solution taken with sub-surface breakdown technique.

for this change in location of breakdown was the presence of particles in the solution which promote breakdown by lowering the breakdown threshold in their immediate vicinity. Because this particle-induced breakdown was affecting the position of plasma formation, and hence light collection geometry, an experiment was setup using a submerged substrate on which to form the plasma.

In this experiment, shown in figure 4-3, the substrate was submerged in a quartz cell and the laser, at an energy of ~200 mJ, was brought to a focus on the surface. Emission was taken at 90°. No delay was used; the gate width was 1 μs. Single shot spectra could be obtained reproducibly with this setup because the breakdown always occurred at the substrate surface.

It was realized early in this experiment that the ideal substrate must have several characteristics. First, it must not produce a large number of interfering emission lines. Second, it must produce an intense plasma when the laser is focused onto its submerged surface. Third, it must show minimum erosion due to being submerged in aqueous solution or due to ablation caused by the focused laser. Several materials including graphite, teflon, and tungsten were examined. Experiments were done using magnesium and sodium as analytes in aqueous solution.

Results and Discussion

The technique of forming the plasma on the surface of the solution was abandoned because of the splashing problem which coated the laser focusing lens with water and made it impossible to maintain an exact lens to sample distance. Of the two remaining

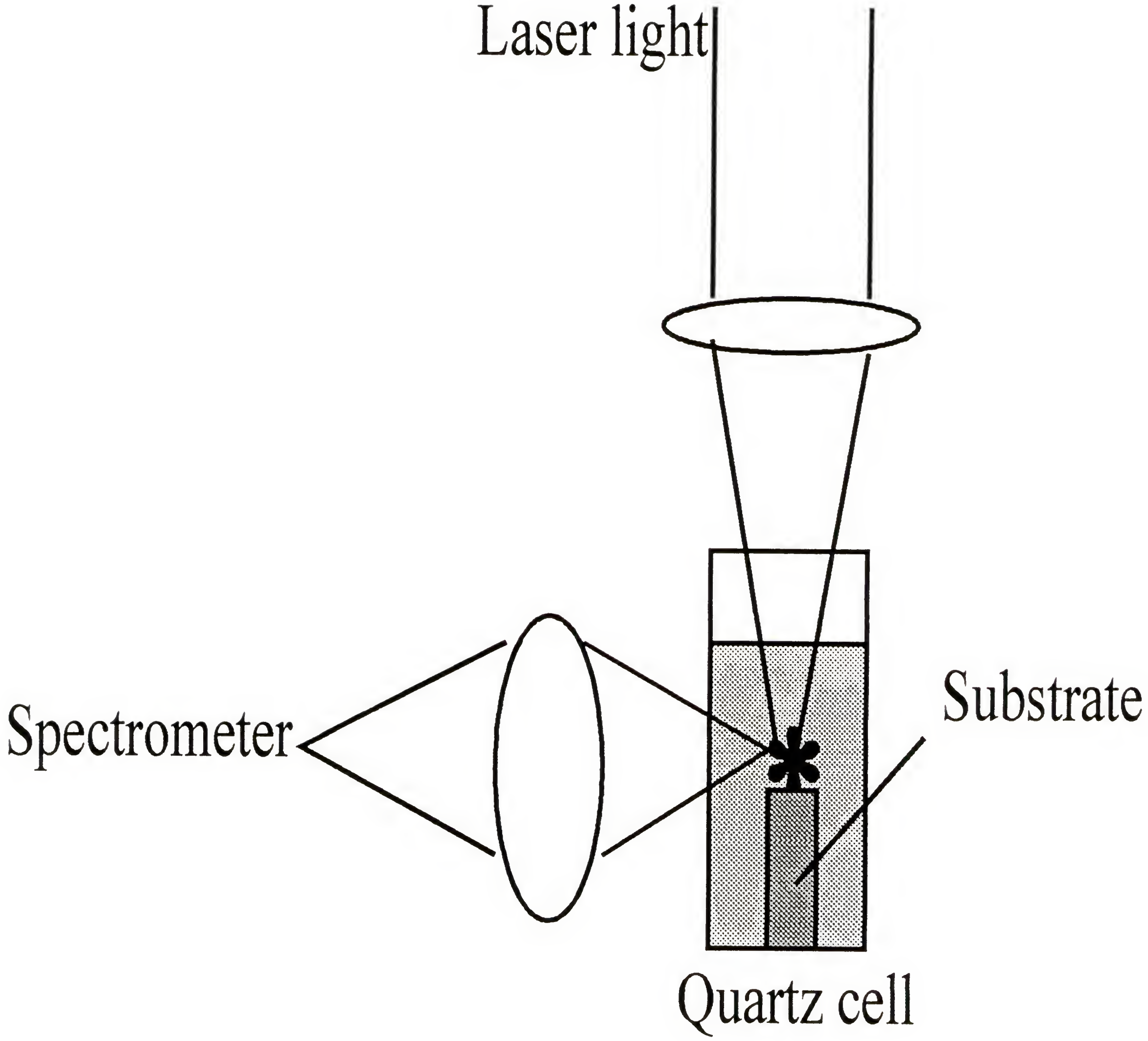

Figure 4-3. Setup for analyzing aqueous solution by breakdown on a submerged substrate.

techniques, formation of the breakdown on a submerged substrate appeared to have an advantage over forming a sub-surface breakdown in the solution because of the reproducibility of the location of the plasma. This substrate breakdown technique was the one chosen to investigate more thoroughly.

A single shot spectrum of 100 ppm sodium on graphite is shown in figure 4-4. The peaks at 589.6 and 590.0 nm are better resolved than those in figure 4-2, the subsurface breakdown. Also, the Na concentration is much lower than in the saline solution used in the subsurface breakdown technique. The graphite substrate produced no spectral interferences in this region of the spectrum. However, the substrate was eroded significantly after a few hundred laser shots. This erosion affected the effective lens to substrate distance and eventually a plasma could no longer be formed on the graphite.

Targets of tungsten and tantalum were used in an attempt to find a substrate that would erode less rapidly. While these metals showed less erosion than the graphite target, they produced a spectrum which was dominated by emission lines of the target. The ablation of these targets beneath the surface of the solution also clouded the solution which in some cases caused particle-induced breakdown to occur above the substrate surface.

The next substrate to be examined was a graphite filled teflon. This substrate showed less erosion than the graphite substrate. Moreover, only the carbon line at 247 nm and some weak CN emission around 388 nm were apparent in the spectra of the submerged substrate. Lastly, the ablation of this substrate produced less clouding of the solution than ablation of the metal targets. This substrate was the one used in generation of analytical curves for Na and Mg in water.

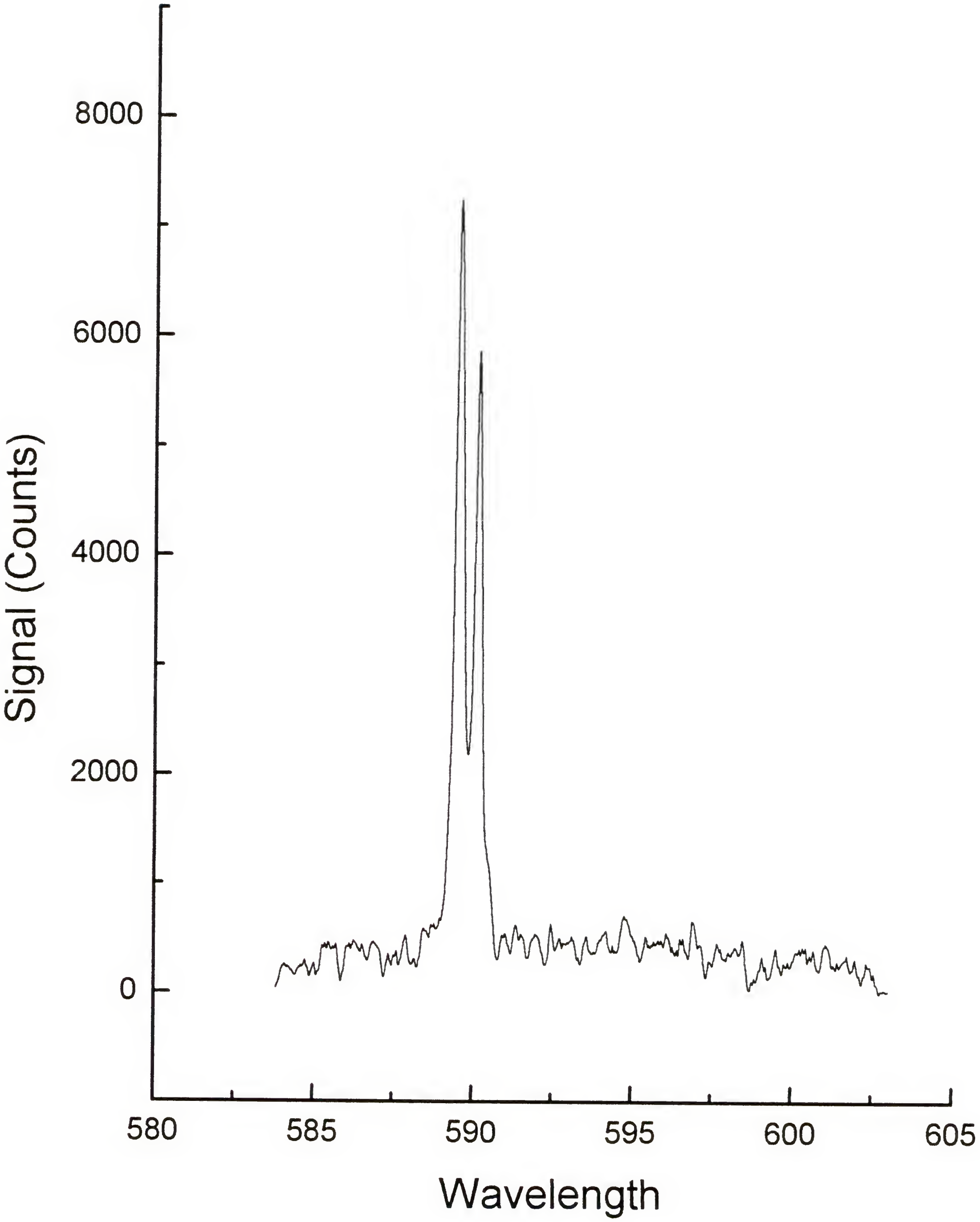

Figure 4-4. Spectra of 100 ppm Na in water taken by forming breakdown on submerged graphite substrate.

Figure 4-5 and 4-6 are calibration curves for sodium and magnesium in water using the submerged graphite filled teflon as a substrate on which to produce a plasma. One determination consisted of the average of 30 shots. Error bars represent one standard deviation between these 30 shot averages.

Conclusions

Laser-induced breakdown spectroscopy of aqueous solutions without the use of a repetitive spark is best performed by submerging a substrate in the solution to be analyzed and forming the laser-induced plasma on this substrate. This technique allows for reproducible location of plasma formation and creates a minimum of physical disturbance in the solution being analyzed.

Graphite filled teflon is a suitable material for the submerged substrate. It shows minimal erosion, contributes few spectral features, and introduces only a minimal amount of particulate into the solution being analyzed. Calibration curves for sodium and magnesium taken using this material as a substrate indicate that detection limits of a few ppm are obtainable.

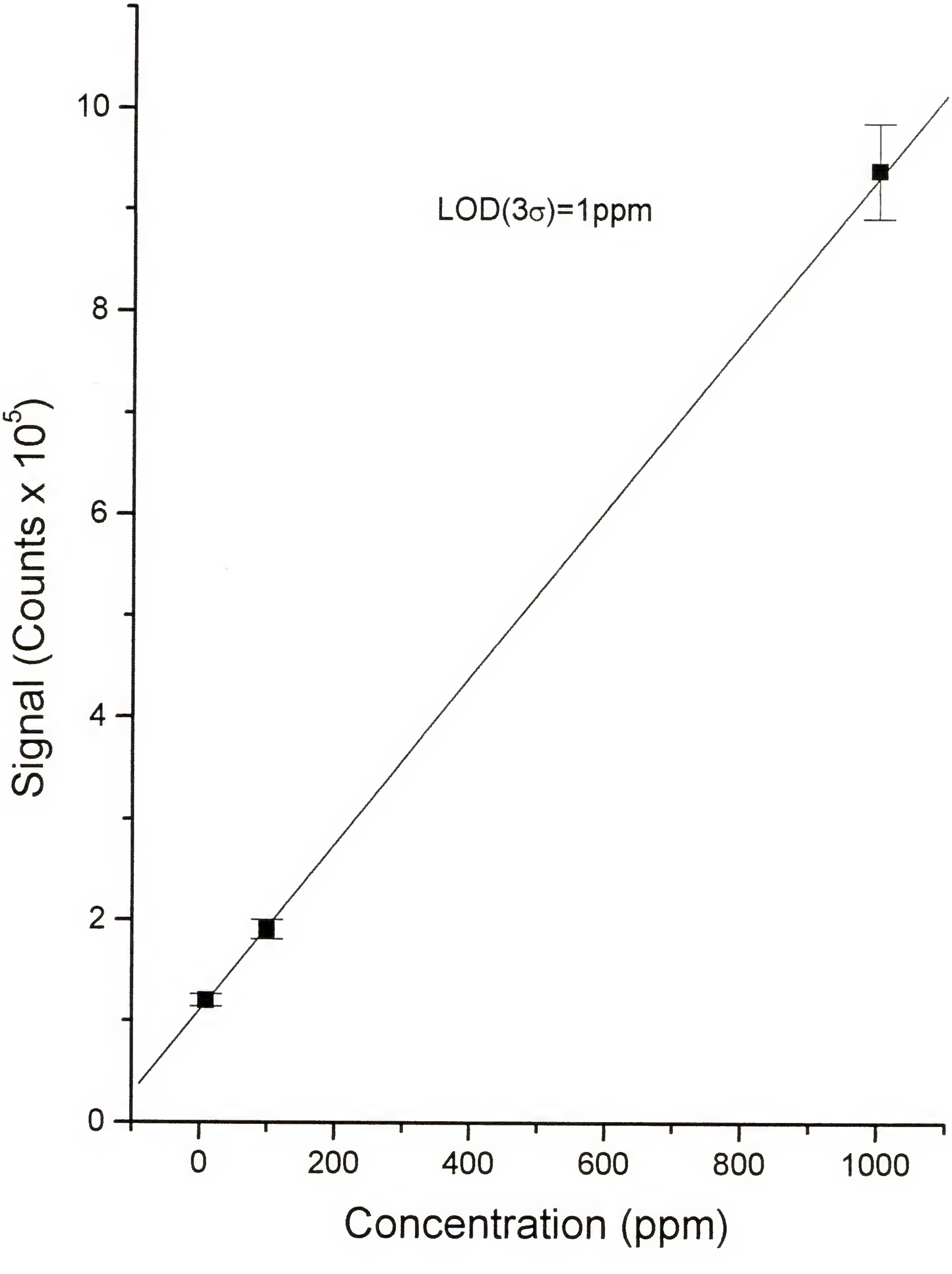

Figure 4-5. Calibration curve for Na in water using breakdown on submerged graphite-filled teflon.

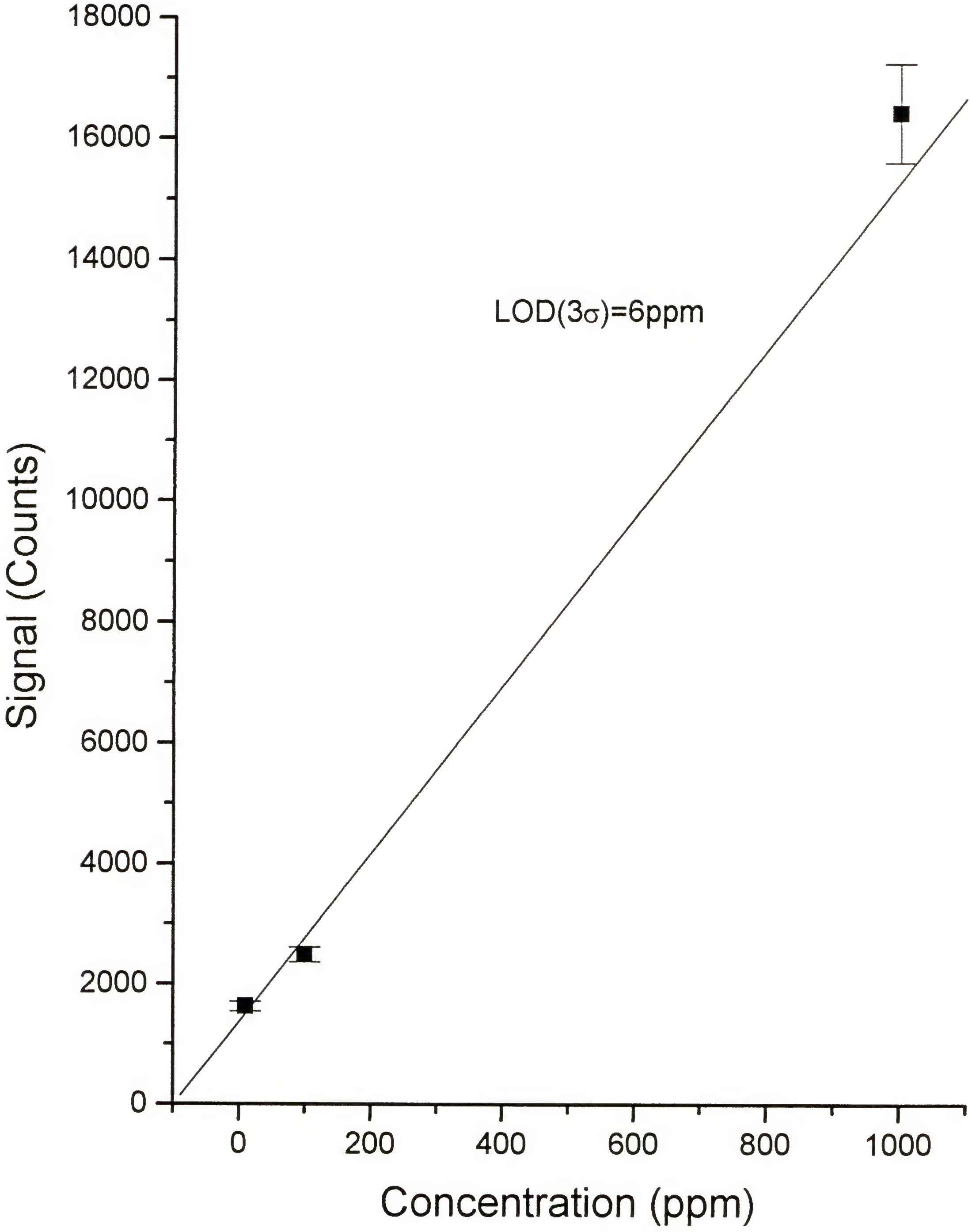

Figure 4-6. Calibration curve for Mg in water using breakdown on submerged graphite-filled teflon.

CHAPTER 5

USE OF A FIBER OPTIC LIBS PROBE TO DETERMINE TEMPORAL EVOLUTION OF ELECTRON NUMBER DENSITIES IN LASER-INDUCED PLASMAS ON METALS

Construction of the Fiber Optic Probe

A number of techniques in analytical chemistry have been performed with fiber optic probes formed by coupling of a laser beam into a fiber optic. Raman spectroscopy is the most common example. This technique has been performed through bifurcated fiber optics which use a large central fiber to carry the excitation light from the laser to the sample and a number of smaller fibers to carry emission light from the sample to a spectrometer.[146-150]

The construction of a laser-induced breakdown spectroscopy (LIBS) probe is more difficult for several reasons. First, the lasers used in LIBS are generally high power pulsed lasers rather than low power continuous wave lasers used in Raman spectroscopy. This means that larger fibers must be used to carry the excitation light. Second, because the power density (W cm^{-2}) at the sample surface varies inversely with the square of the radius of the spot size by

$$P_\rho = \frac{E}{\tau_p \pi r_s^{\,2}} \qquad (5\text{-}1)$$

where E is the pulse energy in J, τ_p is the pulse duration in s, and r_s is the spot size in cm^2, the excitation light emerging from the fiber optic must be focussed to as small a spot as possible to provide the maximum power density.

Because the laser light emerging from the fiber optic is no longer collimated, it is more difficult to focus than a laser beam. Smaller fibers can produce smaller spot sizes. However, because the maximum power that can be transmitted through a fiber varies with the square of the core radius, the power density at the sample is essentially unchanged. This implies that to achieve maximum power density at the sample, the fiber must be carrying as much power as possible.

Different fiber core materials perform better in different wavelength ranges. Figure 5-1 shows some typical transmission spectra of high-OH and low-OH fibers. Choosing the proper core material is essential in achieving maximum power output. Another property of the fiber which must be considered is the numerical aperture (NA). This number defines the maximum angle of incidence at which a fiber will accept light.

A few characteristics of the laser determine the maximum power that can be launched into a fiber. The pulse to pulse reproducibility becomes a factor because any single pulse of anomolously high power can damage the fiber optic. It is desirable that the laser operate just below the maximum power that the fiber can carry with no pulses of power greater than the fiber can carry.

Another laser characteristic that is important in launching a beam into a fiber optic is the beam profile. A flat-top profile is desirable because with this profile no single portion of the beam is more intense than any other. When more intense regions, or hot

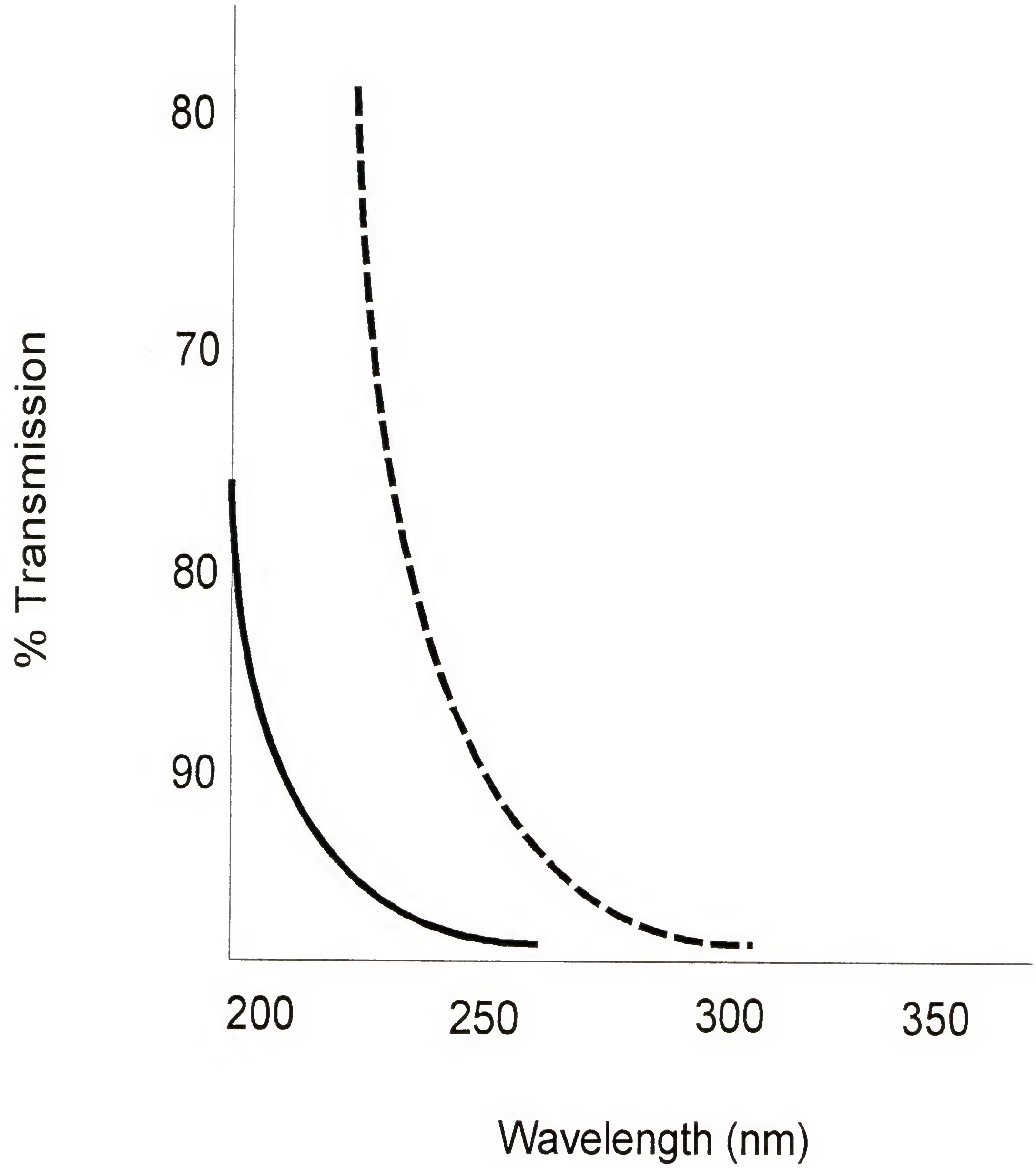

Figure 5-1. Transmission of high-OH (—) and low-OH (---) fiber cores.

spots, exist, they can damage the fiber optic long before the peak power throughput is obtained. For convenience, a nearly Gaussian beam is usually used in coupling a laser into a fiber. When the profile is smooth there is less danger of damaging the fiber. Nevertheless, several devices for converting various beam profiles into flat-top profiles have been described in the literature.[151-154] Figure 5-2 shows some of these devices.

Another tecnnique for reducing the risk of damaging the fiber is coupling the laser into the fiber under vacuum conditions. In the vacuum, breakdown thresholds are increased and the probability for a breakdown to occur at the fiber surface is reduced. This technique is commonly employed in laser drilling applications.[155,156]

In the experiment performed in our lab a Nd:YAG laser (1064 nm, 20 ns, Quantel, Santa Clara, CA) was coupled into a 1000 μm low-OH fiber with a numerical aperture of 0.22. This fiber was part of a bifurcated assembly (Multimode, Meutchen, NJ) which contained 12-200 μm high-OH fibers surrounding the 1000 μm excitation fiber at one end, and terminated in a slit configuration for introducing light to the spectrometer at the other end. In order to achieve an approximately flat beam profile, the center of the Gaussian profile was isolated by use of a 3 mm aperture. The focusing lens had a f/n of 4 which gave an incident angle of ~15 ° at the face of the fiber. This was slightly larger than the maximum incident angle the fiber would accept, which was 12.7 °. A schematic of the laser launching setup is shown in figure 5-3.

A collimating and a focusing lens both with a focal length of 25.4 mm were placed at the common end of the fiber and held in a small metal cylinder. These lenses served to focus excitation light from the central fiber onto the target, and to collect light emitted

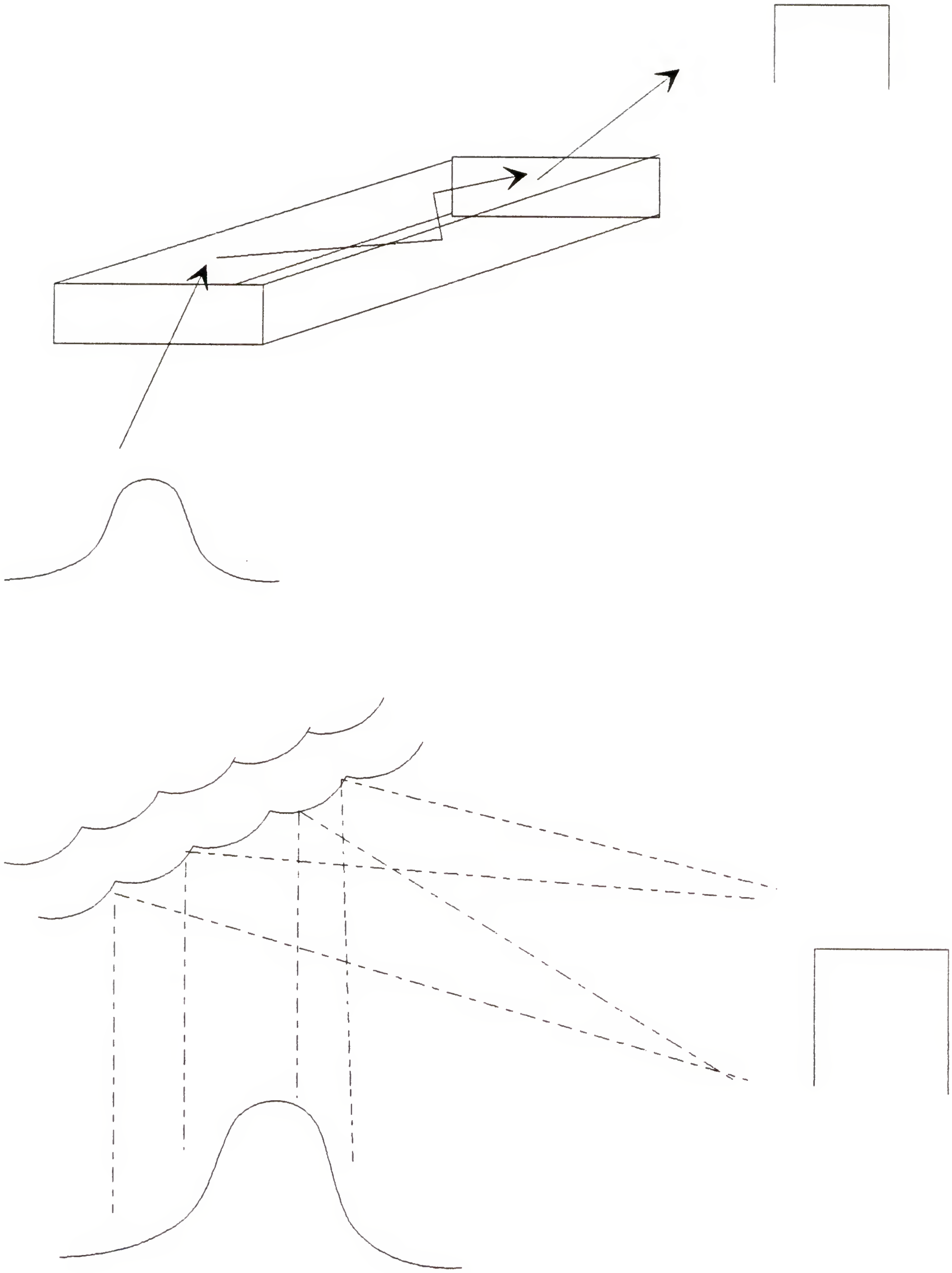

Figure 5-2. Devices for creating flat-top beam profiles. In the top device an incoming laser beam undergoes multiple reflections within a four-sided tunnel to homogenize the beam profile. In the lower device a large number of convex mirrors magnify small portions of the beam to the size of the entire beam effectively averaging the beam profile.

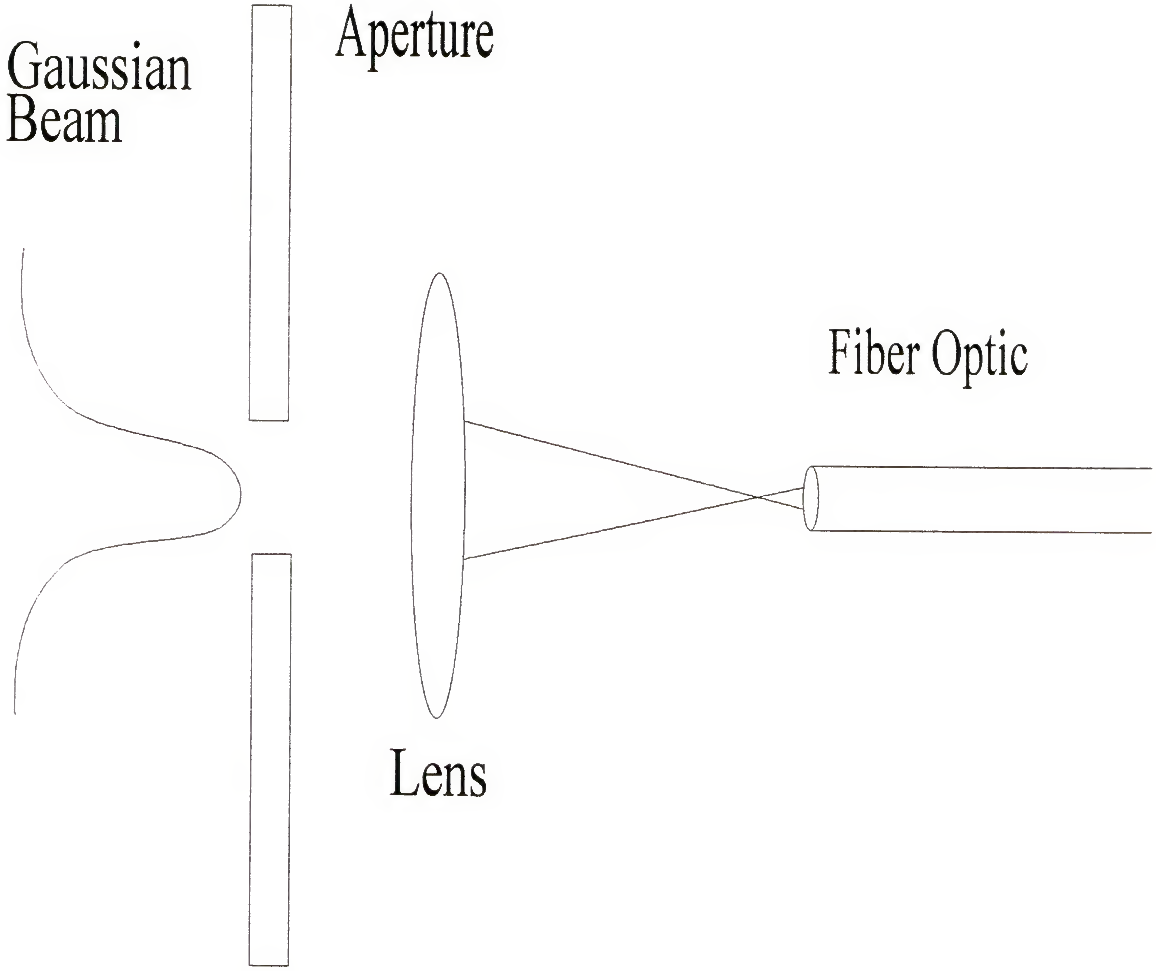

Figure 5-3. Setup for coupling pulsed Nd:YAG laser into a fiber

from the laser-induced plasma and focus it into the smaller fibers which terminated at the entrance slit to the spectrometer. A schematic of the common end of the fiber is shown in figure 5-4.

With this arrangement ~50 mJ could be passed through the fiber and focused to a spot of 1 mm diameter. Referring to equation 5-1, this gives a power density of 318 MW cm^{-2} at the sample surface. This is sufficient power to produce breakdown on most solid targets at atmospheric pressure.

To assure that the excitation/collection geometry of the probe remained constant, a plastic extension was fitted to the end of the probe head. In order to take a measurement, this extension was pressed flush against the sample surface, thus assuring the correct lens to sample distance and incident angle. A spectrum of stainless steel obtained with the fiber optic probe is shown in figure 5-5.

Measurement of Temporal Electron Number Density Evolution in Laser-induced Plasmas on Metals

Introduction

Because the thermal and electronic properties of pure metals are well known, using these metals as targets for laser-induced breakdown spectroscopy provides a way to investigate which of these properties or combination of these properties influence plasma parameters such as electron number density.

Electron number density measurements have been made in several different types of plasmas.[18,46,135] The measurement is important because it allows calculation of the ion to atom ratio using the Saha equation as described in chapter 1.

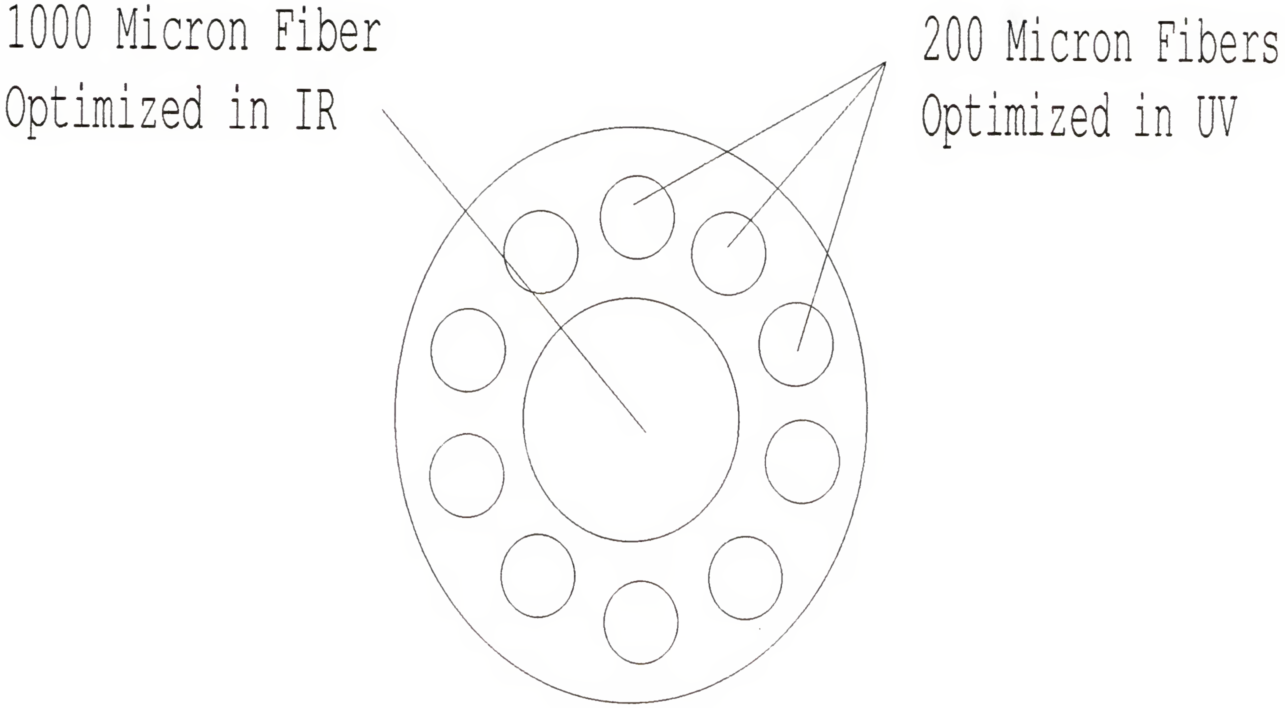

Figure 5-4. Common end of fiber optic LIBS probe

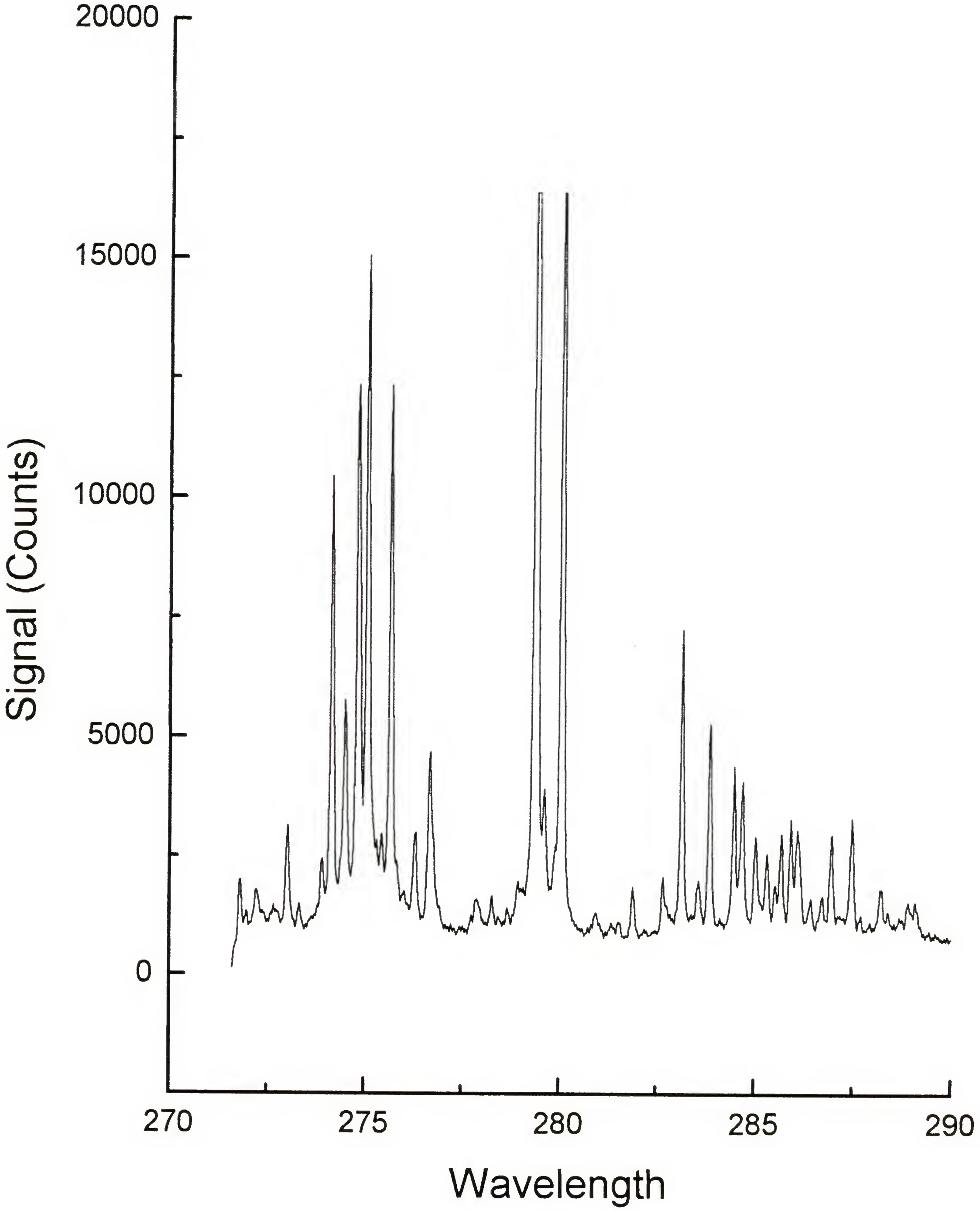

Figure 5-5. Single shot spectra of stainless steel obtained with fiber optic LIBS probe

In this study the temporal evolution of electron number density during the first 2 μs after the laser striking the target is determined for targets of aluminum, zinc, and lead. An attempt is made to correlate the number densities found to properties of the metals. Some properties of Al, Pb, and Zn which are relevant to the laser-material interaction are summarized in figure 5-6.

Experimental

The detector and pulse generator used in the experiment are the same as previously described. In order to measure electron number density evolution in the plasmas produced on metal, the gate width was set to 250 ns, and the gate delay was varied by multiples of 250 ns. The width of the Hα line at 656.56 nm was averaged over 10 shots, and calculation of the electron number density was carried out as described in chapter 1.

Results and Discussion

The temperature in the plasma formed on the lead target, determined by a Boltzmann plot was found to be 10000 ± 1500 K. The Boltzmann plots for Al and Zn targets were difficult to prepare because different spectral windows had to be used in order to observe emission lines from a variety of upper energy levels. Due to variance in detector sensitivity in different spectral windows and to deviation from local

Property Element	Thermal Conductivity W m^{-1} K^{-1}	Molar Heat Capacity a,b* J K^{-1} mol^{-1}	Melting Point °C	Boiling Point °C	Latent Heat of Fusion kJ mol^{-1}	Latent Heat of Vaporization kJ mol^{-1}	Density g cm^{-3}	Work Func. eV
Al	238	4.94 2.96	660.1	2520	10.47	290.9	2.70	5.986
Pb	34.9	5.63 2.23	327.4	1750	4.81	178.8	11.68	7.416
Zn	119.5	5.35 2.40	419.5	907	7.28	114.3	7.14	9.394

Figure 5-6. Selected properties of Al, Pb, and Zn

thermodynamic equilibrium, the Boltzmann plots for Al and Zn targets could not be used to determine a temperature. A temperature of 10000 K was used to calculate electron densities on these targets as well. In figure 5-7 it can be seen that the electron number density *vs* $\Delta\lambda$ curves are similar for temperatures of 5000, 20000, and 40000 K, therefore this assumption will not significantly affect the calculated value.

Figure 5-8 shows the temporal evolution of electron number density on the three targets at 250 ns intervals fit with first-order exponential decay. The Zn target, which has the highest ionization potential, shows the lowest electron number densities at all times up to 2 μs. However, Pb which has a higher ionization potential than Al, shows the highest electron number density. Ionization potential alone does not account for differences in plasma electron densities.

The Pb target shows the highest electron number densities, highest density, and lowest thermal conductivity. However, the ratio of density to thermal conductivity cannot predict the correct order of electron number densities either. The Zn target with a density and thermal conductivity which fell between Pb and Al showed the lowest electron number density.

Conclusions

It is apparent that properties of a metal such as melting point, boiling point, density, and ionization potential are not sufficient to describe the laser-material interaction. One parameter which has not been included in the analysis is the absorption of the sample at the wavelength of the laser. Because this parameter affects the energy deposited into the sample it can also affect plasma formation.

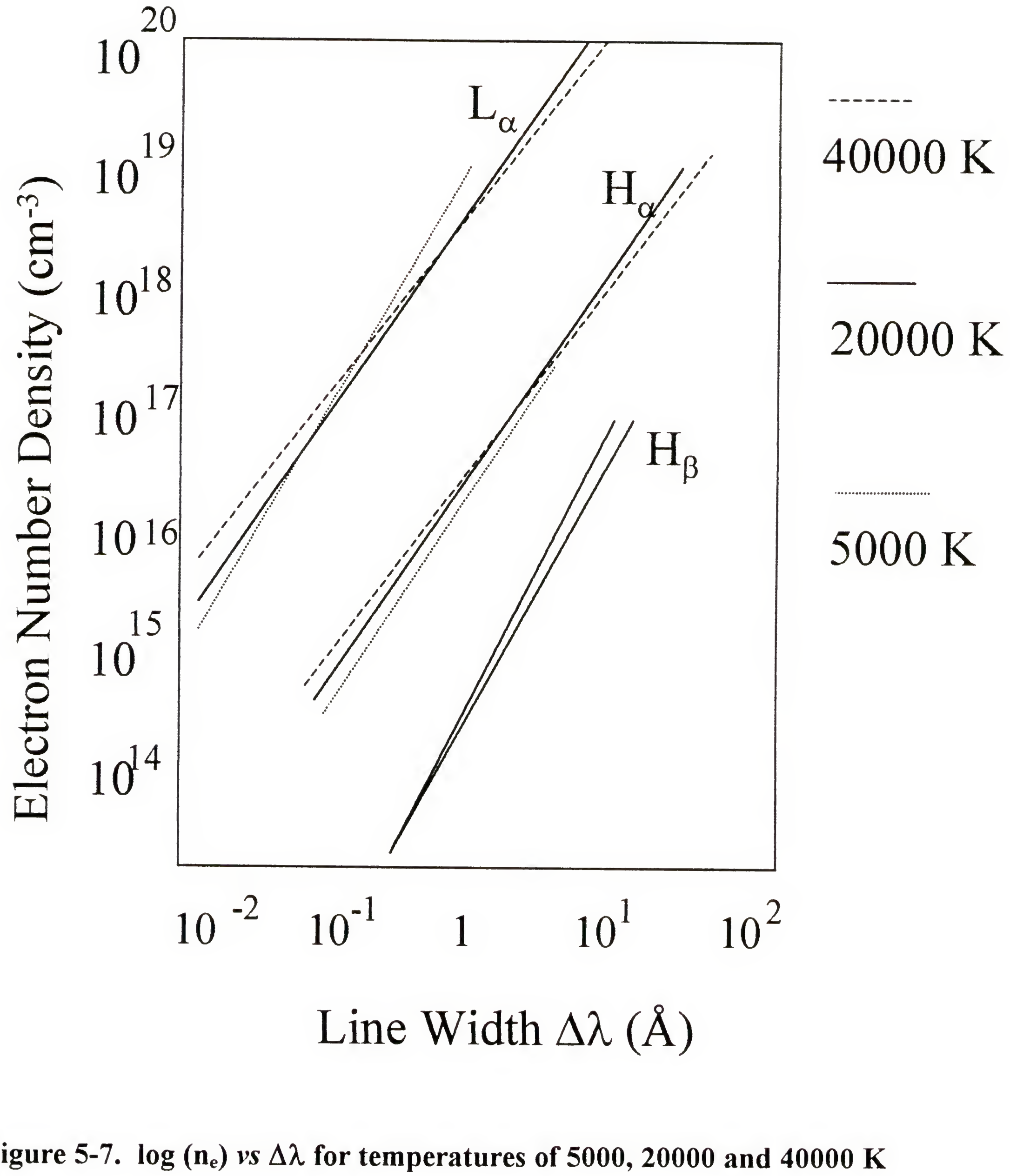

Figure 5-7. log (n_e) *vs* Δλ for temperatures of 5000, 20000 and 40000 K

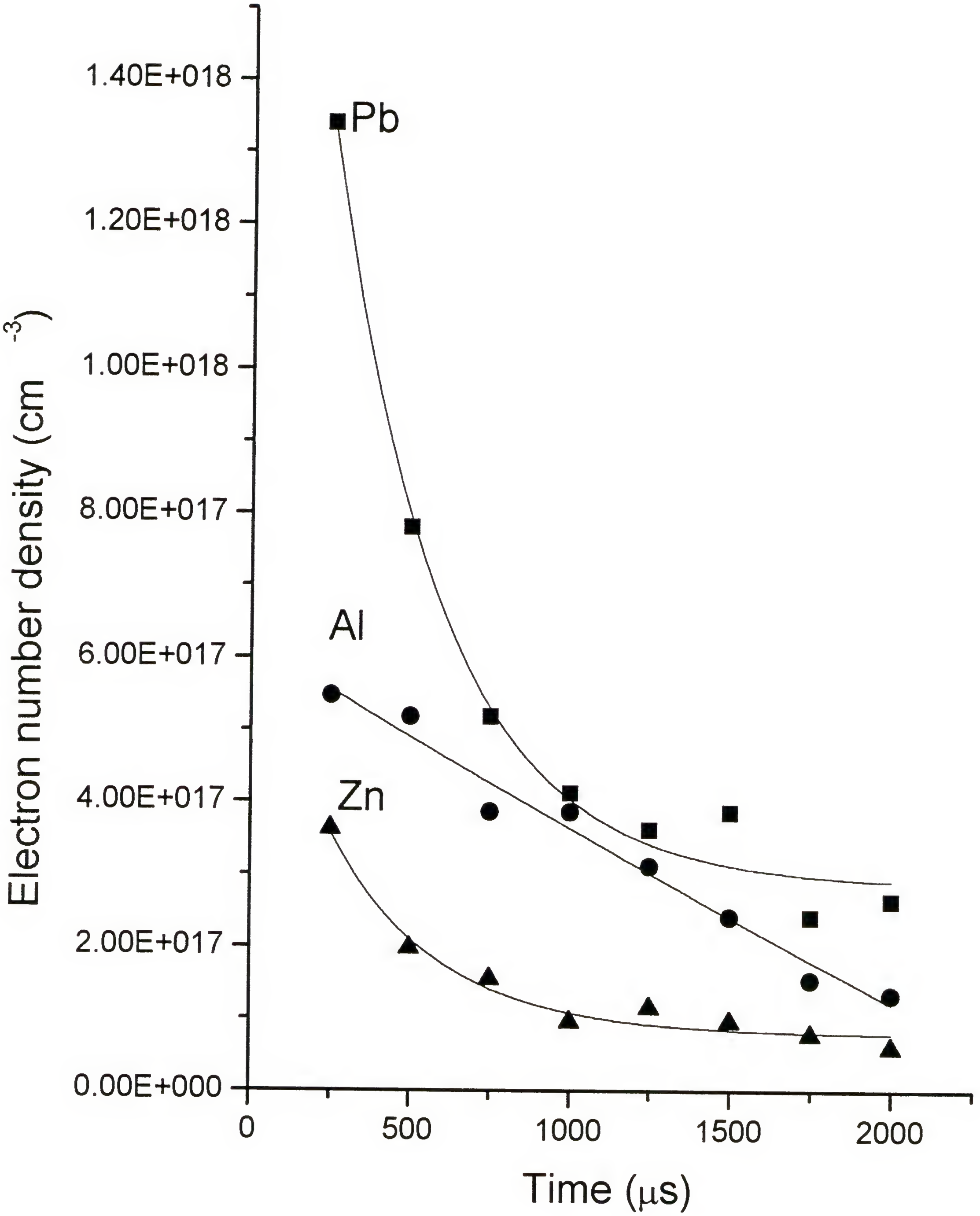

Figure 5-8. Temporal evolution of electron number density on targets of Al, Pb, and Zn

The construction of the fiber optic probe was successful and provided a convenient means for performing laser-induced breakdown spectroscopy on the metal targets. A maximum energy density of 318 MW cm^{-2} was reached at the sample surface by excitation through a 1000 μm fiber. The 200 μm fibers surrounding the excitation fiber effectively collected light and carried it to the spectrometer. Intense, well resolved spectra could be obtained.

CHAPTER 6

EXCITATIONAL, VIBRATIONAL, AND ROTATIONAL TEMPERATURES IN Nd:YAG AND XeCl LASER-INDUCED PLASMAS

Introduction

Laser-induced plasmas formed on graphite by a Nd:YAG laser at 1064 nm and by a XeCl laser at 308 nm were analyzed spectroscopically to determine vibrational, rotational, and excitation temperatures. For determination of vibrational and rotational temperature, the emission of the CN radical in the region between 385.1 and 388.3 nm was used to construct Boltzmann plots. Relative vibrational transition probabilities were calculated. For determination of excitation temperature, a small amount of lead or iron was added to the graphite target and Boltzmann plots were constructed using transition probabilities found in the literature.

In a laser-induced plasma, “temperature” most often refers to excitation, or electronic, temperature. This temperature is a measure of the distribution of atomic or ionic populations within the source and is often used as a quantitative means of comparing different atomic emission sources. The excitation temperature is determined from relative intensities of emission lines, the energy levels from which they originate, and the corresponding transition probabilities.

Molecular spectroscopy has been used to determine vibrational and rotational temperatures in a variety of sources used for atomic emission. Spectra of species such as OH, CN, and N_2^+ can be obtained from a number of sources, and the force constants and equilibrium bond lengths for different excited levels of these molecules are well known. For this reason, they are the most commonly chosen molecules for use in vibrational or rotational temperature determinations.

When the observed plasma volume is in local thermodynamic equilibrium (LTE), the excitation temperature should equal the vibrational, rotational, kinetic, and thermal temperature of the plasma. In an often cited publication, Radziemski *et al.* concluded that local thermodynamic equilibrium was established in the laser plasma created by ablation of aerosols with a Nd:YAG laser (1064 nm, 10 ns pulse duration, 50-300 mJ/pulse) after a time delay of 1 μs relative to the laser pulse.[99] They determined time resolved temperatures ranging from 22000 to 8000 K during the plasma decay.

Relatively few studies have been done comparing excitation, vibrational and rotational temperatures in a laser plasma, and comparison of experiments by different authors is difficult because there is inevitably more than one variable. Laser wavelength and energy density at the target, target composition, the spatial and temporal region of the plasma observed, and the specific atomic and molecular transitions observed are some of the more important parameters that can vary. In the present work, laser wavelength and energy density are chosen as the only two variables and a study of excitation, vibrational, and rotational temperatures produced by irradiation of a graphite target is made.

Background

In order to calculate an excitation temperature, the intensity of atom or ion lines of one element which originate from different upper energy levels and have accurately known transition probabilities must be determined. The excitation temperature can then be obtained by a Boltzmann plot of ln ($I\lambda/gA$) *vs* E_i where I is the relative intensity of the observed transition, λ is the wavelength, A is the transition probability, g is the degeneracy of the upper energy level, and E_i is the energy level of the upper state (cm^{-1}). The slope of this plot will then be equal to (hc/kT).

Several authors have determined excitation temperatures by this method in laser-induced plasmas using various lasers on a variety of solid samples. Mao *et al.* determined a temperature of between 6000 and 11000 K for a plasma formed on a copper target by a KrF excimer laser (248 nm, 30 ns pulse, ~20 mJ/pulse).[157] Castle *et al.* found temperatures close to 10000 K using a Nd:YAG (1064 nm, 15 ns pulse, ~200 mJ/pulse) on a lead target.[158] Sabsabi *et al.* used iron lines to determine time resolved temperatures in the plasma produced by a Nd:YAG laser on alloys and determined a temperature of 6700 K after a rapid initial decrease,[64] and Kagawa *et al.* used a XeCl laser (308 nm, 20 ns pulse 15 mJ/pulse) on a zinc target and found a temperature of 9000 K at low pressure.[28] Typical values for the excitation temperature were 6000-15000 K in the spatial and temporal portion of the plasma used for analytical measurements.

The determination of vibrational temperature requires that the relative populations of the upper energy levels (v') be known. The population of a given level can be deduced by either summing the intensity of all transitions which occur from that level, or by observing one transition from that level for which an accurate transition probability is known or can be calculated. With knowledge of the populations, vibrational Boltzmann plots are constructed and vibrational temperatures are determined.

Vibrational transition probabilities are calculated from wavefunctions of the upper and lower quantum state of the transition of interest. The overlap integral of the two wavefunctions is written as[159]

$$S_{m,n} = \int_{-\infty}^{\infty} \psi_m(R)\psi_n(R)dR \qquad (6\text{-}1)$$

where ψ_m is the wavefunction for the upper level (v') of the transition and ψ_n is the wavefunction for the lower level (v) of the transition. The wavefunctions themselves are given by

$$\Psi_\nu = N_\nu H_\nu(y)e^{-y^2/2} \qquad (6\text{-}2)$$

with

$$N_\nu = \left(\frac{1}{\alpha\pi^{1/2}2^\nu \nu!}\right)^{1/2}, \qquad (6\text{-}3)$$

$$\alpha = \left(\frac{\hbar}{mk}\right)^{1/4} \qquad (6\text{-}4)$$

where k is the force constant (J/m) for the molecule, and

$$y = \left(\frac{R - R_e}{\alpha}\right) \qquad (6\text{-}5)$$

where R_e is the equilibrium internuclear distance (m). H_v is the Hermite polynomial which satisfies the equation

$$H_v'' - 2yHv' + 2vH_v = 0 \qquad (6\text{-}6)$$

and the recursion relation

$$H_{v+1} = 2yH_v - 2vH_{v-1} \qquad (6\text{-}7)$$

The square of the overlap integral $(S_{m,n})^2$ can then be used as the relative transition probability in preparing a Boltzmann plot.

Rotational temperature determination requires that a single vibrational band be resolved into its individual rotational components. The intensity of each of these components must then be determined and each peak must be assigned a rotational quantum number (J). A plot of ln (I/2J+1) *vs* J(J+1) gives a slope equal to (Bhc/kT). When the rotational molecular constant (B) is known, the rotational temperature can be determined. Alternatively, the observed rotational spectra can be fit with a model in which temperature is a parameter.

High resolution spectra of OH in a flame have been used to determine spatially resolved rotational temperatures,[160] and N_2^+ and OH emission have been used to determine both vibrational and rotational temperatures in microwave and inductively coupled plasmas.[161,162] In direct current arcs and in laser-induced plasmas, CN emission has been used to determine rotational and vibrational temperatures.[34,35,108,163]

The CN band was used by Parigger *et al.* to determine vibrational temperature of the plasma produced by a Nd:YAG laser breakdown in carbon monoxide. By fitting the experimental spectra with a model, they determined a temperature of 6000 K which was in agreement with the vibrational temperature determined using C_2 emission.[108]

Studies of graphite ablation with a Nd:YAG laser (1064 nm, 7 ns pulse duration, 240 mJ/pulse) by Hatem *et al.* using CN emission in the spectral range 415.2 to 421.6 nm have shown excitation, vibrational and rotational temperatures all near 9000 K.[34] In contrast, the plasma formed by excimer laser irradiation (351 nm, 20 ns pulse duration, ~100 mJ) of polyimide showed a rotational temperature of only about 800 K as determined by Dreyfus *et al.* using CN emission.[35]

This large temperature discrepancy is probably caused by the different mechanisms by which the excited CN radical is formed. Ablation of the polymer forms CN radicals by decomposition, whereas ablation of the graphite forms highly excited CN by combination of carbon radicals with atmospheric nitrogen.

The kinetic temperature in a laser plasma has also been calculated by using laser-induced fluorescence to determine the velocity of the expanding laser plume.[35] The kinetic temperature was determined from the relationship

$$\mathrm{kT} = \frac{1}{\eta}\left(\frac{1}{2}\,\mathrm{mv}^2\right) \qquad (6\text{-}8)$$

where v is the velocity of the expanding plume (m/s), m is the mass of the molecule observed (kg), and η is a measure of the internal degrees of freedom of the molecule observed (dimensionless). A temperature of between 4600-10000 K was determined for a graphite plasma using C_2 as an indicator, and a value of 34000 K was found for a plasma on polyimide using CN as an indicator.

In our laboratory, images of a laser-induced plasma on lead and tin targets have been obtained by using an unfocused dye laser tuned to an appropriate atomic transition to illuminate the region in which the plasma forms. Absorption of the dye laser beam by neutral atoms in the plasma produced a shadow-like image. Time resolved measurements taken in this way showed that the plasma plume formed on a lead target was expanding at about 1500 m/s during the first 2 μs following ablation laser impact. This velocity corresponded to a kinetic temperature of 9400 K.

Experimental

The experimental setups used for the experiments at 1064 and 308 nm have been described previously by Castle[158] and Gornushkin,[165] respectively, and are summarized in Figure 6-1. All experiments were carried out in air at atmospheric pressure. Spot size at the sample was measured for both the Nd:YAG and XeCl lasers. The Nd:YAG laser spot was larger (900 μm) than the XeCl laser spot (400 μm). Thus, at the same pulse energy, the energy density at the sample was greater for the XeCl laser setup than for the Nd:YAG setup. In the experiments done using equal energy density from both setups, this difference in spot size was accounted for by adjusting laser energy.

The spectra taken on the Nd:YAG setup were acquired with sufficient resolution to determine intensities for the first 10 rotational levels of the R branch in the (0-0) vibrational level. The resolution was approximately 20 pm. With the spectrometer used

Component	**1064 nm**	**308 nm**
Laser	Laser Photonics YQL-102+, Nd:YAG, 1064 nm, 15 ns pulse	Lambda Physics LPX100, XeCl, 308 nm, 15 ns pulse
Spectrometer	Acton Research SP-500, 0.5 m focal length	Thermo-Jarrel Ash 82020 0.33 m focal length
Detector	Princeton Instruments ICCD-576S	Princeton Instruments IRY-1024
Pulse Generator	Princeton Instruments PG-200	Princeton Instruments FG-100
Stage	UniSlide X, Y, Z Computer controlled	Modified syringe pump
Focusing Lens	25 mm diameter, 305 mm focal length	25 mm diameter, 100 mm focal length

Figure 6-1. Experimental Components for Experiments at 1064 nm and 308 nm

on the XeCl setup, the resolution was approximately 100 pm and rotational intensities could not be determined.

All spectra except those taken for the time resolved study were acquired with a delay of 2 μs and a gate width of 2 μs. The light was collected by focusing the middle of the roughly spherical plasma onto the entrance slit of the spectrometer in both setups and at all power densities. Each spectra was composed of 20 accumulated laser shots on a stationary target.

Samples were prepared by pressing ~0.75 g of graphite powder into a 13 mm pellet with a pressure of 6000 kPa. The pellets were approximately 3 mm thick. For the studies of excitation temperature, either Fe_2O_3 or PbO was mixed with the powder, 10% by weight before pressing.

Excitation temperatures were calculated using two different series of emission lines. The first series was based on iron emission and had been used previously by Sabsabi for excitation temperature determination.[64] The second scheme was based on lead emission and had been used previously by Castle.[158] These series of lines were chosen because they were well resolved, fell in a narrow spectral region, originated from a variety of upper energy levels, and had accurately known transition probabilities. The temperature was determined for each series from the slope of the Boltzmann plot.

For the calculation of vibrational temperature, the ($B^2\Sigma^+ \rightarrow X^2\Sigma^+$) CN transitions with $\Delta v=0$ were observed in the spectral region from 385.1-388.3 nm, and transition probabilities were calculated for each observed transition as described above. This approach was chosen to avoid the problem of varying sensitivity at different wavelengths which would cause error when attempting to sum the intensities of transitions in different spectral regions. The relative probabilities found were: (0-0) 0.994, (1-1) 0.975, (2-2) 0.981, and (3-3) 0.966.

Rotational temperature determination could be accomplished only on the setup with the Nd:YAG laser. Using the high resolution grating (3600 grooves/mm), the (0-0) vibrational transition of CN with bandhead at 388.1 nm was observed with a resolution of about 20 pm. At this resolution, the first 10 bands of the R branch were sufficiently resolved so that intensity values could be determined from the areas under each peak. A plot of ln (I/2J+1) *vs* J(J+1) was made and the temperature was determined from the slope of this line using a rotational molecular constant B=1.97 given by Herzberg.[167]

Results and Discussion

Figure 1 is the CN emission spectra from 384.5 to 388.3 nm. The intensities of the vibrational transitions were determined by integrating the entire vibrational band. The (0-0) band was integrated from 387.2-388.3 nm, the (1-1) band was integrated from 386.2-387.2 nm, the (2-2) band was integrated from 385.5-386.2 nm, and the (3-3) band was integrated from 385.1-385.5 nm. Rotational intensities were determined by viewing only the region from 387.1 to 388.3 and peakfitting the first 10 transitions. Rotational quantum numbers were assigned by comparing position of the observed transitions to spectra found in Herzberg.[167]

The Boltzmann plots for rotational temperature were not linear. Plots prepared from spectra taken at four different delay times are shown in Figure 2. Because there is no single value for the slope at any time delay, a single temperature cannot be inferred.

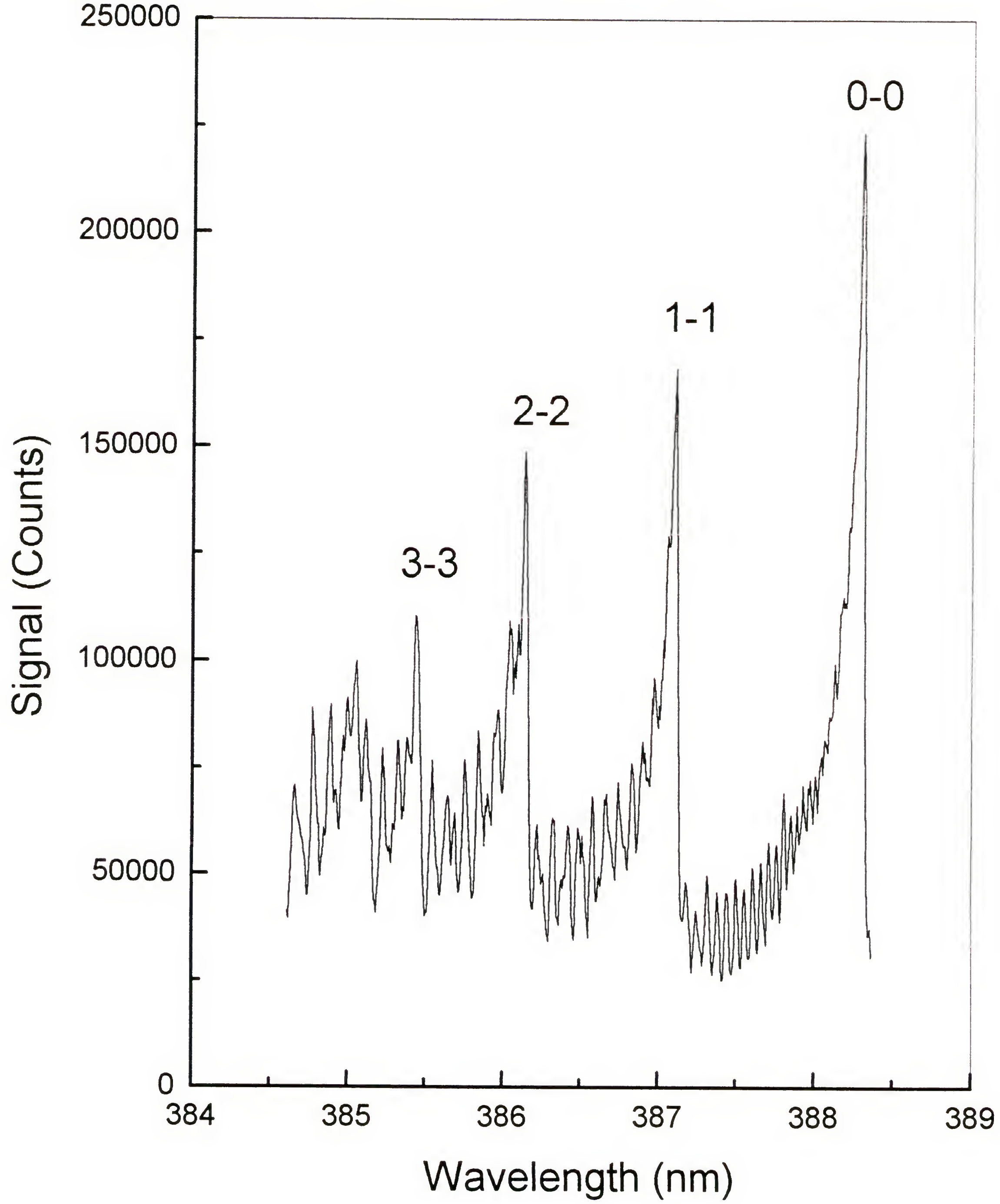

Figure 6-2. CN emission spectra from 384.5 to 388.3 nm. The (0-0), (1-1), (2-2), and (3-3) bandheads are labeled.

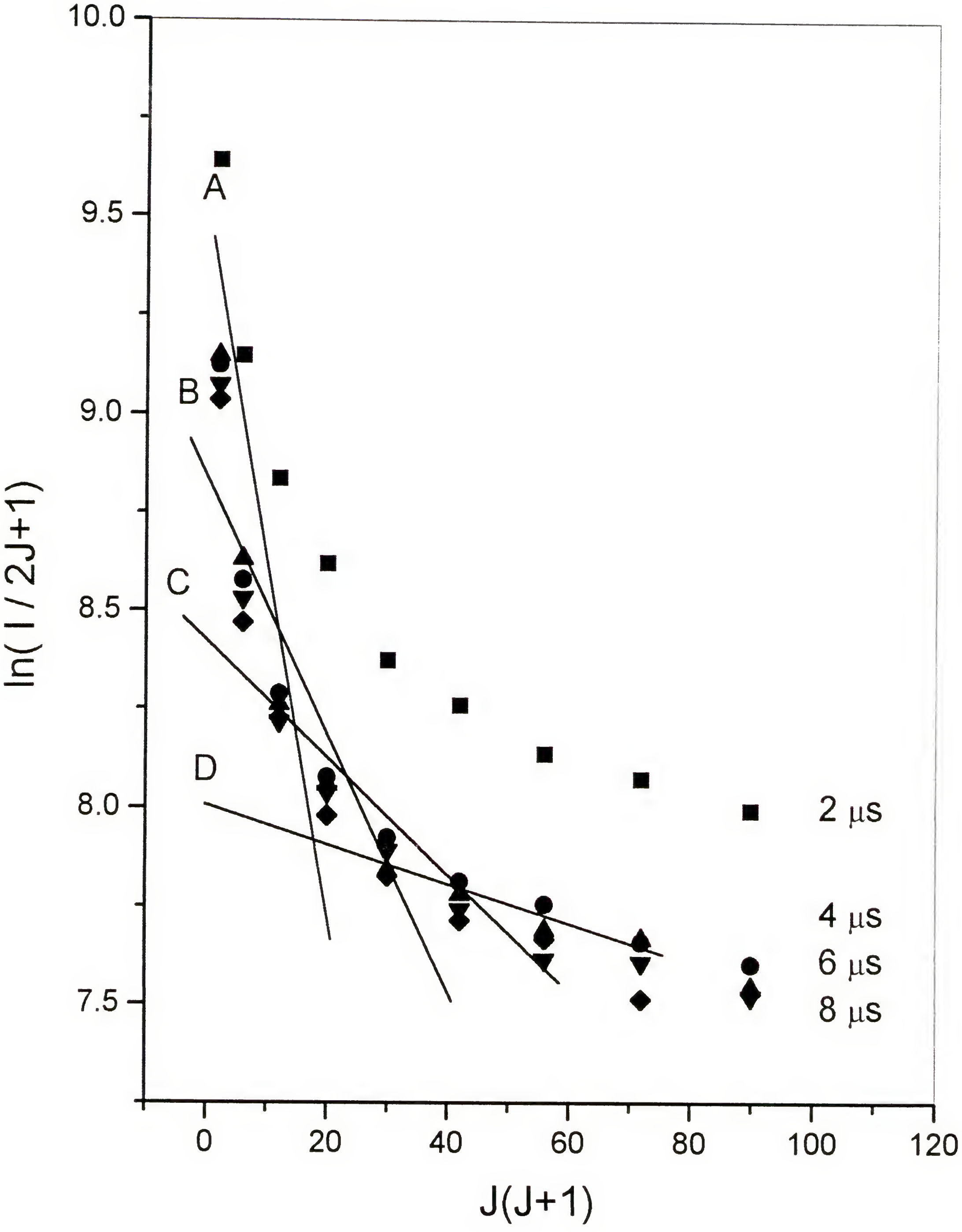

Figure 6-3. Boltzmann plots for the first 9 rotational levels of the R branch in the (0-0) vibrational band at delay times of 2, 4, 6, and 8 μs. The line segments labeled A, B, C, and D are tangents to the plot at increasing energies. The slope of segment A corresponds to a temperature of 5 K, B: 70 K, C: 140 K, and D: 560 K.

However, the shape of these plots is very similar to the shape of the plot observed in a supersonically cooled jet by Rehfuss *et al.* who explained the phenomenon by assuming two different mechanisms for formation of the excited CN radical.[166] These authors postulated that in a supersonic expansion, radicals could either be formed in the excited (B) state directly, in which case they would exhibit a “hot” rotational population distribution, or be formed in the ground (X) state and excited by electron impact, in which case they would exhibit a “cool” rotational population distribution. The shape of the Boltzmann plot reflected this multi-temperature distribution.

The expanding laser plasma is similar to the nozzle expansion into vacuum used by Rehfuss *et al.*,[166] and a similar argument may explain the multi-temperature rotational population distribution found within it. Line segments A, B, C, and D in Figure 2 all represent slopes in different regions of the Boltzmann plot and correspond to rotational temperatures of 5, 70, 140, and 560 K, respectively.

An example of the Boltzmann plots used to determine vibrational temperature is shown in Figure 3. All the plots were nearly linear, and temperatures could be easily determined from the slopes found from linear regression. The Boltzmann plots for excitation temperature for the two series of iron lines and the series of lead lines were also linear and gave temperatures which were in agreement with one another.

Figure 4 shows the temporal evolution of the excitation and vibrational temperature of the plasma produced by the Nd:YAG laser with an energy density of 1.6 GW cm^{-2} on a graphite target. The excitation temperature is the upper trace at ~10000 K After the first 2 μs, during which the temperature drops rapidly, both excitation and vibrational

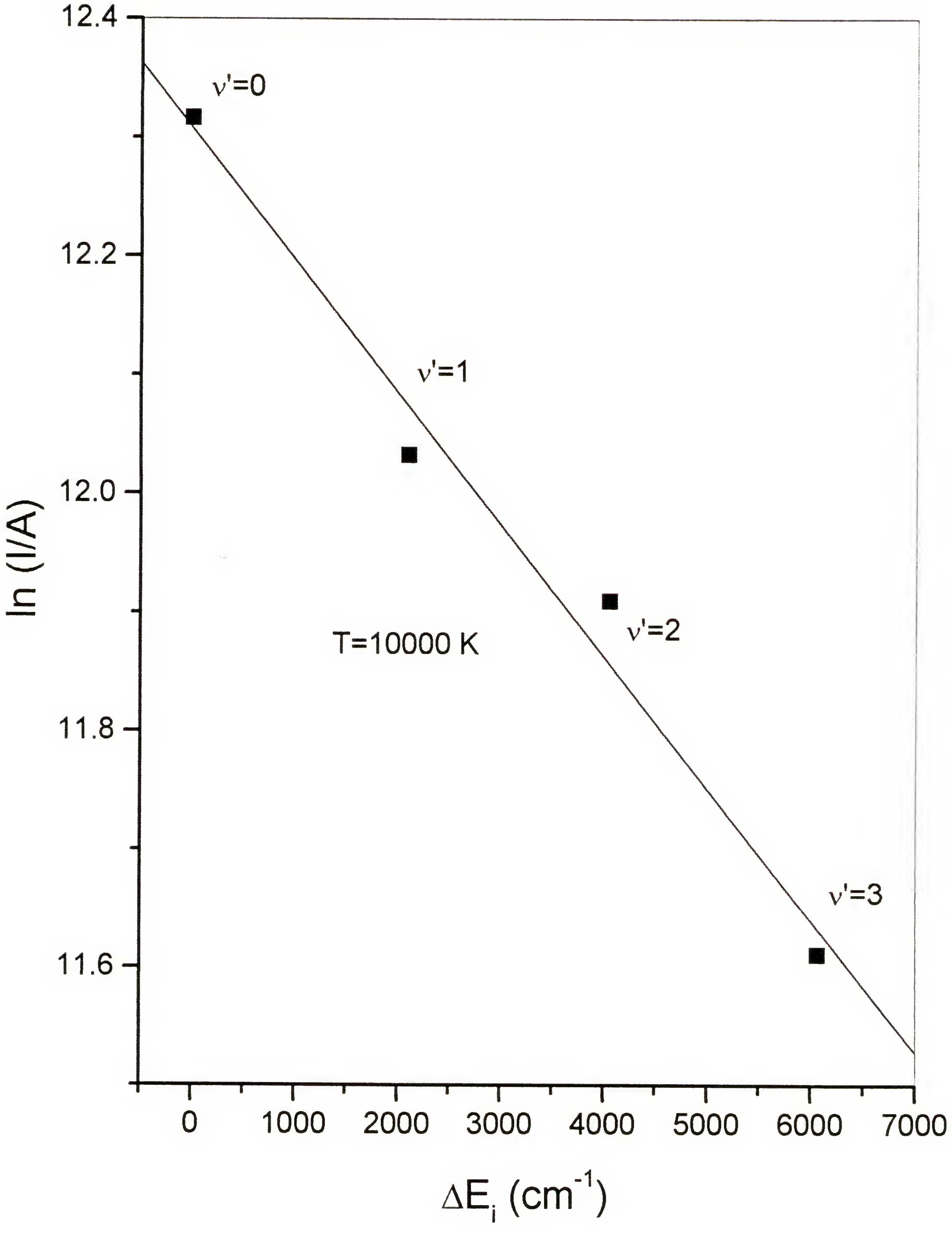

Figure 6-4. Boltzmann plot for vibrational levels (0-0), (1-1), (2-2), and (3-3) of the ($B^2\Sigma^+ \rightarrow X^2\Sigma^+$) CN transition observed in the plasma formed by a XeCl laser on a graphite target. The slope of this plot corresponds to a vibrational temperature of 13000 K.

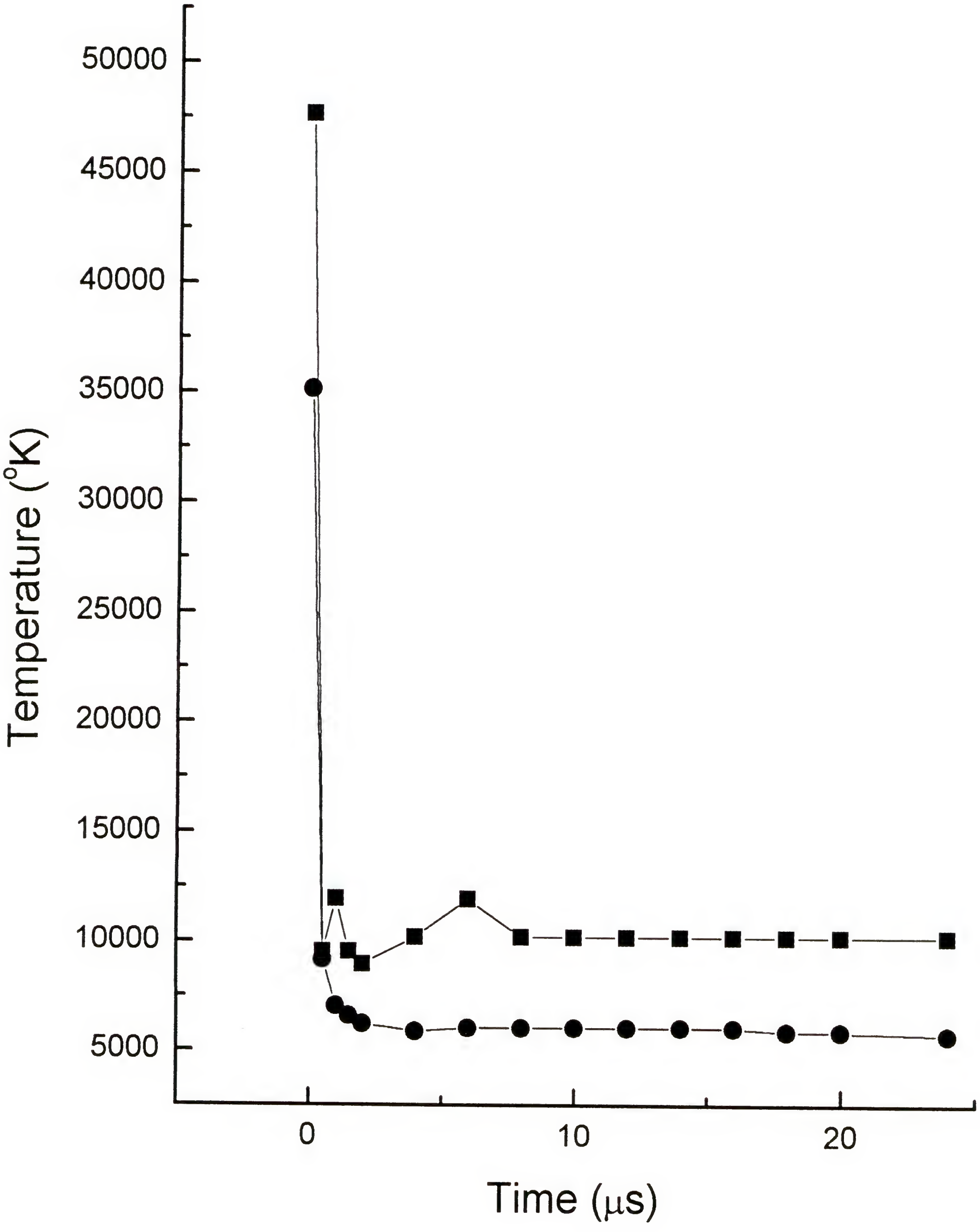

Figure 6-5. Temporal evolution of excitation (■) and vibrational (●) temperature in a plasma formed by a Nd:YAG laser on a graphite target.

temperature remain constant up to a time of at least 25 μs. For this reason, 2 μs was chosen as the delay time for determination of temperature at varying laser energy densities.

Figures 5 and 6 show the excitation and vibrational temperatures for plasmas produced on graphite by the Nd:YAG (1064 nm) and XeCl (308 nm) lasers at different energy densities. The excitation temperatures were found to be constant at all four energy densities observed. With the XeCl laser, the excitation temperature was ~20000 K while for the Nd:YAG the value was ~9800 K. The temperatures determined by the three series of lines were in good agreement. Error in the excitation temperature determination is due, in large part, to inaccurately known transition probabilities. The error bars for excitation temperature have been set at 15 %.

Vibrational temperatures for plasmas produced by both lasers decreased with increasing energy density. For the experiments at 308 nm, the vibrational temperature fell from a value of ~16000 K at 0.4 GW cm^{-2} to ~10000 K at 1.6 GW cm^{-2}. Vibrational temperature for plasmas produced by 308 nm were always less than the excitation temperatures over the energy density range used in this experiment. Error bars on the vibrational temperatures reflect the standard deviation in temperatures obtained from replicate measurements.

For plasmas produced by irradiation at 1064 nm, the vibrational temperature was roughly equal to the excitation temperature (~10000 K) at lower energy densities (0.4-0.8 GW cm^{-2}) and decreased to well below the excitation temperature (~6000 K) at higher energy densities. The decrease in vibrational temperature with increasing energy density

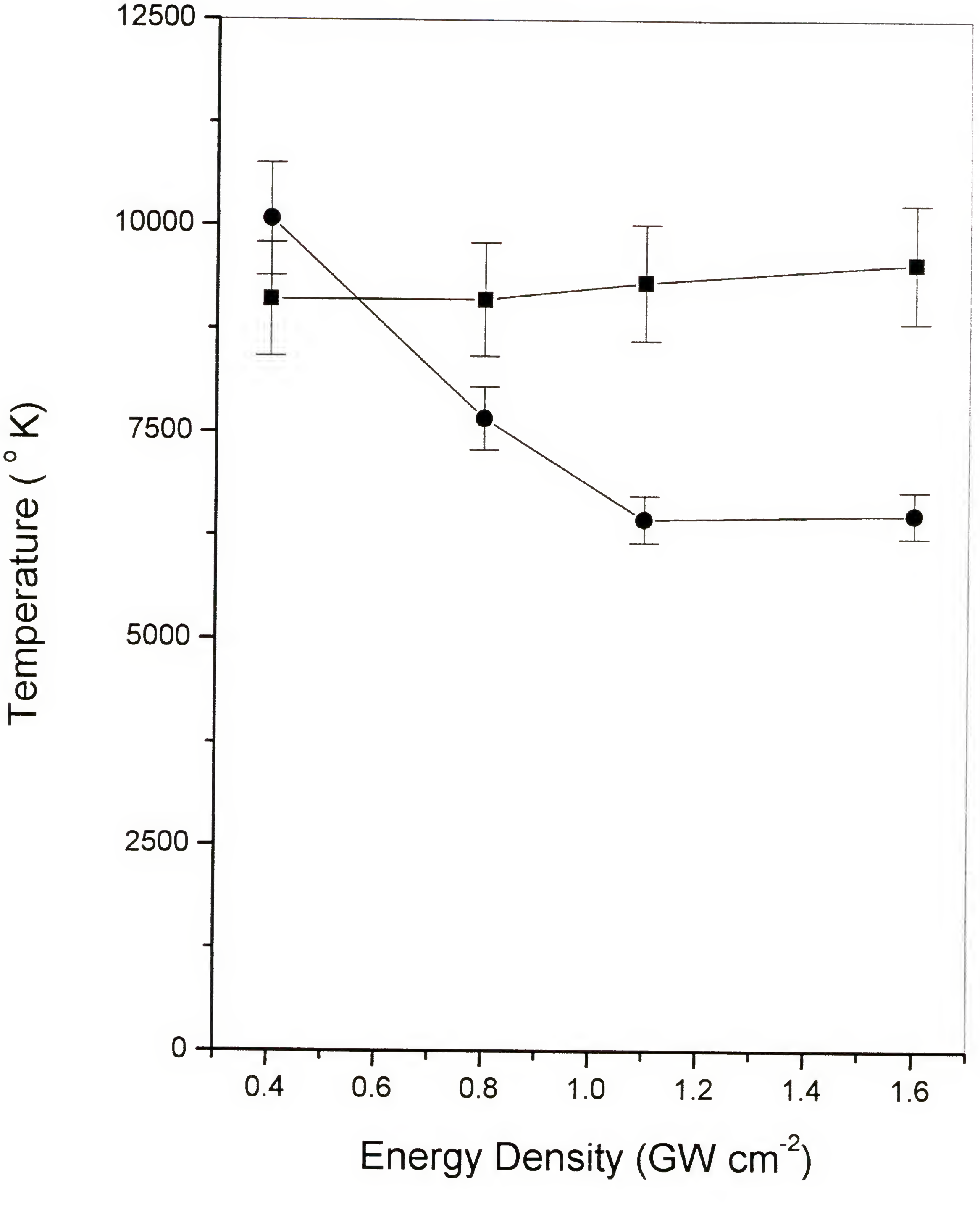

Figure 6-6. Excitation (■) and vibrational (●) temperatures in a plasma formed by a Nd:YAG laser (1064 nm) on a graphite target at a time delay of 2 μs and energy densities of 0.4, 0.8, 1.1,and 1.6 GW cm^{-2}.

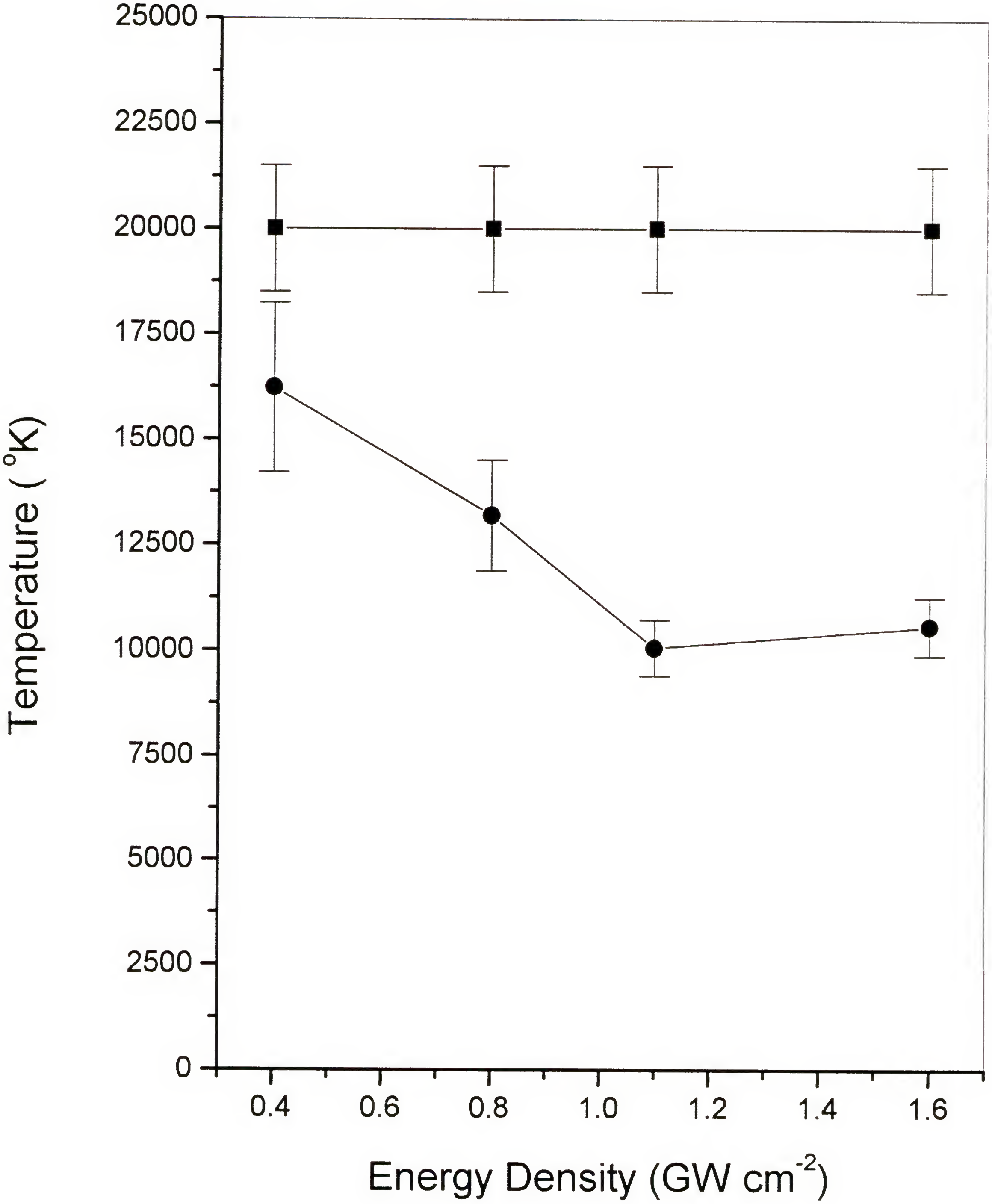

Figure 6-7. Excitation (■) and vibrational (●) temperatures in a plasma formed by a XeCl laser (308 nm) on a graphite target at a time delay of 2 μs and energy densities of 0.4, 0.8, 1.1 and 1.6 GW cm^{-2}.

in both cases may be due to a higher rate of collisions in the plasmas produced at higher energy densities. Collisions provide a mechanism by which molecules formed in a high energy state relax to a lower energy state. The values for both types of laser-induced plasmas suggest that at energy densities below 1 GW cm^{-2}, the excitation and vibrational populations are more likely to be described by a single temperature. The appropriate energy density appears to be about 0.6 GW cm^{-2} for the Nd:YAG laser irradiation and (by extrapolation) about 0.1 GW cm^{-2} for the XeCl laser.

CHAPTER 7

CONCLUSIONS AND FUTURE WORK

The main contributions of this work are the use of plasma diagnostics to correct for matrix effects, such as water content, the use of a submerged substrate to perform determinations in liquids, the construction of a fiber optic LIBS probe, and the comparison of temperatures in plasmas formed by UV and IR lasers. A second LIBS instrument is also nearly complete.

If laser-induced breakdown spectroscopy is to become a valuable tool for elemental analysis outside the laboratory, the majority of work to be done should be in developing efficient multivariate data analysis routines which can take advantage of the wealth of spectral information acquired when CCDs are employed as detectors.

Currently most quantitative LIBS data analysis routines consist of only a background subtraction, peak assignment, and peak height or peak area determination. The area or height of the analyte peak chosen is then assumed to vary with concentration in a way which can be described by a calibration curve (usually first order). Most spectral data are discarded.

When a 10 or 20 nm spectral range is acquired, there is often enough information present to determine an electronic temperature from a Boltzmann plot and an electron number density from either a half-width or ratio of ion line intensity to atom line intensity.

It was shown in chapter 3 that measurement of these parameters allows for correction of signal with respect to matrix effects such as water content. If LIBS is to be performed as an on-line technique requiring no sample preparation, measurements of this type will be essential for accurate quantitation.

Chemometric approaches to analyzing LIBS data, such as principal components analysis (PCA) may show potential. In applications where the goal is to classify samples into different categories based on elemental composition, PCA is particularly applicable. This method was investigated as a means for identifying five different steels from their spectra.

The five steels used in the experiment were NIST samples 1261a, 1264a, 1265a, 807, and 818. These samples differ very slightly in composition and show spectra which are dominated in every wavelength region by iron lines. Figure 7-1 shows superimposed spectra of samples 818 and 1261a around 300 nm.

In the analysis performed, four spectra of each of the five steels were imported into Pirouette™ software. The software is capable of performing PCA with 1024 independent variables. In this experiment, the intensities at each of the 576 pixels composing the wavelength axis of the spectra were read as independent variables. The software then determined loadings for the first 48 principal components. Figure 7-2 is a plot of the 3-dimensional PC space formed by the first three principal components. The five steel samples are denoted by the five different symbols. It can be seen that the samples of the same steel type form clusters which can be distinguished from one another quite easily. In practice, these clusters could comprise a training set that form the basis for identification of unknown samples.

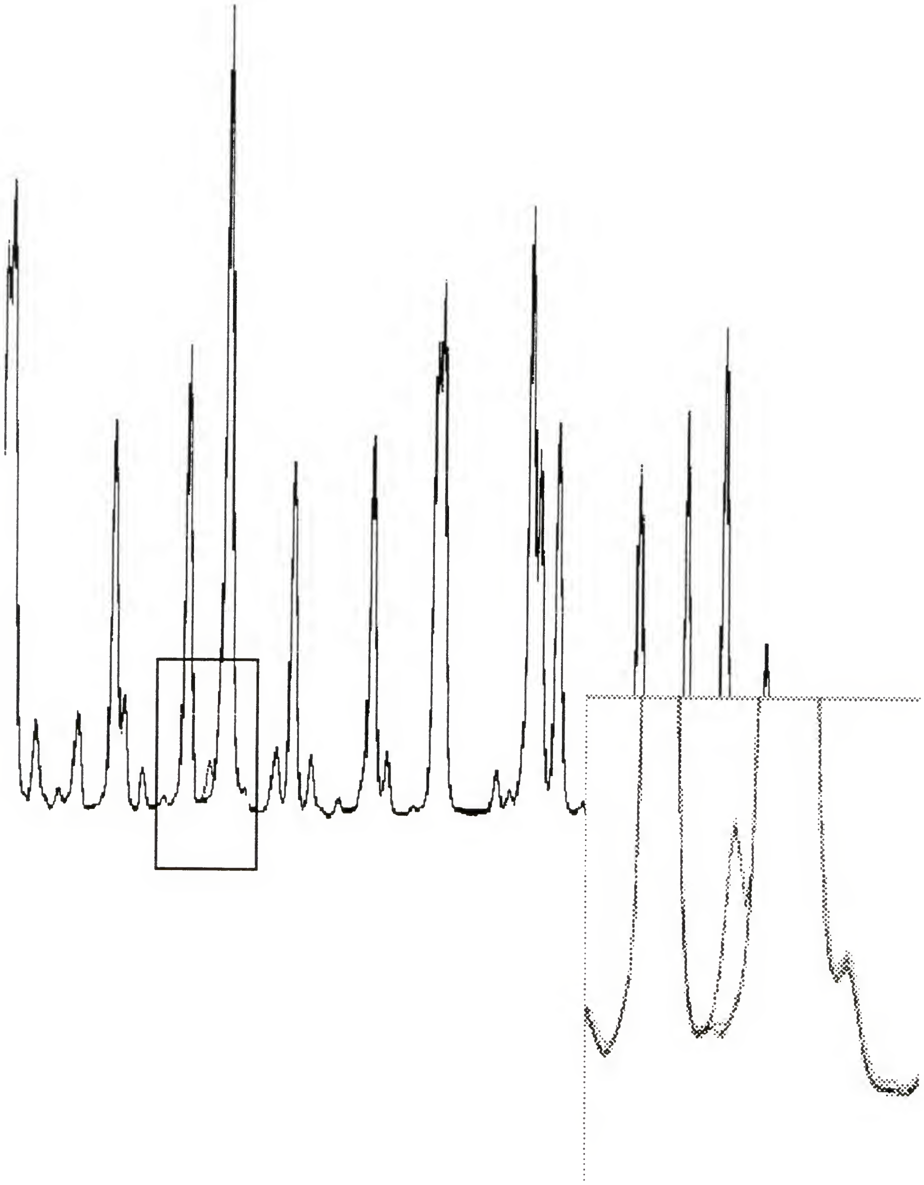

Figure 7-1. Superimposed spectra of NIST steel samples 818 and 1261a. The 1261a sample shows a small Ni peak which is absent in the 818 sample.

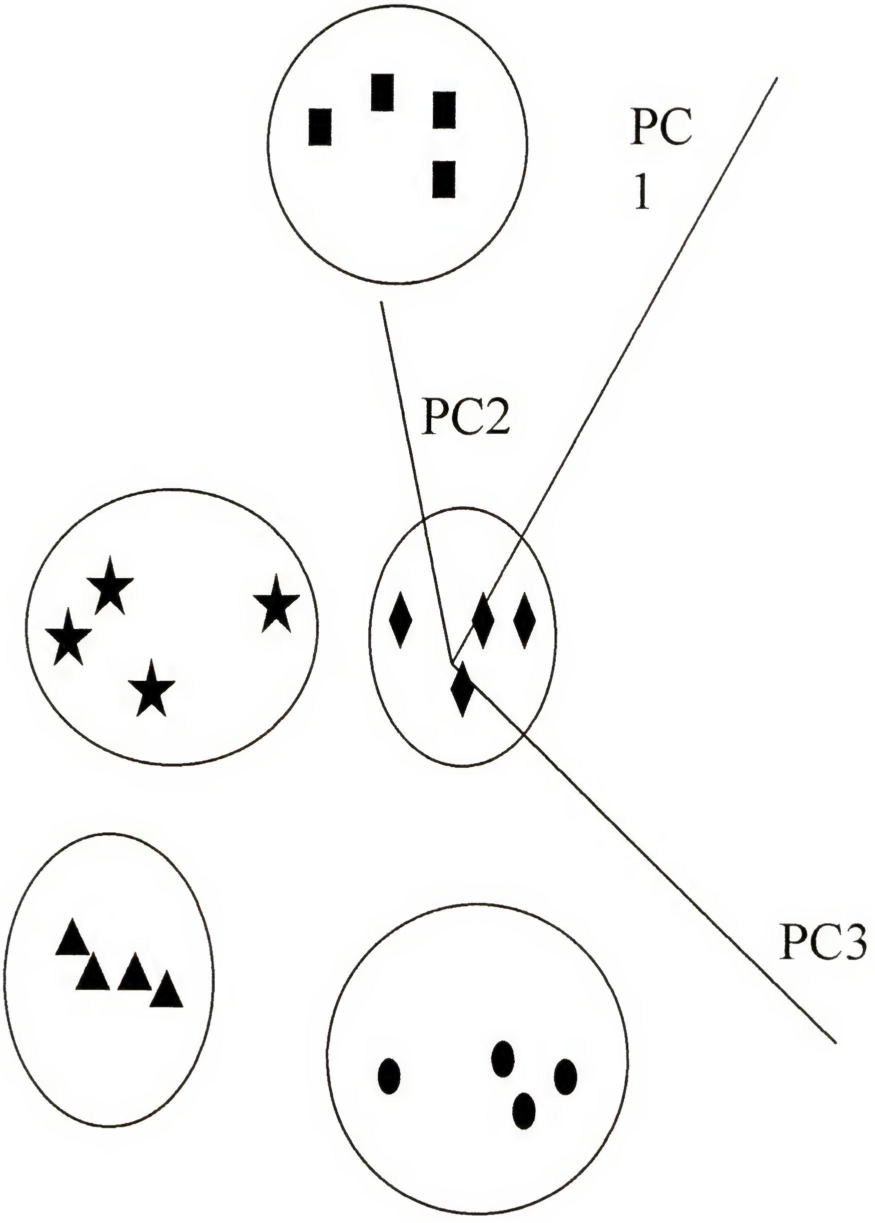

Figure 7-2. A plot of the 3-dimensional principal components space defined by the first three principal components determined by Pirouette™. The symbols represent spectra from the five steel samples: ▲1265a, ●807, ♦1261a, ★818, and ■ 1264a.

Analysis of this type can be performed without the need for background correction or peak assignment. When the goal is merely to identify a sample from a limited number of possibilities it is certainly the method of choice. Forensic analysis is an obvious example.

LIBS is far from being a mature technique. The first commercial instruments are just beginning to appear on the market. Small Nd:YAG lasers and CCDs which do not require water cooling are being employed in portable LIBS instrumentation. The key to the success of LIBS in industry may well lie in the development of application specific software.

LIST OF REFERENCES

1. **Ingle, J. D., and Crouch, S. R**. Spectrochemical Analysis, Prentice Hall, Englewood Cliffs, NJ, 1988.

2. **Boumans, P. W.** Theory of Spectrochemical Excitation, Adam Hilger, Bristol England, 1966.

3. **Marcus, K**. Glow Discharge Spectroscopies, Plenum Press, NY, 1993.

4. **Perryman, M. A., Foden, C. L., and Peacock, A**., *Nuclear Instruments and Methods in Physics Research*, 325A, 319, 1993.

5. **deGalan, L. and Winefordner, J. D**., *Spectrochimica Acta*, 23B, 521, 1968.

6. **Griem, H. R**., Spectral Line Broadening by Plasmas, Academic Press, NY, 1974.

7. **Lochte-Holtgreven, W**., Plasma Diagnostics, Wiley Interscience, NY, 1968.

8. **Adrain, R. S. and Watson, J.,** *J. Appl. Phys. D*, 17, 1915, 1984.

9. **Radziemski, L. J. and Cremers, D. A.,** *SPIE*, 1318, 71, 1990.

10. **Thiem, T. L., Lee, Y., and Sneddon, J.,** *Microchemical Journal*, 45, 1, 1992.

11. **Majidi, V. and Joseph, M. R.,** *Critical Reviews in Analytical Chemistry*, 23, 143, 1992.

12. **Ibrahim, A. and Goddard, B. J.,** *Jurnal Fizik Malaysia*, 14, 43, 1993.

13. **Darke, S. and Tyson, J.,** *J. Analytical Atomic Spectroscopy*, 8, 145, 1993.

14. **Noll, R., Sattmann, R., and Sturm, V.,** *SPIE*, 2248, 50, 1994.

15. **Sharp, B. L., Chenery, S., Jowitt, R., Fisher, A., and Sparkes, S. T.,** *J. Analytical Atomic Spectroscopy*, 10, 139, 1995.

16. **Chen, G. and Yeung, E. S.,** *Analytical Chemistry*, 60, 2258, 1988.

17. **Wood, O. R., Silfvast, W. T., Tom, H. W. K., Knox, H., Fork, R. L., Brito-Cruz, C. H., Downer, M. C., and Maloney, P. J.,** *Appl. Phys. Lett.*, 53, 654, 1988.

18. **Coche, M., Berthoud, T., Mauchien, P., and Camus, P.,** *Applied Spectroscopy*, 43, 646, 1989.

19. **Iida, Y.,** *Applied Spectroscopy*, 43, 229, 1989.

20. **Balazs, L., Gijbels, R., and Vertes, A.,** *Analytical Chemistry*, 63, 314, 1991.

21. **Mason, K. J. and Goldberg, J. M.,** *Applied Spectroscopy*, 45, 1444, 1991.

22. **Owens, M. and Majidi, V.,** *Applied Spectoscopy*, 45, 1463, 1991.

23. **Lee, Y., Sawan, S. P., Thiem, T. L., Teng, Y. Y., and Sneddon, J.,** *Applied Spectroscopy*, 46, 436, 1992.

24. **Marine, W., Gerri, M., d'Aniello, J. M. S., Sentis, M., Delaporte, P., Forestier, B., and Fontaine, B.,** *Applied Surface Science*, 54, 264, 1992.

25. **Kuzuya, M., Matsumoto, H., Takechi, H., and Mikami, O.,** *Applied Spectroscopy*, 47, 1659, 1993.

26. **Okano, A., Matsuura, A. Y., Hattori, K., and Itoh, N.,** *J. Appl. Phys.*, 73, 3158, 1993.

27. **Yago, H., Furuta, K., Ishikawa, K., and Komura, H.,** *Phys. Stat. Sol.*, 179, 223, 1993.

28. **Kagawa, K., Kawai, K., M.Tani, and Kobayashi, T.,** *Applied Spectroscopy*, 48, 198, 1994.

29. **Tambay, R. and Thareja, R. K.,** *Laser Chemistry*, 14, 225, 1994.

30. **Blanco, F., Botho, B., and Campos, J.,** *Physica Scripta*, 52, 1995.

31. **Jensen, L. C., Langford, S. C., Dickinson, J. T., and Addlman, R. S.,** *Spectrochimica Acta*, 50B, 1501, 1995.

32. **Tasaka, Y., Tanaka, M., and Usami, S.,** *Japanese Journal of Applied Physics*, 34, 1673, 1995.

33. **Thareja, R. K. and Dwivedi, R. K.,** *Laser and Particle Beams*, 13, 481, 1995.

34. **Hatem, G., Colon, C., and Campos, J.,** *Spectrochimica Acta*, 49A, 509, 1993.

35. **Dreyfus, R. W., Kelly, R., and Walkup, R. E.,** *Nuclear Instruments and Methods in Physics Research*, B23, 557, 1987.

36. **Koren, G. and Yeh, J. T. C.,** *J. Appl. Phys.*, 7, 2120, 1984.

37. **Deshmukh, S. and Rothe, E. W.,** *J. Appl. Phys.*, 66, 1370, 1989.

38. **Al-Wazzan, R. A., Lewis, C. L. S., and Morrow, T.,** *Rev. Sci. Instrum.*, 67, 85, 1996.

39. **Al-Wazzan, R. A., Hendron, J. M., and Morrow, T.,** *Applied Surface Science*, 96-98, 170, 1996.

40. **Bulatov, V., Xu, L., and Schechter, I.,** *Analytical Chemistry*, 68, 2966, 1996.

41. **Multari, R. A., Foster, L. E., Cremers, D. A., and Ferris, M. J.,** *Applied Spectroscopy*, 50, 1483, 1996.

42. **Multari, R. A. and Cremers, D. A.,** *IEEE Transactions on Plasma Science*, 24, 39, 1996.

43. **Nemet, B. and Kozma, L.,** *Fresenius J. Anal. Chem.*, 355, 904, 1996.

44. **Kurniawan, H. and Kagawa, K.,** *Applied Spectoscopy*, 51, 304, 1997.

45. **Martin, P., Campos, J., and Santander, J. L. G.,** *J. Quant. Spectrosc. Radiat. Transfer*, 57, 459, 1997.

46. **Granse, G., Vollmar, S., Lenk, A., Rupp, A., and Rohr, K.,** *Applied Surface Science*, 96-98, 97, 1996.

47. **Aguilera, J. A., Aragon, C., and Campos, J.,** *Applied Spectroscopy*, 46, 1382, 1992.

48. **Hader, W.,** *Tech mitt Krupp Engl. Ed.*, 2, 97, 1992.

49. **Lorenzen, C. J., Carlhoff, C., Hahn, U., and Jogwich, M.,** *J. Analytical Atomic Spectrometry*, 7, 1029, 1992.

50. **Sabsabi, M., Cielo, P. G., Boily, S., and Chaker, M.,** *SPIE*, 2069, 191, 1993.

51. **Thiem, T. L., Salter, R. H., Gardner, J. A., Lee, Y. I., and Sneddon, J.,** *Applied Spectroscopy*, 48, 58, 1994.

52. **Thiem, T. L. and Wolf, P. J.,** *Microchemical Journal*, 50, 244, 1994.

53. **Borthwick, I. S., Ledingham, K. W. D., and Singhal, R. P.,** *Spectrochimica Acta*, 47B, 1259, 1992.

54. **Allen, T. M., Kelly, P. B., Anderson, J. E., Taylor, T. N., and Nogar, S. S.,** *J. Appl. Phys.*, 61, 221, 1995.

55. **Anderson, D. R., McLeod, C. W., English, T., and Smith, A. T.,** *Applied Spectroscopy*, 49, 691, 1995.

56. **Arnold, S. D. and Cremers, D. A.,** *AIHA Journal*, 56, 1180, 1995.

57. **Sattmann, R., Sturm, V., and Noll, R.,** *J. Appl. Phys. D*, 28, 2181, 1995.

58. **Davies, C. M., Telle, H. H., and Williams, A. W.,** *Fresenius J. Anal. Chem.*, 355, 895, 1996.

59. **Cremers, D. A., and Koskelo, A. C.,** *Applied Spectroscopy*, 49, 857, 1995.

60. **Cremers, D. A.,** *Applied Spectroscopy*, 41, 572, 1987.

61. **Bescos, B., Castano, J., and Urena, A. G.,** *Laser Chemistry*, 16, 75, 1995.

62. **Gonzalez, A., Oritz, M., and Campos, J.,** *Applied Spectroscopy*, 49, 1632, 1995.

63. **Hakkanen, H. J. and Korppi-Tommola, J. E. I.,** *Applied Spectroscopy*, 49, 1721, 1995.

64. **Sabsabi, M. and Cielo, P.,** *Applied Spectroscopy*, 49, 499, 1995.

65. **Ciucci, A., Palleschi, V., Rastelli, S., Barbini, R., Colao, F., Fantoni, R., Palucci, A., Ribezzo, S., and Steen, H. J. L. v. d.,** *J. Appl. Phys. B*, 63, 185, 1996.

66. **Ernst, W. E., Farson, D. F., and Sames, D. J.,** *Applied Spectroscopy*, 50, 306, 1996.

67. **Geertsen, C., Lacour, J. L., Mauchien, P., and Pierrard, L.,** *Spectrochimica Acta*, 51B, 1403, 1996.

68. **Marquardt, B. J., Goode, S. R., and Angel, S. M.,** *Analytical Chemistry*, 68, 977, 1996.

69. **Miziolek, A. W.,** *Optics and Photonics News*, 10, 39, 1996.

70. **Radziemski, L. J., Loree, T. R., and Cremers, D. A.,** *Optical Sciences*, 39, 1983.

71. **Palleschi, V., Arca, G., Ciucci, A., Rastelli, S., and Tognoni, E.,** *IEEE-International Geoscience and Remote Sensing Symposium*, 2, 854, 1996.

72. **Vadillo, J. M. and Laserna, J. J.,** *Talanta*, 43, 1149, 1996.

73. **Vadillo, J. M., Palanco, S., Romero, M. D., and Laserna, J. J.,** *Fresenius J. Anal. Chem.*, 355, 909, 1996.

74. **Kim, D. E., Yoo, K. J., Park, H. K., Oh, K. J., and Kim, D. W.,** *Applied Spectroscopy*, 51, 22, 1997.

75. **Maravelaki, P. V., Zafiropulos, V., Kilikoglou, V., Kalaitzaki, M., and Fotakis, C.,** *Spectromchimica Acta*, 52B, 41, 1997.

76. **Armstrong, R. L.,** *J. Appl. Phys.*, 56, 2142, 1984.

77. **Alexander, D. R. and Armstrong, J. G.,** *Applied Optics*, 26, 533, 1987.

78. **Chylek, P., Jarzembski, A., and Chou, N. Y.,** *Appl. Phys. Lett.*, 49, 1475, 1986.

79. **Hsieh, W. F., Eickmans, J. H., and Chang, R. K.,** *J. Optical Society of America*, 4, 1816, 1987.

80. **Biswas, A., Latifi, H., and Radziemski, L. J.,** *Applied Optics*, 27, 2386, 1988.

81. **Zheng, J., Hsieh, W. F., Chen, S., and Chang, R. K.,** *Optics Letters*, 13, 559, 1988.

82. **Hammer, D. X., Thomas, R. J., Noojin, G. D., Rockwell, B. A., Kennedy, P. K., and Roach, W. P.,** *IEEE Journal of Quantum Electronics*, 32, 670, 1996.

83. **Kitamori, T., Yokose, K., Suzuki, K., Sawada, T., and Gohshi, Y.,** *Japanese Journal of Applied Physics*, 27, L983, 1988.

84. **Vogel, A., Busch, S., and Parlitz, U.,** *J. Acoust. Soc. Am.*, 100, 148, 1996.

85. **Sacchi, C. A.,** *J. Optical Society of America*, 8, 337, 1991.

86. **Pinnick, R. G., Biswas, A., Pendleton, J. D., and Armstrong, R. L.,** *Applied Optics*, 31 No. 3, 311, 1992.

87. **Nyga, R. and Neu, W.,** *Optics Letters*, 18, 747, 1993.

88. **Feng, Q., Moloney, J. V., Newell, A. C., Wright, E. M., Cook, K., Kennedy, P. K., Hammer, D. X., Rockwell, B. A., and Thompson, C. R.,** *IEEE Journal of Quantum Electronics*, 33, 127, 1997.

89. **Cremers, D. A., Radziemski, L. J., and Loree, T. R.,** *Applied Spectroscopy*, 38, 721, 1984.

90. **Wachter, J. R. and Cremers, D. A.,** *Applied Spectroscopy*, 41, 1042, 1987.

91. **Aragon, C., Aguilera, J. A., and Campos, J.,** *Applied Spectroscopy*, 47, 606, 1993.

92. **Stolarski, D. J., Hardman, J., Bramlette, C. M., Noojin, G. D., Thomas, R. J., Rockwell, B. A., and Roach, W. P.,** *SPIE*, 2391, 100, 1995.

93. **Ito, Y., Ueki, O., and Nakamura, S.,** *Analytica Chimica Acta*, 299, 401, 1995.

94. **Nakamura, S., Ito, Y., Sone, K., Hiraga, H., and Kaneko, K.,** *Analytical Chemistry*, 68, 2981, 1996.

95. **Knopp, R., Scherbaum, F. J., and Kim, J. I.,** *Fresenius J. Anal. Chem.*, 355, 16, 1996.

96. **Ho, W. F., Ng, C. W., and Cheung, N. H.,** *Applied Spectroscopy*, 51, 87, 1997.

97. **Paksy, L., Nemet, B., Lengyel, A., Kozma, L., and Czekkel, J.,** *Spectrochimica Acta*, 51B, 279, 1996.

98. **Arca, G., Ciucci, A., Palleschi, V., Rastelli, S., and Togononi, E.,** *IEEE-International Geoscience and Remote Sensing Symposium*, 1, 520, 1996.

99. **Radziemski, L. J., Loree, T. R., Cremers, D. A., and Hoffman, N. M.,** *Analytical Chemistry*, 55, 1246, 1983.

100. **Eickmans, J. H., Hsieh, W. F., and Chang, R. K.,** *Applied Optics*, 26, 3721, 1987.

101. **Essien, M., Radziemski, L. J., and Sneddon, J.,** *J. Analytical Atomic Spectroscopy*, 3, 985, 1988.

102. **Archontaki, H. A. and Crouch, S. R.,** *Applied Spectroscopy*, 42, 741, 1988.

103. **Ng, K. C., Ayala, N. L., Simeonsson, J. B., and Winefordner, J. D.,** *Analytica Chimica Acta*, 269, 123, 1992.

104. **Parigger, C. and Lewis, J. W. L.,** *Applied Physics Communications*, 12, 163, 1993.

105. **Poulain, D. E. and Alexander, D. R.,** *Applied Spectroscopy*, 49, 569, 1995.

106. **Haisch, C., Paine, U., and Niessner, R.,** *Technical Digest- European Quantum Electronics Conference*, 25, 1996.

107. **Kumar, V. and Thareja, R. K.,** *J. Appl. Phys.*, 64, 5269, 1988.

108. **Parigger, C., Plemmons, D. H., Hornkohl, J. O., and Lewis, J. W. L.,** *J. Quant. Spectrosc. Radiat. Transfer*, 52, 707, 1994.

109. **Yagi, T. and Huo, Y.,** *Applied Optics*, 35, 3183, 1996.

110. **Yalcin, S., Crosley, D. R., Smith, G. P., and Faris, G. W.,** *Hazardous Waste and Hazardous Materials*, 13, 51, 1996.

111. **Cremers, D. A. and Radziemski, L. J.,** *Analytical Chemistry*, 55, 1252, 1983.

112. **Cremers, D. A. and Radziemski, L. J.,** *Applied Spectroscopy*, 39, 57, 1985.

113. **Sneddon, J.,** *Trends in Analytical Chemistry*, 7, 222, 1988.

114. **Ottesen, D. K., Wang, J. C. F., and Radziemski, L. J.,** *Applied Spectroscopy*, 43, 967, 1989.

115. **Morris, J. B., Forsch, B. E., and Miziolek, A. W.,** *Applied Spectroscopy*, 44, 1040, 1990.

116. **Cheng, E. A. P., Fraser, R. D., and Eden, J. G.,** *Applied Spectroscopy*, 45, 949, 1991.

117. **He, K. X., Hammond, T. D., Winstead, C. B., Gole, J. L., and Dixon, D. A.,** *J. Chem. Phys*, 10, 7183, 1991.

118. **Joseph, M. R. and Majidi, V.,** *J. Trace and Microprobe Techniques*, 10, 207, 1992.

119. **Casini, M., Harith, M. A., Palleschi, V., Salvetti, A., Singh, D. P., and Vaselli, M.,** *Laser and Particle Beams*, 9, 633, 1991.

120. **Flower, W. L., Peng, L. W., Bonin, M. P., French, N. B., Johnsen, H. A., Ottesen, D. K., Renzi, R. F., and Westbrook, L. V.,** *Fuel Processing Technology*, 39, 277, 1994.

121. **Lazzari, C., Rosa, M. D., Rastelli, S., Ciucci, A., Palleschi, V., and Salvetti, A.,** *Laser and Particle Beams*, 12, 525, 1994.

122. **Zhang, H., Singh, J. P., Yueh, F. Y., and Cook, R. L.,** *Applied Spectroscopy*, 49, 1617, 1995.

123. **Nordstrom, R. J.,** *Applied Spectroscopy*, 49, 1490, 1995.

124. **Parigger, C., Plemmons, D. H., and Lewis, J. W.,** *Applied Optics*, 34, 3325, 1995.

125. **Haisch, C., Niessner, R., Matveev, O., Panne, U., and Omenetto, N.,** *Fresenius J. Anal. Chem*, 356, 21, 1996.

126. **Yamamoto, K. Y., Cremers, D. A., Ferris, M. J., and Foster, L. E.**, *Applied Spectroscopy*, 50, 222, 1996.

127. **Pahkomov, A. V., Nichols, W., and Borysow, J.**, *Applied Spectroscopy*, 50, 1175, 1996.

128. **Eppler, A. S., Cremers, D. A., Hickmott, D. D., Ferris, M. J., and Koskelo, A. C.,** *Applied Spectroscopy,* 50, 1175, 1996.

129. **Case, M. E., and Hofeldt, D. L.,** *Aerosol Science and Technology*, 25, 46, 1996.

130. **Telle, H. H.,** *SPIE Optical Engineering,* 2730, 160, 1996.

131. **Wisbrun, R., Schechter, I., and Neissner, R.**, *SPIE Optical Engineering*, 1716, 2, 1992.

132. **Lapinski, M.**, Modern Methods for the Control and Measurement of Humidity and Moisture, National Center for Scientific Technical and Economic Information, Warsaw, Poland, 1976.

133. **Ahmad, I., and Goddarad, B. J.**, *Jurnal Fizik Malaysia*, 14, 43, 1993.

134. **Perkins, L. D., and Long, G. L.**, *Applied Spectroscopy*, 43, 499, 1989.

135. **Masamba, W. R., Ali, A. H., and Winefordner, J. D.**, *Spectrochimica Acta*, 47B, 481, 1992.

136. **Klein, A. J.,** *Microwave Power*, 16, 284, 1981.

137. **Cutmore, N., Evans, T., McEvan, A.**, *Journal of Microwave Power and Electromagnetic Energy*, 26, 237, 1991.

138. **Brosio, E., Conti, F., DiNola, A., Scorano, O., and Balestrieri, F.**, *Journal of Food Technology*, 16, 629, 1981.

139. **Hester, R. E., and Quine, D. E.**, *Journal of Dairy Research*, 44, 125, 1977.

140. **Davenal, A., and Marchal, P**, *Transactions of the American Society of Agricultural Engineers*, 35, 1891, 1992.

141. **Delwiche, S.**, *Cereal Chemistry*, 73, 399, 1996.

142. **Nilsson, M. B.**, *Environmental Science and Technology*, 30, 2586, 1996.

143. **Windham, W. R.**, *Journal of the Association of Official Analytical Chemists*, 72, 255, 1989.

144. **Seyfried, M. S.**, *Soil Science*, 161, 87, 1996.

145. **Schroeder, I., Schlechter, R., Wisbrun, R., and Niessner, R.**, Excimer Lasers and Applications ed. by L. D. Laude Kluwer Academic Publishers, Dordrecht, 1994.

146. **Allred, C. D., McCreery, R. L.**, *Applied Spectroscopy*, 44, 1229, 1990.

147. **Newman, C. D., Bret, G. G., and McCreery, R. L.**, *Applied Spectroscopy*, 46, 262, 1992.

148. **Schwab, S. D., and McCreery, R. L.**, *Analytical Chemistry*, 56, 2199, 1984.

149. **Lewis, I. R., and Griffiths, P. R.**, *Applied Spectroscopy*, 50, 12A, 1996.

150. **Zimba, C. G., and Rabolt, J. F.**, *Applied Spectroscopy*, 45, 162, 1991.

151. **Kawamura, Y., Itagaki, Y., Toyoda, K., and Namba, S.**, *Optical Communications*, 48, 44, 1983.

152. **Lacombat, M., Dubroeucq, G. M., Massin, J., and Brevignon, M.**, *Solid State Technology*, 23, 115, 1980.

153. **Latta, M. R., and Jain, K.**, *Optical Communications*, 49, 435, 1984.

154. **Rhodes, P. W., and Shealy, D. L.**, *Applied Optics*, 19, 3545, 1980.

155. **Hand, D., Peters, C., Haran, F., and Jones, J.,** *Measurement Science and Technology,* 8, 587, 1997.

156. **Pratisto, H., Frenz, M., Koenz, F., Altermatt, H., and Weber, H**., *SPIE Optical Engineering,* 2681, 201, 1996.

157. **Mao, X. L., Shannon, M. A., Fernandez, A. J., and Russo, R. E.,** *Applied Spectroscopy,* 49, 1054, 1995.

158. **Castle, B. C., Visser, K., Smith, B. W., and Winefordner, J. D**., *Spectrochimica Acta B,* in press.

159. **Atkins, P. W**., Physical Chemistry 4th Edition, Ch. 11,12, Oxford University Press, 1990.

160. **Petrucci, G. P., Imbroisi, R. D., Guenard, R. D., Smith , B. W., and Winefordner, J. D.,** *Applied Spectroscopy,* 49, 655, 1994.

161. **Spencer, B. M., Smith, B. W., and Winefordner, J. D.,** *Applied Spectroscopy,* 48, 289, 1994.

162. **Zeeman, P. B., Terblanche, S. P., Visser, K., and Hamm, F. H.,** *Applied Spectroscopy*, 32, 572, 1978.

163. **Smit-Miessen, M. M., and Spier, J. L.,** *Physica IX,* 422, 1942.

164. **Harilal, S. S., Issac, R. C., Bindhu, C. V., Varier, G. K., Nampoori, V. P., and Vallabhan, C. P.,** *Pramana Journal of Physics,* 46, 145, 1996.

165. **Gornushkin, I., Smith, B. W., and Winefordner, J. D.,** *Spectrochimical Acta B,* in press.

166. **Rehfuss, B. D., Suh, M., and Miller, T. A.,** *Journal of Molecular Spectroscopy,* 151, 437, 1992.

167. **Herzberg, G.,** Molecular Spectra and Molecular Structure I. Spectra of Diatomic Molecules, pg. 520, D. Van Nostrand Company, Inc., New York, 1967.

BIOGRAPHICAL SKETCH

David Alexander Rusak was born August 9, 1971, in Grand Forks, North Dakota. He is the oldest child in a family which includes his parents, Al and Sharon, brother, Steve and sister, Karen. David attended high school at East Mecklenburg in Charlotte, North Carolina, and college at The University of North Carolina at Chapel Hill, where he received a B.S. degree in Chemistry in 1993.

I certify that I have read this study and that in my opinion it conforms to acceptable standards of scholarly presentation and is fully adequate, in scope and quality, as a dissertation for the degree of Doctor of Philosophy.

James D. Winefordner

James D. Winefordner
Graduate Research Professor of
Chemistry

I certify that I have read this study and that in my opinion it conforms to acceptable standards of scholarly presentation and is fully adequate, in scope and quality, as a dissertation for the degree of Doctor of Philosophy.

Richard A. Yost
Professor of Chemistry

I certify that I have read this study and that in my opinion it conforms to acceptable standards of scholarly presentation and is fully adequate, in scope and quality, as a dissertation for the degree of Doctor of Philosophy.

Robert T. Kennedy
Associate Professor of Chemistry

I certify that I have read this study and that in my opinion it conforms to acceptable standards of scholarly presentation and is fully adequate, in scope and quality, as a dissertation for the degree of Doctor of Philosophy.

Randolph Duran

Randolph S. Duran
Associate Professor of Chemistry

I certify that I have read this study and that in my opinion it conforms to acceptable standards of scholarly presentation and is fully adequate, in scope and quality, as a dissertation for the degree of Doctor of Philosophy.

E. Dow Whitney

E. Dow Whitney
Professor of Materials Science and
Engineering

This dissertation was submitted to the Graduate Faculty of the College of the Department of Chemistry in the College of Liberal Arts and Sciences and to the Graduate School and was accepted as partial fulfillment of the requirements for the degree of Doctor of Philosophy.

May 1998

____
Dean, Graduate School